STRUCTURAL EVOLUTION OF THE VIRGIN SPRING PHASE OF THE AMARGOSA CHAOS, DEATH VALLEY, CALIFORNIA, USA

by

SAMUEL ROBERT CASTONGUAY

A THESIS

Presented to the Department of Geological Sciences
and the Graduate School of the University of Oregon
in partial fulfillment of the requirements
for the degree of
Master of Science

September 2013

THESIS APPROVAL PAGE

Student: Samuel Robert Castonguay

Title: Structural Evolution of the Virgin Spring Phase of the Amargosa Chaos, Death Valley, California, USA

This dissertation has been accepted and approved in partial fulfillment of the requirements for the Master of Science degree in the Department of Geological Sciences by:

Marli Miller	Chair
Ray Weldon	Member
Mark Reed	Member

and

Kimberly Andrews Espy	Vice President for Research and Innovation/Dean of the Graduate School

Original approval signatures are on file with the University of Oregon Graduate School.

Degree awarded September 2013

THESIS ABSTRACT

Samuel Robert Castonguay

Master of Science

Department of Geological Sciences

September 2013

Title: Structural Evolution of the Virgin Spring Phase of the Amargosa Chaos, Death Valley, California

The Amargosa Chaos and Fault of Death Valley are complex features that play important roles in various tectonic models. Some recent models claim the fault is a regional detachment accommodating 80 km of NW-directed transport that produced the Chaos in its hangingwall. I offer an alternative interpretation: the chaos is a product of multiphase deformation that likely spanned the late Mesozoic and Cenozoic. The Amargosa Fault represents just one of six deformation events.

The accompanying map (supplemental file) shows the cross-cutting relationships among fault populations: (D1) 25% north-northwest directed shortening across an imbricate thrust and tight fold system; (D2) E-SE extension on five normal faults; (D3) extension-related folding, which folded the D2 faults; (D4) normal-oblique slip on the Amargosa Fault; (D5) E-W extension on domino faults; (D6) extension on the Black Mountains Frontal Fault. The D2 faults, not the Amargosa, created the enigmatic attenuation observed in the Chaos.

CURRICULUM VITAE

NAME OF AUTHOR: Samuel Robert Castonguay

GRADUATE AND UNDERGRADUATE SCHOOLS ATTENDED:

University of Oregon, Eugene
Lane Community College, Eugene, Oregon

DEGREES AWARDED:

Master of Science, Geology, 2013, University of Oregon
Bachelor of Science, Geological Science, 2010, University of Oregon
Associate of Arts Oregon Transfer Degree, Lane Community College

AREAS OF SPECIAL INTEREST:

Structural Geology
Neotectonics
Volcano-tectonic Interactions
Geoscience Education

PROFESSIONAL EXPERIENCE:

Geology Lecturer, Department of Geology, University of Wisconsin-Eau Claire, Eau Claire, 2013-2014

Graduate Teaching Fellow, Department of Geological Sciences, University of Oregon, Eugene, 2012-2013

Research Assistant, Department of Geological Sciences, University of Oregon, Eugene, 2011-2012

Student Intern, Alaska Department of Geological and Geophysical Surveys, Fairbanks, 2008

Undergraduate Research Assistant, Department of Geological Sciences, University of Oregon, Eugene, 2007-2010

GRANTS, AWARDS, AND HONORS:

Graduate Teaching Fellowship, 2011- 2013

Geologic Society of America Student Travel Grant, 2012

PUBLICATIONS:

Castonguay, S.R., 2012, Starting a Geology Student Club Public Outreach Program, The Professional Geologist, Jan/Feb

Carver, G.A., Bemis, S.P., Solie, D.N., Castonguay, S.R., Obermiller, K.E., 2010, Active and Potentially Active Faults in or near the Alaska Highway Corridor, Dot Lake to Tetlin Junction, Alaska,Alaska Department of Geological and Geophysical Surveys, Preliminary State Report

ACKNOWLEDGEMENTS

I would like to thank the people of Faith, South Dakota. Particularly, Mr. Dutton, Mr. Meyer, Mrs. King, Mrs. Storm, Mr. and Mrs. Fernau, Mrs. Peterson, Ms. Mollman, Pastor Muriel and Jim Oats, and Nancy Vance.

I thank my peers and teachers, both in the Geological Sciences Department at University of Oregon and the Earth and Environmental Science Department at Lane Community College, for the years of input; I thank Sarah Ulerick, Gene Humphreys, the students of Geology Field Camp ’09, ’10, and ’12, and the UO Geology club. I express special thanks to the office staff within the Geological Sciences Department: Vicki Arbeiter, Dave Stemple, and Shari Douglas. I thank my thesis and guidance committees, Greg Retallack, Mark Reed, Ray Weldon, and Marli Miller, for assisting me during my academic journey. Thank you Marli, for your academic, geologic, emotional, and financial support. Watch out for bears!

Thanks to Susan Sorrels, Birgitta Jansen, Cynthia Kienitz, the Timbisha-Shoshone Tribe, the staff and rangers of Death Valley National Park Service, and the town folk of Shoshone and Tecopa. I thank the community of Death Valley geological researchers: Bennie Troxel, Darrel Cowan, Terry Pavlis, Laura Serpa, David Topping, John Caskey, John Niles, and Robert Mahon. Tom Robbins and Kris Hornsby helped me immensely during field work.

To my family and friends that have created me, guided me, and stood by my side, I thank you deeply. I thank my ancestors for your hand in raising and perpetuating our blood line. I thank my Grandmother Verella and her children for their special influence in my young life. I thank my cousins and second cousin for our experiences as developing

children. I thank the Mees for raising my wife and providing me soil to work with. A special thanks to Anastasia Raichart. I thank Rocky Castonguay, Amy Cox, Lex Palmer, Jayme Williams and Andy Castonguay. I thank Ivan Campbell, for years of philosophical discussions and camping trips. I thank my dear sisters, Nicole Singer and Desireé Anzalone, and your families for our cherished experiences. I thank my step-father Gary Palmer for taking me in and teaching me the ways of the working world. I thank my mother—my dear mother—for raising me in hard and good times.

I am eternally thankful for the support of my nuclear family-Laurie, Oshen, and Neva-for letting me go on rock hunting expeditions. Thank you Laurie; you have always stood by my side and encouraged my work…gushem gushem.

My thanks to the deities of the ether, that are so completely mysterious and sensible, while chaotic and organized. Thanks to the place called Death Valley and the Amargosa Chaos for not killing me. Gaia, I thank you for your humble allowance and fierce disgust during my work. I thank Jesus for your guidance of love and patience with humanity and civilization. I thank Pan for your guidance of wildness and intolerance of humanity and civilization. I thank the great gods of duality, female and male, that is one God in all things. And most essentially, I thank the cells, molecules, and elements that flux through me and connect me to the Universe.

It is star dust that wrote this manuscript.

For my beautiful wife and children, Laurie, Oshen and Neva. I love you.

And in memory of Lauren Wright, a great researcher.

TABLE OF CONTENTS

LIST OF FIGURES

CHAPTER I

INTRODUCTION

This manuscript is the result of my exploration of the structural origin of the Virgin Spring Phase of the Amargosa Chaos and how the Chaos relates to the proximal Amargosa Fault. The study includes a review of significant concepts and literature, field descriptions of rocks and structures from 48 days of field data collection, and an interpretation of the observations. This work recognizes the systematic assemblage defined as "Chaos" as a relic of distributed and multiphase crustal faulting, which supports a distributed-faulting model for the Neogene evolution of southern Death Valley. The accompanying map (supplemental file) was created in ArcGIS to display the data.

The following introduction covers a broad range of topics relevant to Death Valley, but is ultimately focused on the local geology. I first discuss the general geography, biology, and culture of the area and then offer a brief introduction to western North American Tectonics. I then offer a review of the relevant literature, a section introducing the purpose of the study, and lastly a general description of the local stratigraphy.

The Ultimate Desert Valley

Death Valley is a National Park in southeastern California, USA in the northeastern Mojave Desert and lies 180 km west of Las Vegas, Nevada (Figure 1). Badwater basin in Central Death Valley is the lowest point in the United States at 282 feet below sea level. Only 134 km to the west, Mt. Whitney is the highest point in the contiguous United States at 14,505 feet. Death Valley is supremely arid and hot.

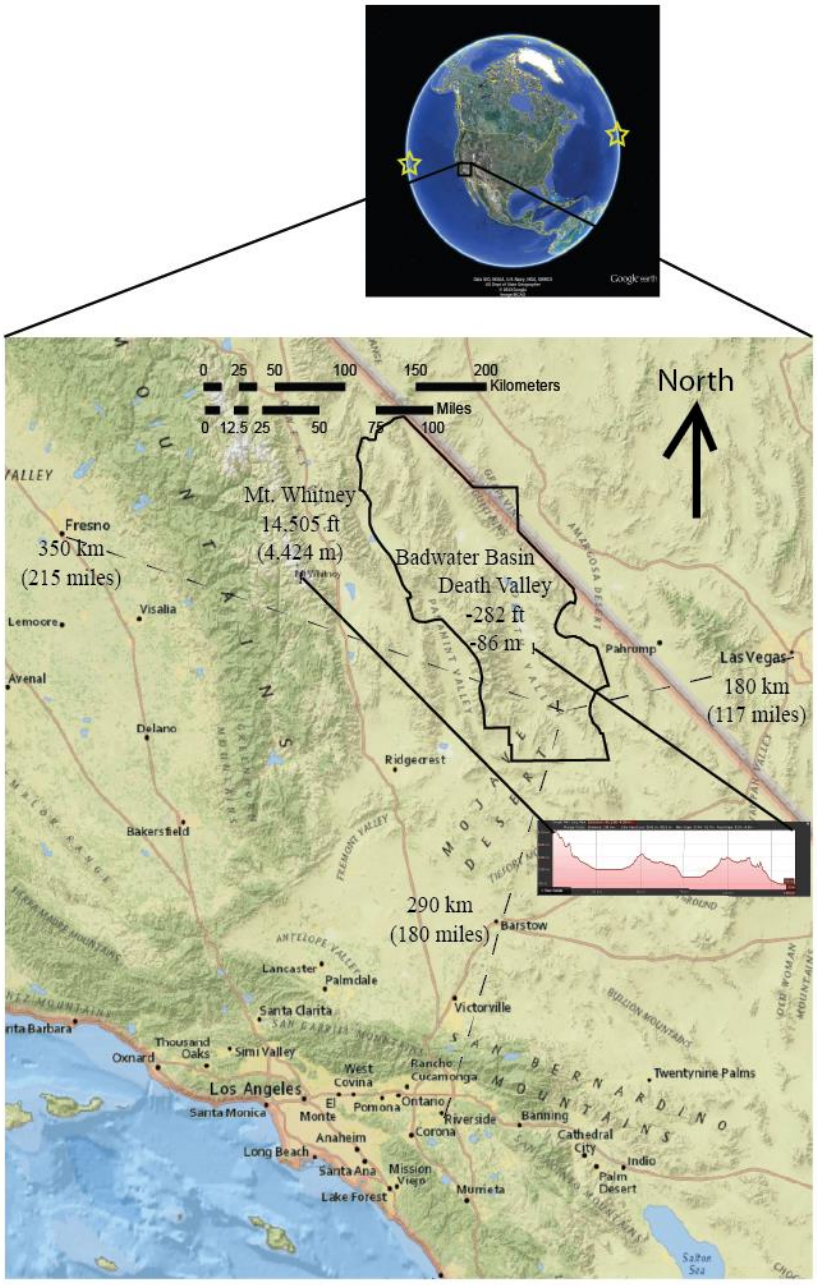

Figure 1: (top) Google Earth image showing the location of the regional map, the Açores islands of Portugal, and the Hawaiian islands of the United States of America. (right) Death Valley is a National Park in the Mojave Desert. Approximate distances to significant cities from the study area are shown in kilometers and miles. Badwater basin, the lowest point in the United States, is 282 feet below sea level. Mt. Whitney (14,505 feet) is the highest point and is only 140 km northwest of Badwater. The inset elevation profile (6.5x vertical exaggeration) from Google Earth shows the elevation contrast.

This combination of low precipitation and high heat produces extremely well-exposed rock that is mostly free of vegetation and soil.

Despite the minimal vegetation, the Death Valley region, and much of the Mojave, contains several endemic plant species. I observed many animal species that live in this region including, mountain sheep, coyote, rabbits, lizards, tarantulas, and hawks. Moreover, dozens of migratory and resident bird species use the Amargosa River oasis as a biannual refuge.

Culturally, this valley and region is the ancestral territory of the Timbisha-Shoshone tribe of Native Americans. Currently, the Timbisha-Shoshone have a local tribal headquarters and small village one mile south of the National Park Service Furnace Creek Visitor Center. The tribe became federally recognized in 1983 but did not receive land until 2000, at which time it was allotted a meager 7,000 acres, including 90 acres within the park. Verbal communication with some of the local Timbisha-Shoshone tribal members and associates revealed insightful stories of the area. A short and comprehensive collection of facts about the indigenous occupants of Southern California is provided by Heizer (1954).

This region is rich in late 1800s pioneer culture. The hills are pitted with hundreds of small to large prospect pits and adits, very few of which yielded enough valuable material to sustain an established mine. The materials extracted for economic value include gold, silver, talc, and borate. The book Death Valley and the Amargosa: A Land of Illusion by Richard E. Lingenfelter encapsulates much of the pioneer history.

The valley lies between two primary mountain ranges: the Panamint Range on the west and the Black Mountains on the east. The Funeral Mountains loosely border the

north, while the Avawatz and Owlshead ranges loosely define the south and southwest margins, respectively. The southern-most portion of the Black Mountains is split into the smaller but geographically distinct ranges called the Ibex and Saddle Peak Hills. Other significant ranges include the Dublin Hills, Greenwater, Nopah, and Resting Spring Ranges to the east, and the Sperry Hills, Kingston Range, and Silurian Hills to the southeast. Figure 2 shows these local ranges labeled on a satellite image.

The Amargosa Chaos assemblage is located in the southern Black Mountains, with portions possibly extend to the Kingston Range. The section of Chaos focused on in this study, occupies the area between Ashford Canyon and Jubilee Wash and is one of the type sections described by Noble (1941). The map area is approximately 150 km^2 and contains many unique canyons, peaks, passes, and washes that are used in this manuscript to describe locations of geologic structures. Many of these features were named by geologists, prospectors, and explorers. The features in quotations, labeled in Figure 3, were originally and spontaneously named during the field work for this study.

Tectonic Reference Frame

The western margin of North America has a complex tectonic history; much of this history is recorded in the rock record of the Death Valley region. Figure 4 (sources in Appendix A) illustrates the following broad introduction to western United States tectonics, which is focused on the interaction between the structures accommodating active deformation and the inherited structures over which they developed.

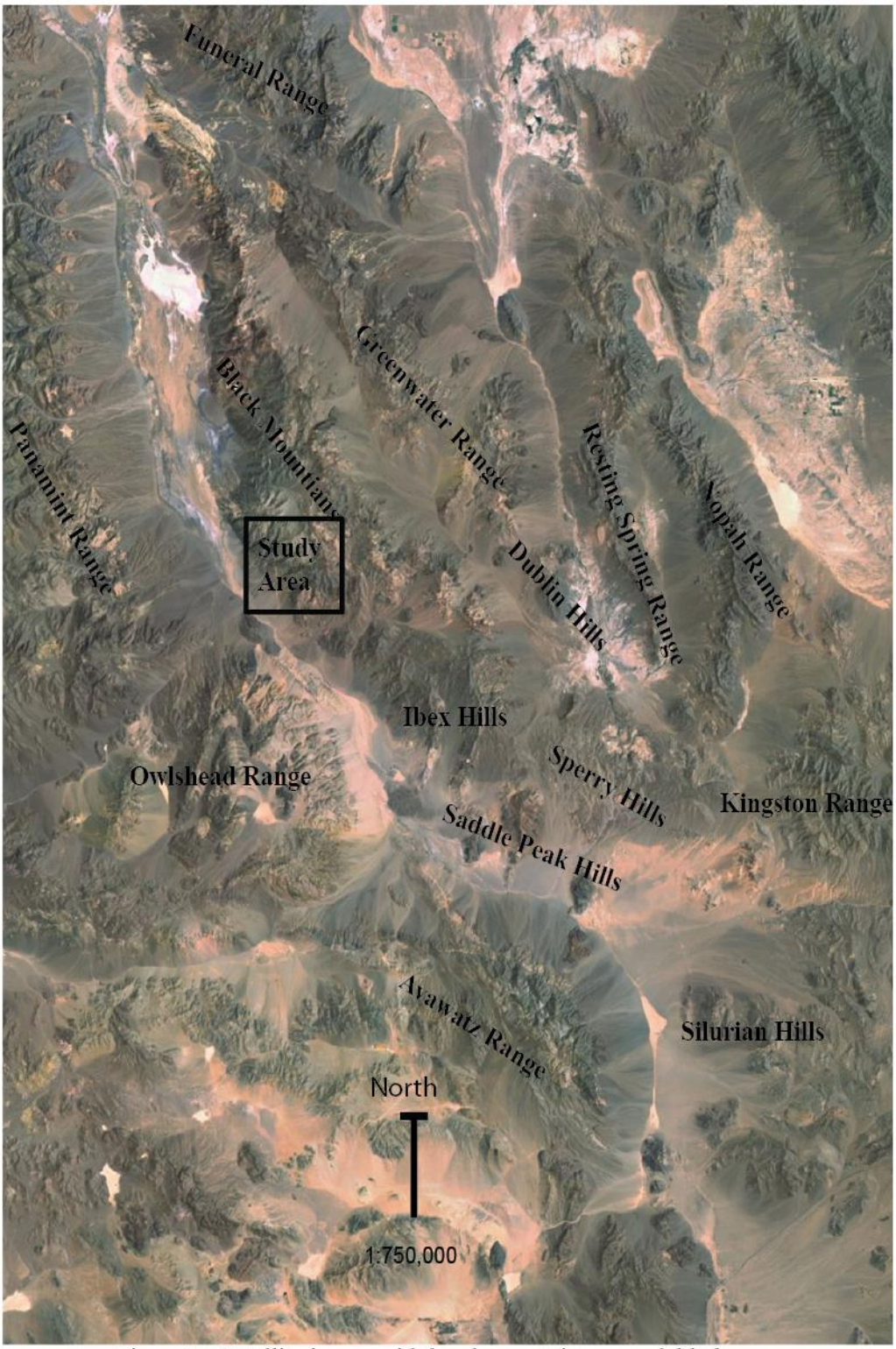

Figure 2: Satellite image with local mountain ranges labled.

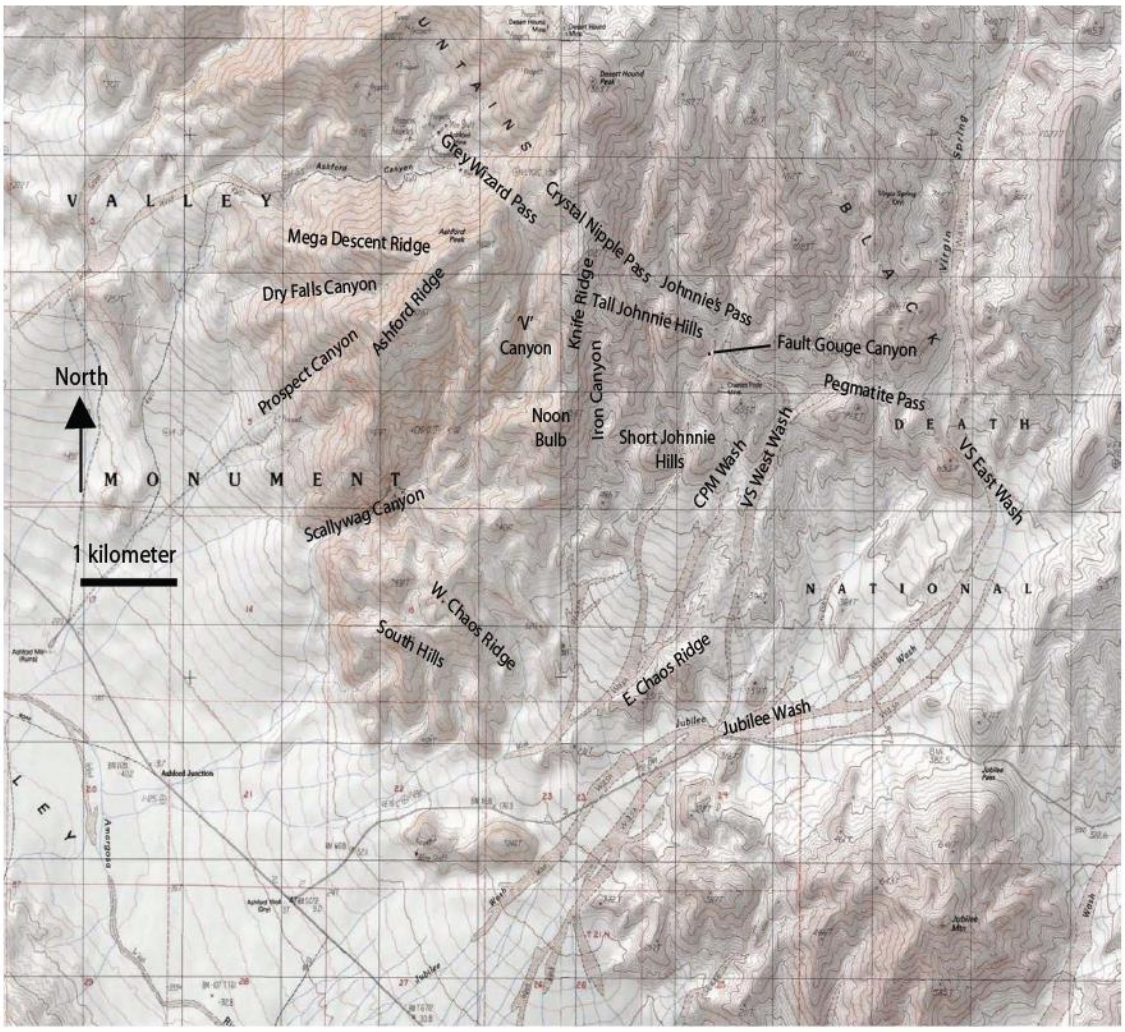

Figure 3: Spontaneously named local topographic features. In the text: these features are used to describe locations of geologic structures or stratigraphic sections are contained in 'single quotation marks' to distinguish them from formally named features.

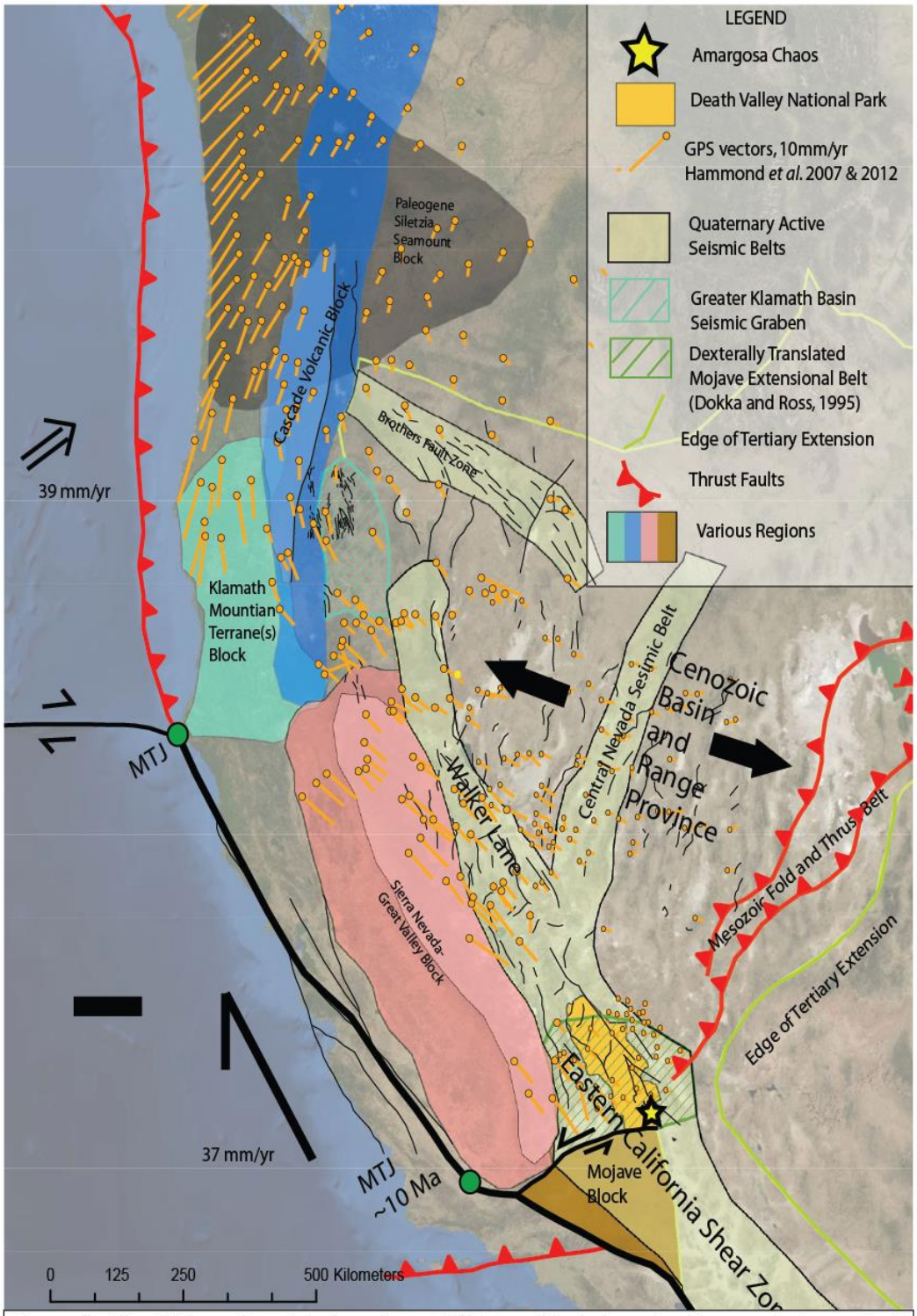

Figure 4: The diffuse microplate boundary of Western North America. Sources in Appendix A

Tectonic Regime Shift

The tectonic history of western North American is one of shifting stress regimes. During the course of the last 60 Ma, the region transitioned from a compressionally-supported mountainous plateau, through a great gravitationally-induced extensional collapse, to a right-laterally deformed, captured-microplate margin. Hypotheses regarding the geodynmaics are ever-evolving. Examples of current hypotheses include abandoned slabs (Schmidt and Humphreys, 2011), whole lithosphere deformation (Flesch and Bendick, 2012), and regional megadetachements (Wernicke, 2008). Figures from these articles are shown in Figure 5 and illustrate the diversity of thought on the tectonic evolution of western North America.

In context to this regime shift, the study area lies in a crucial region. It has been affected by the mid- to upper-crustal organization accommodating the shift. The Keystone Thrust, ~100 km east, records Mesozoic shortening. The region has a record of some of the earliest extension of the Basin and Range Province related to the Mojave Extensional Belt about 30 Ma (Dokka and Ross, 1995). The Eastern California Shear Zone, or ECSZ, overprints the region with active structures. The Basin and Range has accommodated up to 1000% extension of western North America (Snow and Wernicke, 2000), while the ECSZ is now accommodating 15-20% of shear movement between North America and the Pacific Plate. Faulds *et al.* (2005) hypothesized the Walker Lane-ECSZ will become the future plate boundary.

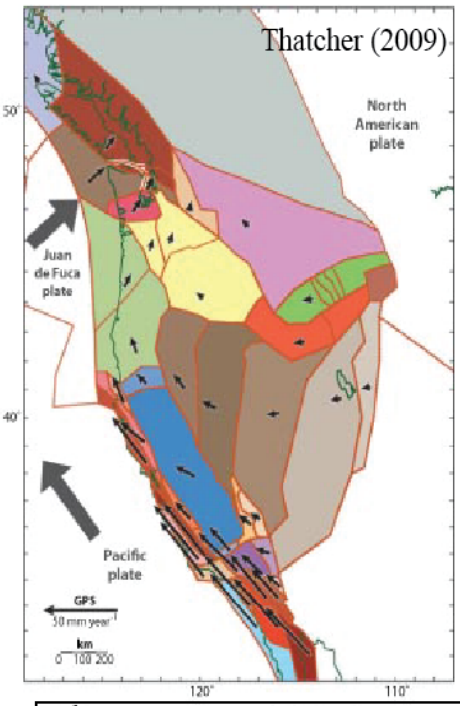

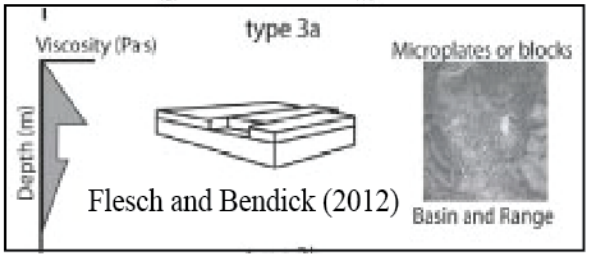

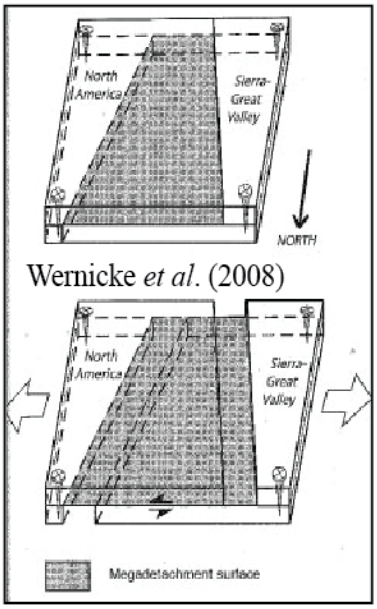

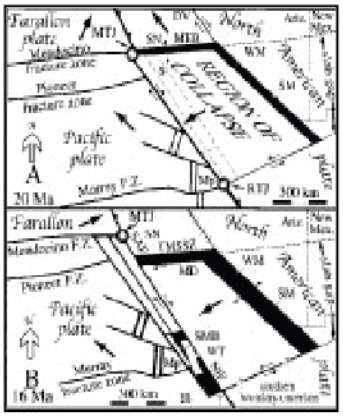

Dokka and Ross (1995)

Figure 5: Thatcher (2009) shows diffuse plate boundaries and microplate tectonics. Wernicke *et al*. (2008) shows the extent of the hypothesized megadetachment underlying the Basin and Range province. The block diagram illustrates the crustal lithosphere coupling of the Sierra Nevada block. Similarly, Flesch and Bendick (2012) developed this model for whole-lithosphere deformation as brittle crustal blocks over a less rigid (or missing) mantle lithosphere. Locally, Dokka and Ross (1995) discussed a slab window that enabled crustal collapse of the Mojave Extensional Basin starting ~30Ma.

More locally, the Kingston Detachment of 13.4-12.4 Ma records Basin and Range extension (Fowler and Calzia, 1999). The right-lateral Furnace Creek Fault Zone records the 14 Ma beginning of the shear-dominated regime (Wright *et* al., 1999).The relationship between the Grandview Fault and the Northern Death Valley Fault Zone remains unclear (Wright *et* al., 1999).

Literature Review

The geologic literature regarding the Death Valley area is vast and ever expanding. This literature review focuses on the key publications that pertain to the Amargosa Chaos.

Early Research

The early research recognized the diversity of rock formations and deformation structures. Much of the research was particularly focused on the development of the basement rock anomalies known as the "turtlebacks" (Curry, 1938). Rock formations of Death Valley, California by Noble (1934) offered first attempt to understand the relative ages and stratigraphic relations of the region's rocks. The term "chaos" was first introduced into the geologic literature by Noble (1941) with the type section as the Amargosa Chaos of Southern Death Valley. Noble described the Amargosa Chaos assemblage using five criteria:

(1) The arrangement of blocks is confused and disordered—chaotic,

(2) The blocks are vastly larger . . . than . . . a breccia,

(3) The blocks are tightly packed . . . not separated by finer grained material,

(4) Each block is . . . a fault block

(5) Each block is minutely fractured throughout, yet the original bedding in each

block of sedimentary rock is clearly discernible

(Noble, 1941, pp. 964)

Noble observed that these blocks and slices were in fault contact with the underlying metamorphic basement and he defined the contact as the Amargosa Fault. He described three phases of the Amargosa Chaos, which were designated by dominant lithology and relative age of the rocks, but not the relative age of the structures. The Virgin Spring Phase, which is the focus of this study, is the most structurally complex phase and consists of Neoproterozoic-Cambrian age sedimentary rocks. Overlying the Virgin Spring Phase is the Calico Phase, composed primarily of Cenozoic volcanic rocks. Also overlying the Virgin Spring Phase, but never in contact with the Calico Phase, is the Jubilee Phase. The Jubilee Phase consists of Cenozoic mass-wasting deposits, rock avalanche deposits, and alluvial fan deposits.

The Amargosa Chaos formation was originally interpreted as a sort of mega-tectonic breccia that formed above a major thrust fault, which Noble termed the "Amargosa Thrust". "Some of the blocks moved under much heavier load than others," indicating the three phases may or may not have formed contemporaneously above the Amargosa Fault (Noble, 1941).

Three prominent basement-composed antiformal features in the Virgin Spring area were mapped by Noble (1941). He correlated them to the turtleback antiforms at the Black Mountain front. He named these folds, the Graham, Rhodes, and Desert Hound Anticlines, from north to south respectively, and interpreted them to have formed after the "Amargosa Thrust" because the trace of the fault outlines the folds.

The Death Valley turtleback surfaces were first described by Curry (1938) as are

convex upward and have smooth topographic surfaces that resemble the carapace of a turtle, and were then later interpreted, by Curry (1954), as fault surfaces. Curry (1954) concluded, as Noble (1941) previously did, the Mormon Point turtleback and the Desert Hound Anticline are a continuous feature comprising a doubly plunging anticline. Both authors conclude the turtleback surfaces are the underlying remnants of a major fault. Drewes (1959) offered a reinterpretation of the turtleback surfaces, suggesting they are normal fault surfaces that are younger than the "thrust fault." He elaborated "[the] turtleback surfaces are not surfaces that were folded after movement on the turtleback faults but are the exhumed surfaces of resistant layers in folds of Precambrian age."

Sears (1953) offered a reinterpretation of the origin of the Amargosa Chaos. He noted the unique geometric relationship between the basement folds and the overlying Chaos and the lack of evidence of greater compressive forces that could have formed the Amargosa "Thrust." Sears (1953) offered a hypothesis in which the folding event that created the Desert Hound anticline was also responsible for the formation of the Virgin Spring and Calico phases of the Amargosa Chaos. The hypothesis essentially suggests the Chaos formed *in situ* as a result of gravitationally induced normal faulting as the basement rose into a great anticline.

Noble and Wright (1954) adopted parts of the Sears (1953) hypothesis in their explanation of the Amargosa Fault as being "produced by the squeezing and arching of the Black Mountain wedge under intense compression". They also hypothesized the origin of the Jubilee phase as debris-flow accumulations.

1950's to 1980's

During this period, perceptions regarding the evolution of the Basin and Range province were changing. This paradigm shift occurred locally as the Amargosa Fault was recognized as a normal fault rather than a thrust fault.

In 1954, Special Report 170 was published by the California Division of Mines and Geology. The publication brought together the work of many of the area's researchers. Noble and Wright (1954) discussed the geology of central and southern Death Valley. Wright and Troxel (1954) presented a field trip guide through this area of the Mojave Desert. Hunt and Mabey (1966) released an updated stratigraphic and structural review of the general geology of Death Valley. This publication, along with the works of Wright (1968), remains the basis for any comprehensive study of the region's stratigraphy. Hunt and Mabey (1966) pointed out the observed sense of slip of the Amargosa Fault as normal displacement (pg. A99). Wright and Troxel (1969) were the first to suggest the Amargosa Chaos actually formed in the footwall of a Basin and Range style normal fault. They referred to the "Amargosa Thrust" as an "illusion."

Fleck (1970) expanded on the concept and stated the "formation of the chaos by a mechanism of over-thrust faulting is . . . highly improbable." He concluded that the Chaos may represent individual fault blocks telescoped and broken during movement down planes that flatten at depth. This interpretation reflects elements of Noble's original description. Fleck (1970) compiled ages from volcanic rocks from within the Calico Phase of the Chaos. The data reveal the Calico Phase of the Amargosa Chaos formed since 6 Ma.

Two other geologic assemblages have been described using the term chaos. Kupfer (1960) mapped a chaotic assemblage in the Silurian Hills he called the Riggs Chaos, which is ~50 km south of the study area. The description of the Riggs Chaos closely resembles that of the Virgin Spring Phase of the Amargosa Chaos and it is composed of the same rocks. However, the Riggs Chaos differs because it lies in the footwall of its bounding fault, rather than in the hangingwall. Another chaotic province in west-central Nevada, the Mineral Ridge Chaos, was described by Kirsch (1971). However, review of both of these localities suggests the assemblages did not form by the same processes as that of the Amargosa Chaos.

Anderson (1971) described the process of thin-skinned tectonics in the Basin and Range explicitly, but the concept was pre-dated by Hill and Troxel (1966) and Burchfiel and Stewart (1966) who identified the pull-apart nature of Death Valley tectonics (Figure 6). Stewart (1983) introduced a hypothesis that involved the transport of the Panamint Range 80 km to the northwest on a low-angle detachment fault, which unroofed the Black Mountains (Figure 6). This hypothesis provided an explanation for the previous discrepancies in the literature, including the vastly different offsets of the Death Valley-Furnace Creek Fault zone and the Southern Death Valley Fault zone. The hypothesis necessitates the Amargosa Fault as the major detachment surface responsible for most, or all, of this 80 km offset.

Wright and Troxel conducted many studies on the stratigraphic and structure of the Death Valley area (Wright *et al.*, 1976; Wright and Troxel, 1974). Many student theses and dissertations, journal and special articles, and maps pertaining to Death Valley were published under their guidance and benefited from their expertise in the area. They

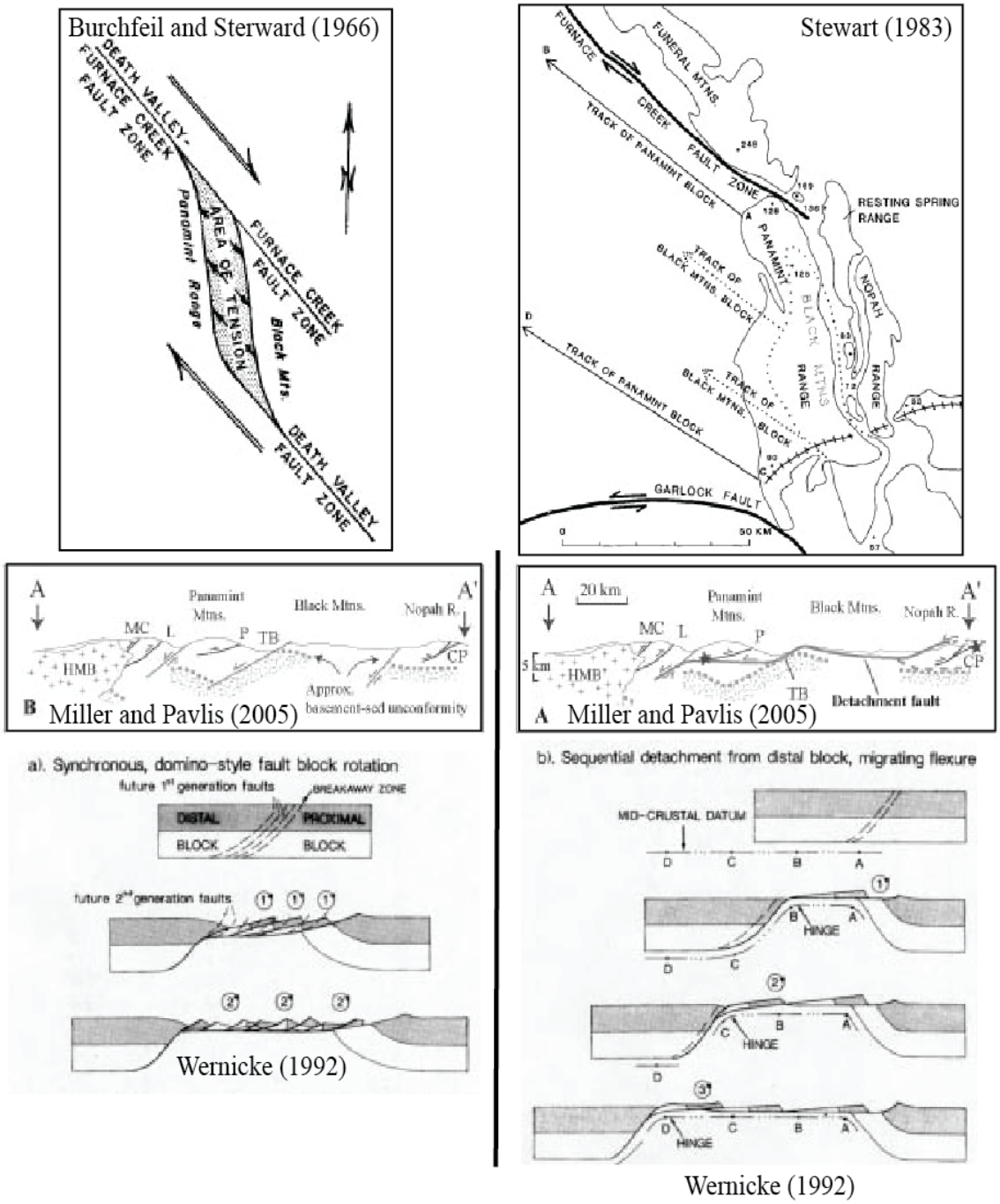

Figure 6: The upper left figure shows the 'Pull-Apart' model of DV extension. From this model, Stewart (1983) proposed the Panamint Range was transported 80 km NW. Below, the two dominant models for accommodating extension are presented. On the left is shown two conceptions of the 'distributed faulting' model, with the 'Rolling-Hinge' model on the right.

released a map of the Amargosa Chaos and an accompanying text that describes their observations and interpretations (Wright and Troxel, 1984). Wright and Troxel recognized three broad deformation events, beginning with the metamorphism of the basement, followed by a rift basin formed that collected Precambrian-Cambrian sediments. Lastly, Cenozoic extension created the Amargosa Chaos. Their observations and interpretations can be paraphrased in the following three points: 1) discrepancies of rock mechanics between the sedimentary rocks and crystalline basement gave rise to the appearance of a single Tertiary structure, 2) involving a range of processes from normal faulting, erosion, basinal sedimentation, and volcanism; the Chaos formed over many intervals of time, 3) the Chaos is composed of a variety of conjugate structures that contribute to the disordered appearance because of the east-west directed extensional stress of the southern Great Basin.

Regionally, Wernicke *et al*. (1988) concluded that the Death Valley region extended up to 500% by correlating a thrust systems exposed in the Nopah Range, the Chicago Pass Thrust) to those in the Panamint Range, the Last Chance Thrust. They suggested the "Death Valley System" accommodated the extension and implied the Amargosa Fault was the primary fault of the system.

Research after 1990

The regional tectonic picture had been generally defined during the previous 30 years of research. During the 1990s, the investigations became focused testing the tectonic hypotheses and deriving more specific evidence.

Holm and Wernicke (1990) discussed their conclusion on the evolving crustal structure of the Black Mountains. Afterwards, Miller (1991) showed multiple discrete,

but not contemporaneous, faults that accommodated movement at the Badwater Turtleback. The concluding evidence of Miller (1991), that the Black Mountain turtlebacks are record of multiple faults, supported a "distributed-faulting" model (Wright and Troxel, 1973) to describe Death Valley extension. Wernicke (1992) devised a model involving a "rolling hinge." In this model, the detachment surface was uplifted while the crystalline basement was unroofed (Figure 6). Holm *et al.* (1992) and Holm and Dokka (1993) presented thermochronology that documented the complex unroofing history of the Black Mountains. Keener *et al*. (1993) mapped complex relationships between the discrete faults responsible for the uplift. Topping (1993) studied the stratigraphic remnants the unroofing history, the Jubilee and Funeral Formations. The results show evidence for a preexisting basin. He termed this basin the Greater Amargosa-Buckwheat-Sperry wash (GABS) basin, based on the geographic distribution of the formation. Friedmann and Burbank (1995), interpreted the basin in context of modern Death Valley: 1) the rift-like basin of modern Death Valley, 2) superposed across a supradetachment-like basin or GABS Basin, and 3) which is in turn being superposed upon by the Walker Lane-ECSZ dextral systems.

Mancktelow and Pavlis (1994) compared the accommodation structures of the Death Valley system to those on the Simplon Fault Zone in Switzerland. They concluded that broad folding accommodated the transpression that formed perpendicular to the direction of transport. The transpression is manifested as folds that plunge opposite the extension direction. Similarly, Holm *et al*. (1994) reinterpreted the turtleback surfaces as Miocene-Pliocene folds. Mancktelow and Pavlis, (1994) and Holm *et al.*, (1994) made

the pivotal connection between the extensional system and the associated transpression structures.

A study on the geometry and kinematics of the Amargosa fault was conducted by Rogers (2000). The results suggested a separate formation for the Chaos on either side of Desert Hound Peak. Topping (2003) compared the distribution of the GABS basin to the known major Death Valley faults. The comparison resulted in a regional model that represents a distributed-faulting mechanism of transport. He included the Amargosa Fault as a minor component. Miller and Pavlis (2005) (Figure 6) combined the reported thermochrology, the crustal structure of the Black Mountains, and the geometries of the turtlebacks, with measurements from distinct mylonite zones, observations of cross-cutting relationships, and kinematic indicators to conclude the turtleback structures are most compatible with a distributed faulting model of extension. Norton (2011) called on a "two-stage" formation of central Death Valley. The first stage started 15-18 Ma as an extensional system, then underwent a transition between 8-3 Ma at which time the second stage formed the modern pull-apart basin. Figure 7 is a collection of photos of many of the above mentioned Death Valley researchers.

Figure 7: As the literature review indicates, many researchers have worked in the Death Valley area. In the above photos are the sources of the published and unpublished maps from this study. (Clockwise, Top left) Noble and young Wright, possibly discussing collaboration. Troxel and Wright (RIP), probably after field work. Topping and myself, after finishing discussion on Jubilee Chaos. Hornsby, my data collecting partner, and Troxel, after discussing our new mapping. Miller, moments before seeing the Beck Fault in the field. The top photos are from the publication *Fifty Years of Death Valley Research*, edited by J.P. Calzia.

Purpose of the Study

This study aims to explain the structural geology of the Virgin Spring phase of the Amargosa Chaos that lies south of Desert Hound Peak. It addresses two main questions:

-Is there a greater order to the Chaos that is indicative of the processes that created it?

-What is the relationship of the Amargosa Fault to the Virgin Spring phase of the Amargosa Chaos?

Leads to the main questions from the existing literature

Noble (1941) referred to "[the] rude system in the arrangement of the large blocks in the chaos" and elaborated:

> The rude shingling, or imbricate structure, of the chaos, which is, very broadly, a piling up of tabular blocks that for the most part dip easterly, accounts in part for the progressive rise from older to younger rocks in the chaos from west to east.

(pp. 967)

That insightful description of the Chaos provided the best basis of understanding the structure while beginning this study.

Wright and Troxel (1984) illustrated the complex systems of faults that dissect the area. It is evident from their map that the structures did not all form contemporaneously because some faults clearly truncate others. The second question, regarding the relationship to the Amargosa Fault, can first be explained using their map.

Figure 8 shows two conceptual diagrams of the primary normal fault geometries seen in the area. The top shows domino blocks, which are the dominant fault type in the

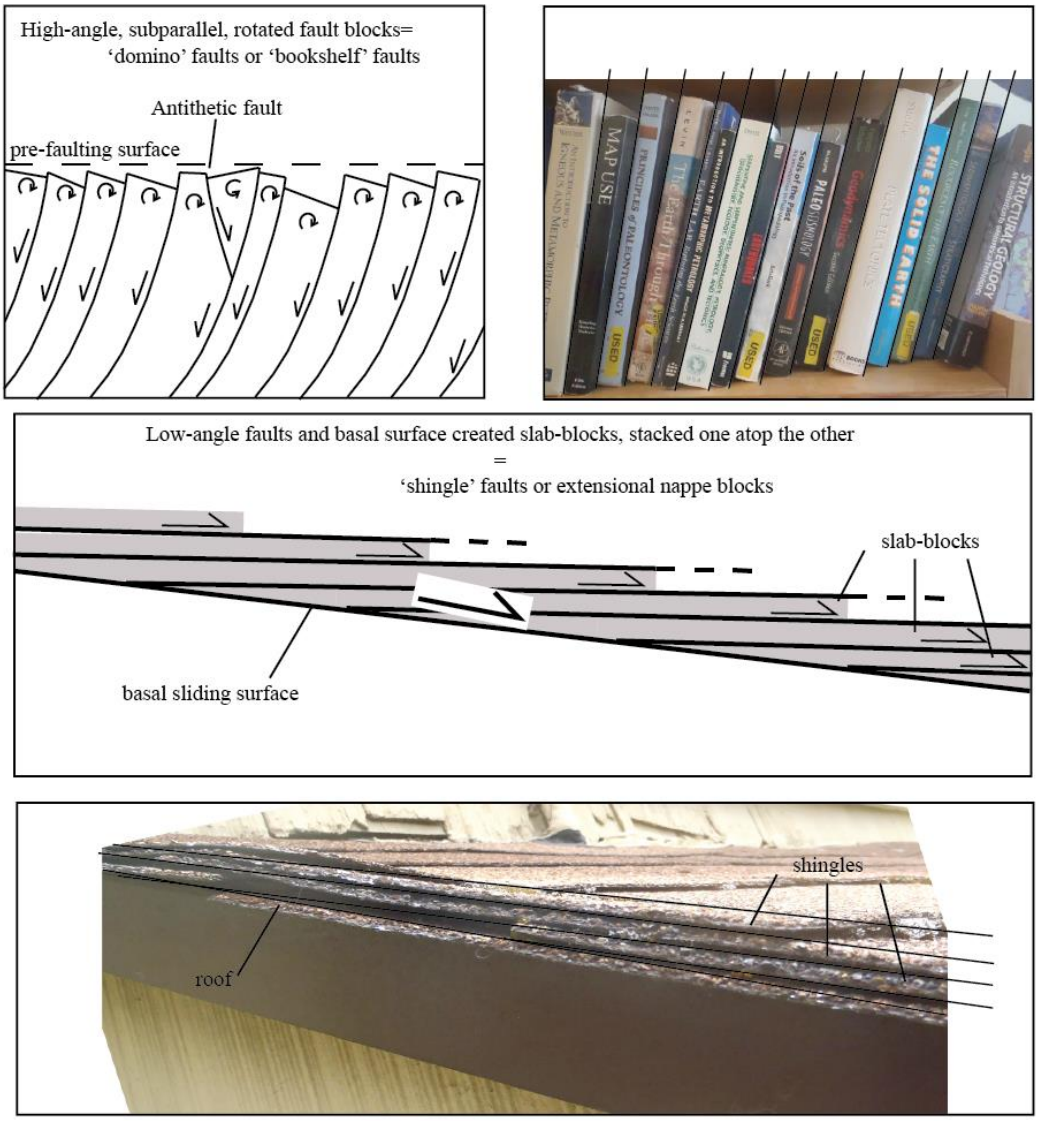

Figure 8: These simple diagrams and physical analogies are offered to define two types of normal faults. Above, domino faults are illustrated as sub-parallel and high angle faults, which dissect the crust into rotated fault blocks and do not accommodate much slip. These type of fault are sometimes referred to as 'bookshelf-style' faults because of the resemblance to leaning books on a shelf. 'Shingle-style' fault blocks (slabs) are the dominant feature of the Chaos. As illustrated below, this style is defined by the resemblance to shingles on a roof. The blocks have been referred to as 'extensional nappes'.

region (Wright and Troxel, 1974). The bottom figure shows a shingled pile of tabular blocks, with an analogy to shingles on a roof.

The Amargosa Fault has been described as the Amargosa Detachment and thought to be solely responsible for creating the overlying chaos (Wright *et al.*, 1974). However, as mapped in Wright and Troxel (1984) the basal unconformity of the Crystal Springs Formation occurs in both the hangingwall and footwall of the fault. Miller (2002) investigated this relationship and indicated no more than 15 km of offset occurred. The Chaos is in the hanging wall of the fault and is assumed to have formed over a long-lived, major fault zone. The offset suggested above does not require a long lived, major fault zone. In response to this conundrum, some researchers have hypothesized that the classically defined Amargosa Fault is more likely made up of several fault surfaces telescoped together along local structures (Rogers, 2000; Miller, 2002), probably normal faults.

The Amargosa Fault is not concisely defined. Instead, it is broadly defined as:

(1) generally as the fault contact between the Paleoproterozoic basement gneiss and the Neoproterozoic sedimentary Pahrump group (Noble, 1941)

(2) specifically as the low-angle fault seen on the west wall of 'V Canyon' (Wright and Troxel, 1984)

(3) locally as the zone of thick fault gouge between Highway 178 and 'Fault Gouge Canyon' (Rogers, 2000)

These three descriptions do not describe the same structure. A more clear definition of the Amargosa Fault is needed.

Generalized Stratigraphy

The rock formations in the study area were first described by in Noble (1934), but a more thorough description of the units can be found in Hunt and Mabey (1966). A concise description of the major rock units is given here, but Appendix B contains detailed descriptions from the field area and literature. A detailed stratigraphic section, modified from Mahon (2012), of the Mesoproterozoic-Cambrian sedimentary rocks unconformably above the paleoproterozoic gneiss is given in Figure 9. A simplified cartoon version of the stratigraphic section is shown in Figure 10. The cartoon version highlights the local section and is displayed in later figures to represent generalized stratigraphic relationships and thicknesses.

The regional basement rock, the World Beater Complex, is composed of numerous metamorphic rock types. There are three major lithologies in the field area: a biotite-quartz schist, a quartz-feldspar gneiss, and an augen gneiss. Unconformably atop the basement is the Pahrump (Super)group composed of three formations: the Crystal Springs Formation, the Beck Springs Dolomite, and the Kingston Peak Formation. The Noonday Dolomite and time-equivalent Ibex Formation rest disconformably above the Pahrump (Super)group. Continuing up section is the Johnnie Formation, which is separated from the Noonday/Ibex by a disconformity. The Sterling Quartzite and Wood Canyon Formation, respectively up section, are the uppermost Proterozoic-Paleozoic rocks exposed in the study area. A summary of the tectonostratigraphic development of the Mesoproterozoic-Cambrian section is described below.

The Virgin Spring Phase of the Amargosa Chaos is composed of the above described section and is overlain unconformably by the Jubilee Phase of the Chaos. The

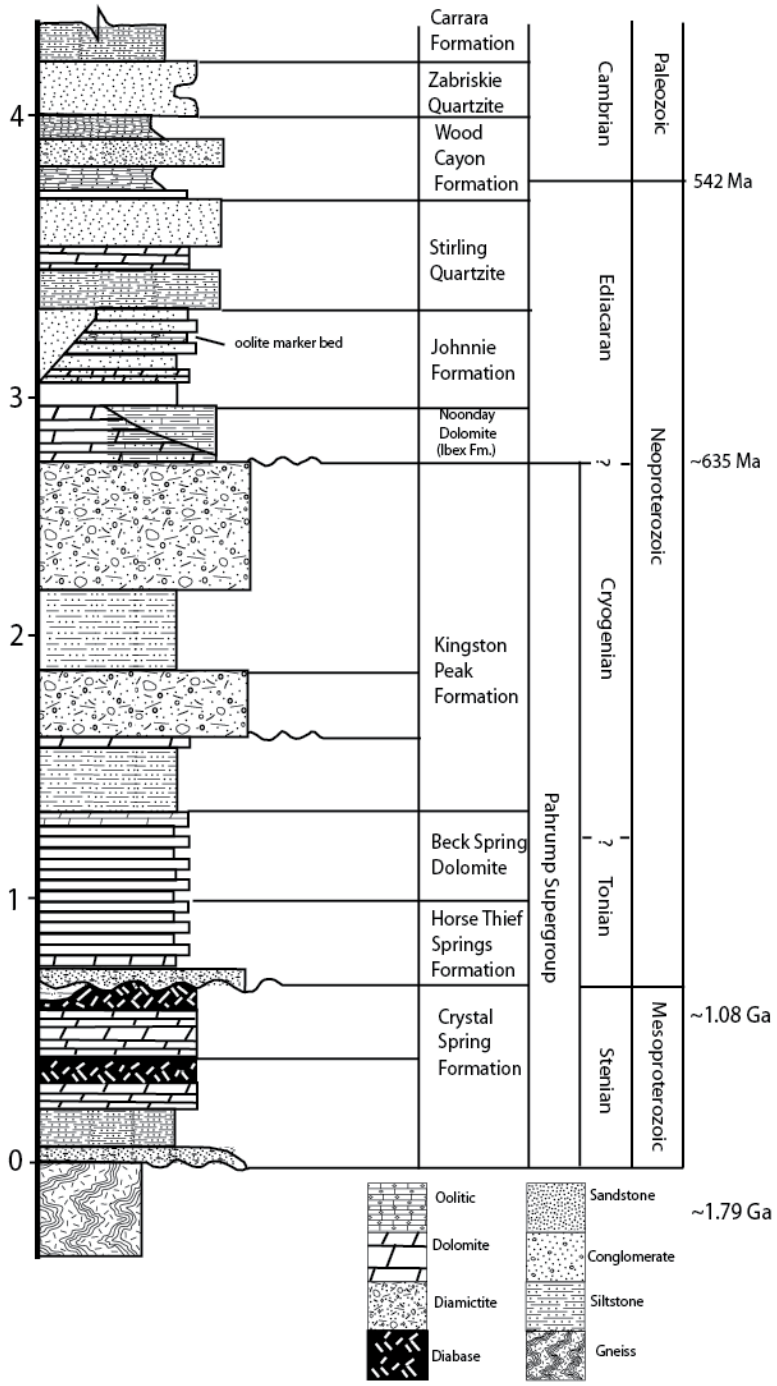

Figure 9: Generalized stratigraphic column modified after Mahon (2012), including suggested stratigraphic revisions therein.

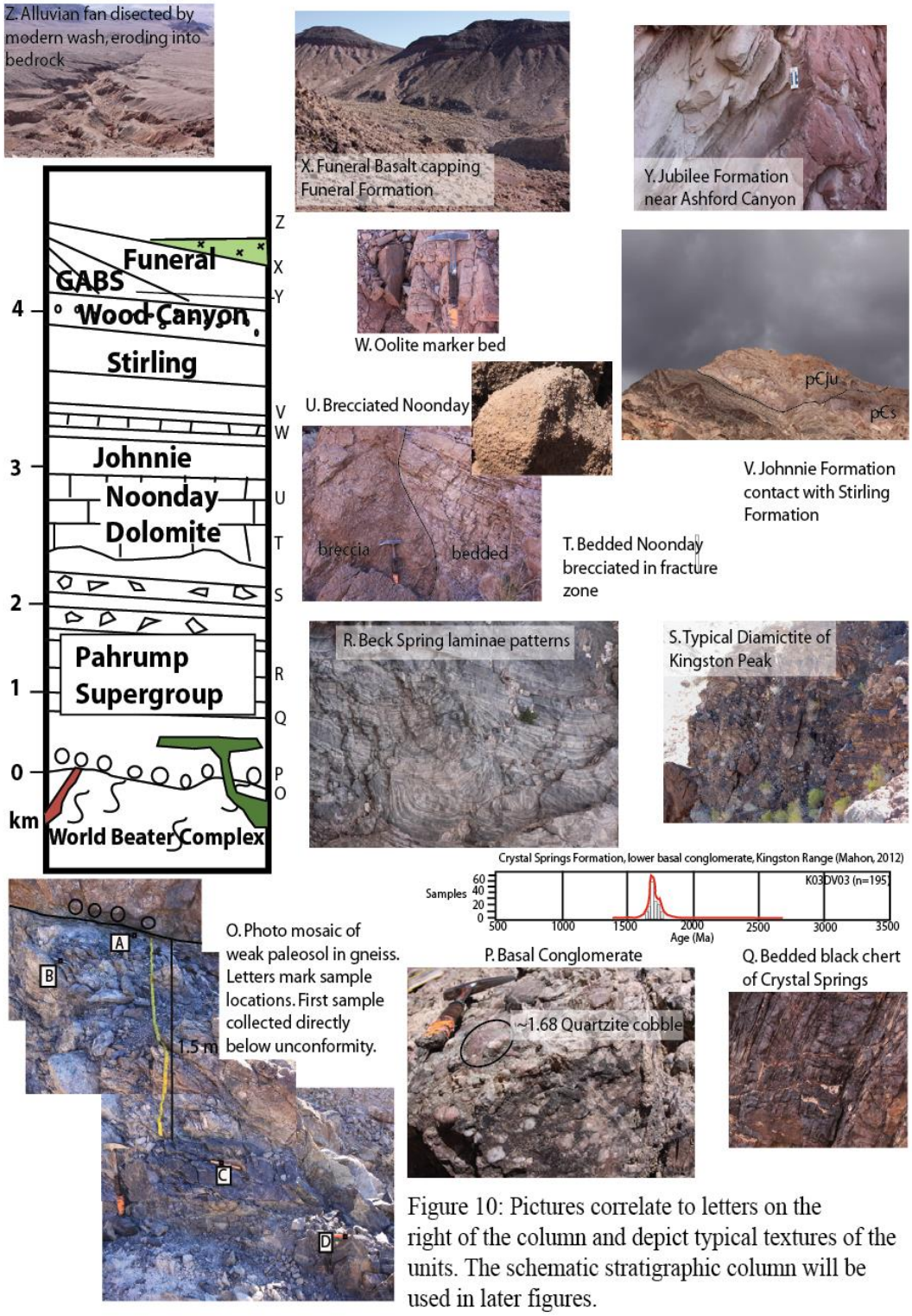

Figure 10: Pictures correlate to letters on the right of the column and depict typical textures of the units. The schematic stratigraphic column will be used in later figures.

Funeral Formation overlies both the Virgin Spring and Jubilee Chaos Formations and has a capping basalt flow. Quaternary formations developed on top of these.

Summary of Tectonostratigraphic Development

The late Mesoproterozoic to Cambrian section represent deposits on a craton-margin hinge zone that formed in response to the breakup of the Proterozoic supercontinent Rodinia (Fedo and Cooper, 2001). This sequence began with the deposition of the Pahrump group in the initial rift (Amargosa Aulocogen). This tectonostratigraphic development occurred in three phases (Fedo and Cooper, 2001). Phase I is represented by the latest Pahrump Group formation (Kingston Peak Formation) which records the formation and filling of syn-rift basins by locally derived materials. Phase II is represented by the Noonday through lower Wood Canyon formations that form a wedge-shaped sediment package consisting of local and distally derived materials. Phase III is then represented by the middle Wood Canyon member and younger Cambrian sedimentary rocks that on-lap the passive-margin and consist of terrestrially derived sediments. Figure 11, from Fedo and Cooper (2001), illustrates the tectonostratigraphic development.

Descriptions of Mineral Alterations

Iron-Oxide Mineralization Zone on 'Knife Ridge'

An iron-oxide rich mineralization fills faults and fractures in the upper plate of a major fault mapped on ‘Knife Ridge’, which is schematically shown in Figure 12. Green circles represent sample locations, labeled with the last three digits of the sample

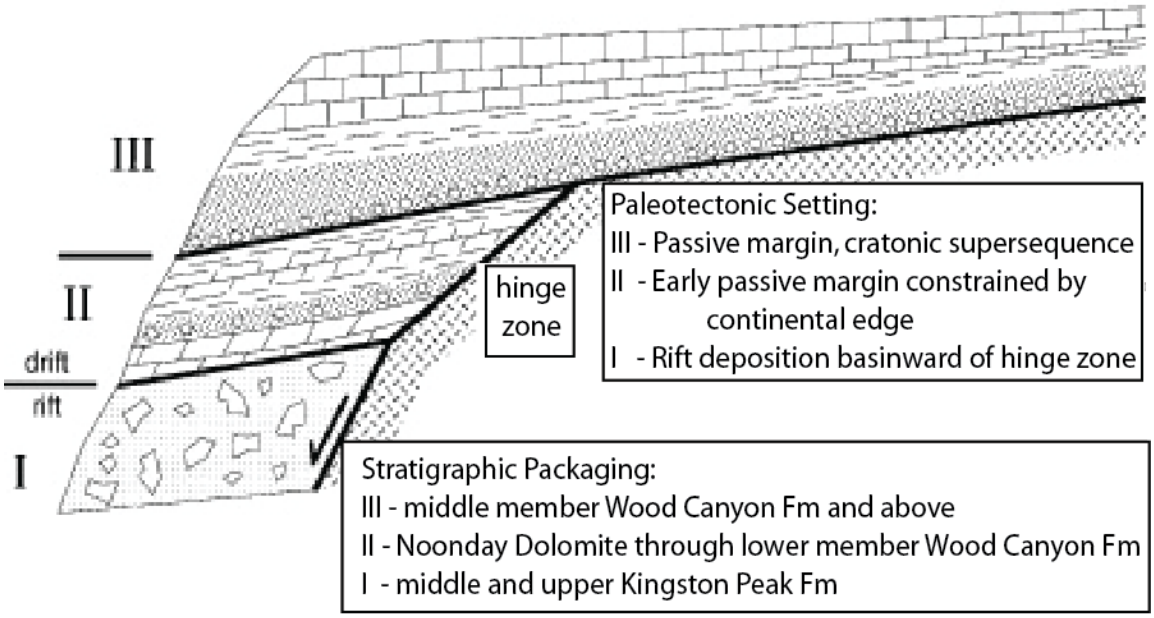

Figure 11: Modified from Fedo and Cooper (2001), this figure depicts their interpretation of the development of supersequence package stacking. First rifting occurs and fills (Phase I), then the early passive margin developed (Phase II), and lastly the passive margin matured (Phase III). Phase III is represeted by the middle Wood Canyon Formation onlapping the craton.

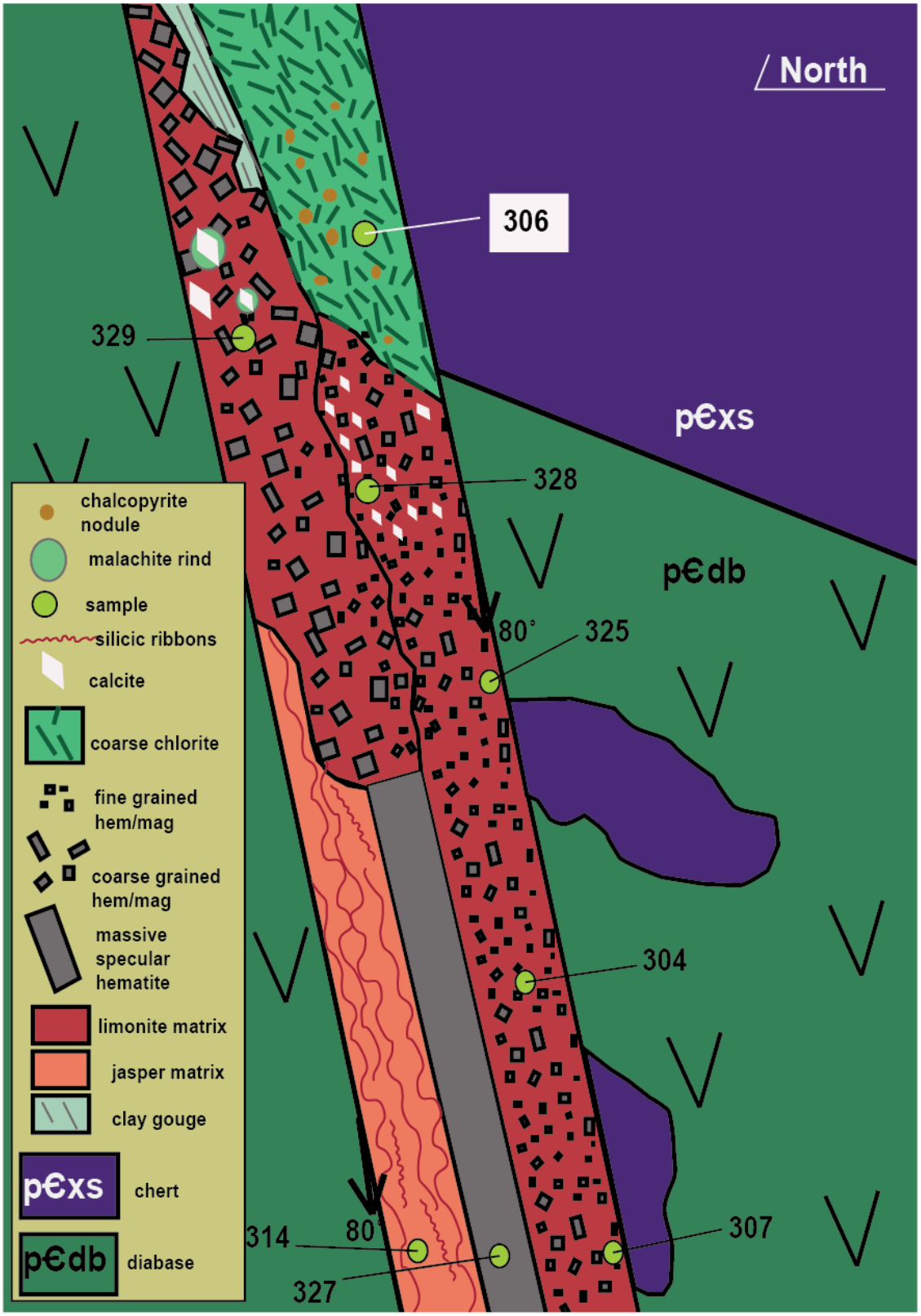

Figure 12: Schematic of field observations of iron-oxide mineralized zone.

number. The main fault dips 80º to the south-southwest but mineralized zones were observed distally from this main fault. The relationship remains unclear whether these distal mineralized zones are part of the same fault system, are cross-cutting faults through which the fluid also passed, or just fractures. Figure 13 is an increased scale excerpt from the main map that shows the mineralization zone pattern, outcrops, and prospect pits.

The mineralization has an upward gradation of mineralization. From the deepest to the highest levels the mineralization grades from fine-grained magnetite-hematite, massive specular hematite, coarse-grained hematite-magnetite-calcite, hematite-magnetite-calcite-chlorite-chalcopyrite. Figure 14 is a photo collage of the collected samples.

The upper end of the exposed section, in the northwest, contains the most economically significant mineralization. The deep adit, moderate spoil piles, and evidence of railing suggest this mineralization was once exploited. The mineralization at the adit consists of coarse, randomly arranged chlorite mixed with magnetite, calcite, and hematite where it contacts the diabase. Also within this zone are small 0.5-1mm of chalcopyrite. The nodules are surrounded by limonite that formed later by alteration from meteoric waters. Those waters mobilized copper and enabled malachite formation where they reacted with calcite. Malachite precipitated and surrounded the original calcite. Sample 329, shown in Figure 14, shows this relationship between calcite and malachite.

Based on these observations, I hypothesize a moderately acidic, iron-rich, sulfur-poor saline hydrothermal fluid passed through the fractures in this rock. When the fluid encountered the carbonate units of the Crystal Springs Formation, the pH increase

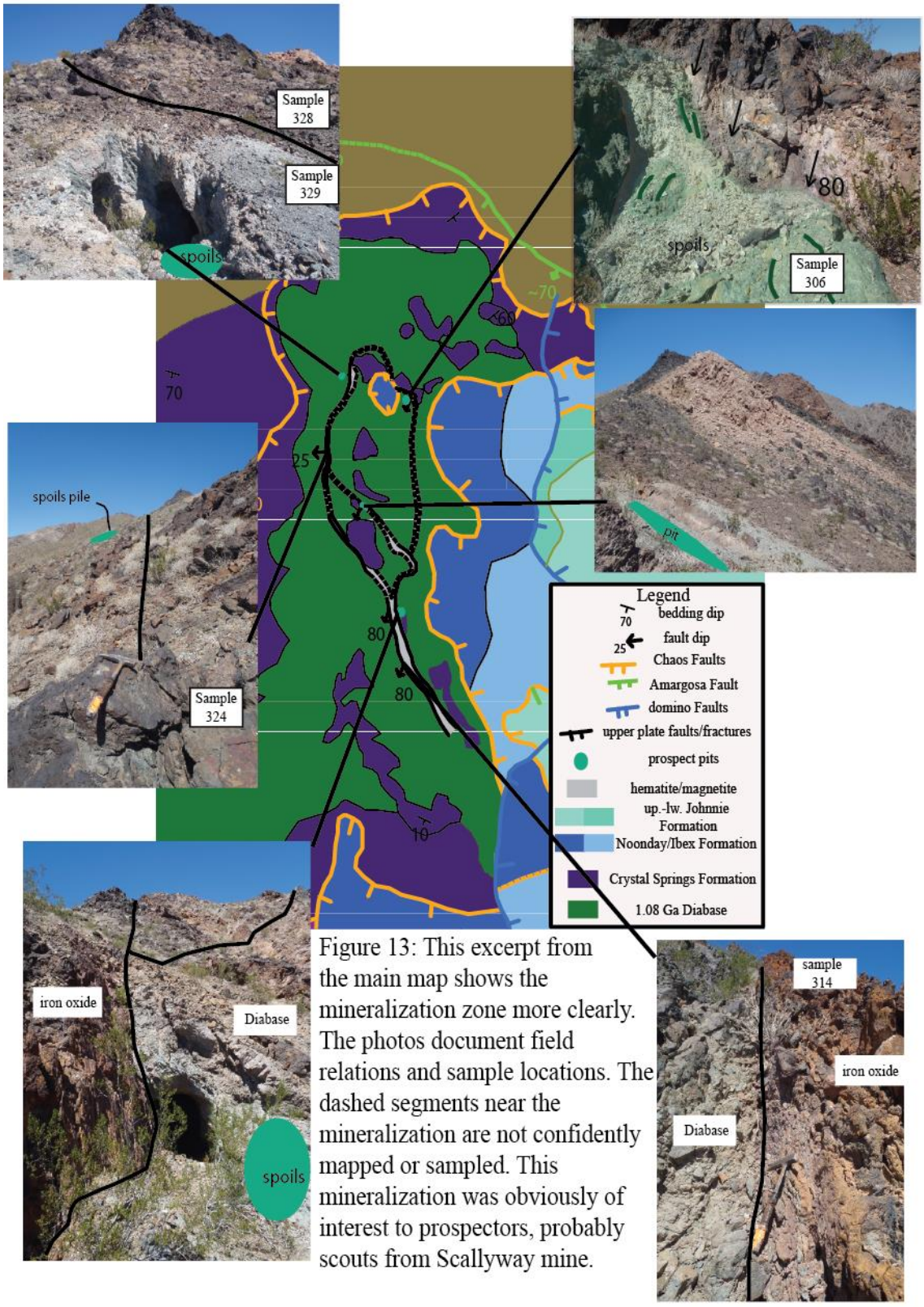

Figure 13: This excerpt from the main map shows the mineralization zone more clearly. The photos document field relations and sample locations. The dashed segments near the mineralization are not confidently mapped or sampled. This mineralization was obviously of interest to prospectors, probably scouts from Scallyway mine.

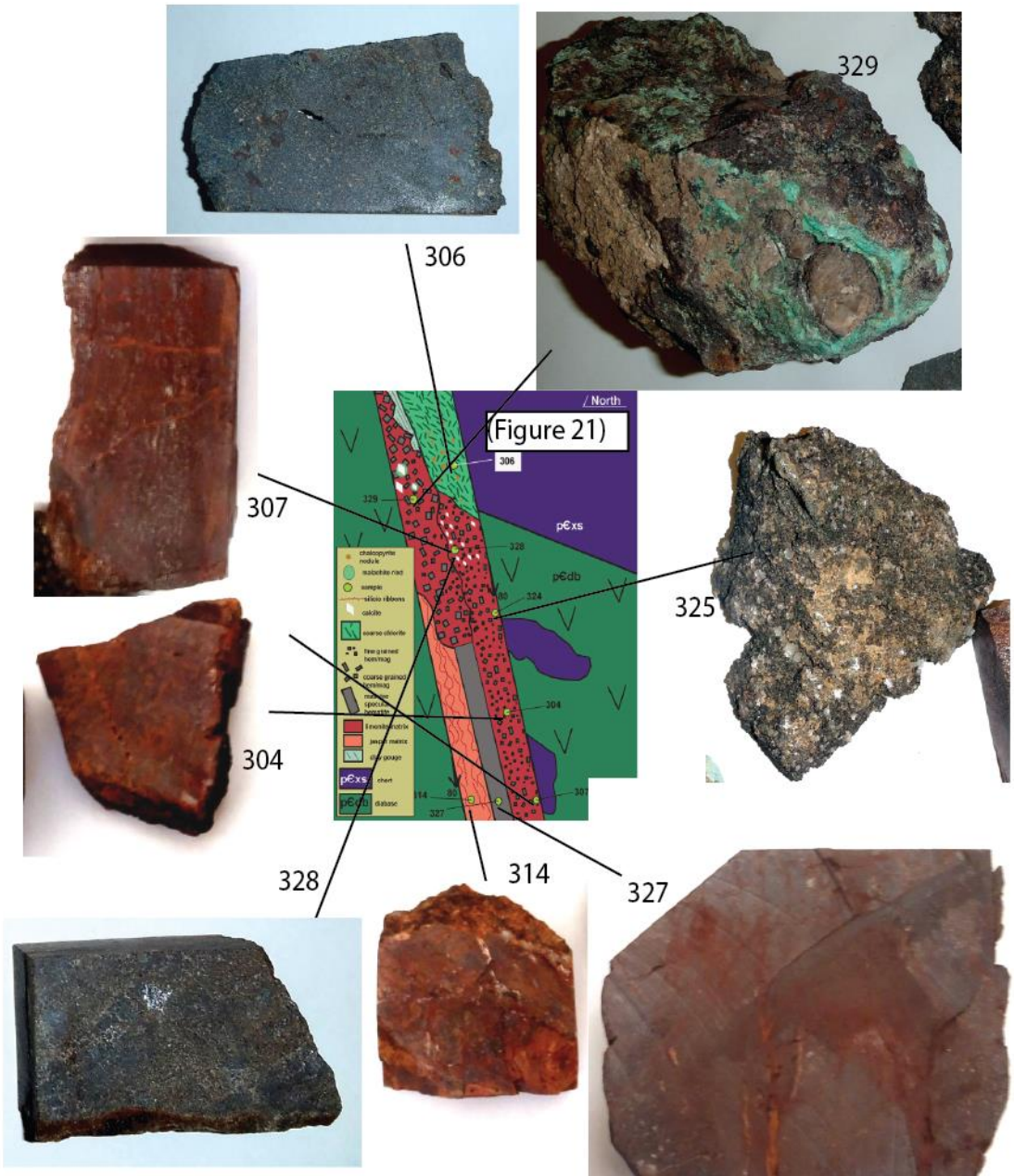

Figure 14: Photos of Samples. Counter-clockwise beginning from upper right: (329) calcite crystal with secondary malachite ring; (306) coarse-grained chlorite, fine-grained hematite, calcite, and chalcopyrite; (307) euhedral medium-grained hematite with jasperitic matrix and whispy calcite fabric; (304) euhedral coarse-grained hematite-magnetite in jasperitic matrix; (328) fine-grained hematite and calcite in fabric, some chlorite; (314) hematite-silica rich minerlized gouge, jasper, with broken peices of hematite and calcite veinlets; (327) massive specular hematite with veins of jasper filling fractures and exposed surfaces oxidizing; (325) coarse-grained hematite-magnetite-calcite cystals in an aplitic texture.

forced the iron to precipitate as iron-oxides (hematite and magnetite), while the available sulfur was consumed to create chalcopyrite. This mineralization and fluid occurrence is one way to generate an Iron-Oxide-Copper-Gold (IOCG) deposit. To test this hypothesis, I have analyzed selected zones of the mineralization for trace elements that would be indicative of such a system.

Hematite-Galena Alteration near Scallywag mine

In 'Scallywag Canyon', near the Scallywag mine, there are many cobbles and boulders of iron oxides, in some ways similar to those described above. Notably different, the rock type surrounding the alteration zones, where preserved in the clasts, is dolomite of the both the Beck Spring and Noonday Dolomite instead of black chert. The veins also contain galena, which is not seen in the other alteration zone. The Scallywag mine was a lead-zinc-silver mining operation, as described by Lingenfelter (1988).

Talc

The talc deposits of this region are best documented and described by Wright (1968), which is a special publication dedicated to the subject. In general, talc-tremolite schist occurs as a silicification deposit at the contact of the dolomitic members of the Crystal Spring Formation and the 1.08 Ga diabase (Figure 15). Veins of pure tremolite exist locally in the deposits. Though much larger deposits from outside the study area were commercially mined, the local deposits are small and impure, and not heavily exploited. The deposits are stark white, especially where prospecting or mining occurred. The white color is a vibrant contrast to the surrounding diabase, which makes the deposits easy to sight and map from a distance.

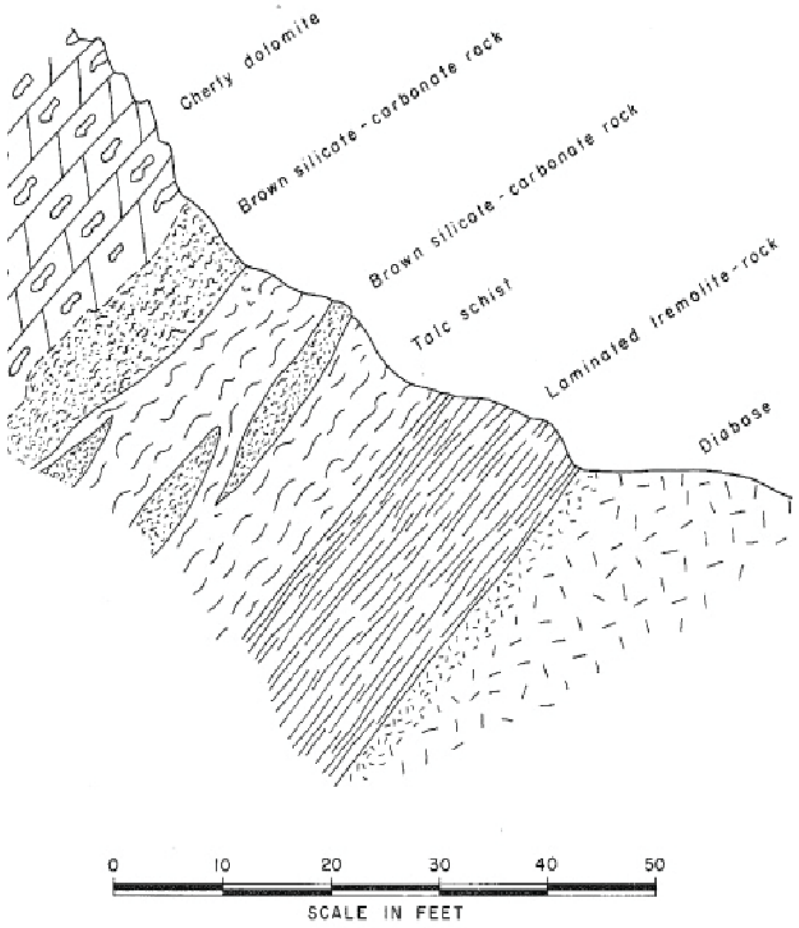

Figure 15: This diagram is from Wright (1968). The publication was written to describe the details of each occurrence and commercial talc mine in the Death Valley region. As Wright described in the text, the alteration is usually stratigraphically above the diabase and below the upper carbonate rocks of the Crystal Springs Formation.
The alteration is a talc-tremolite schist.

CHAPTER II

DATA COLLECTION METHODS

This investigation included three primary data collection methods: geologic mapping and analysis of previous maps, spatial analysis using ArcGIS, and stereonet analysis. Three other methods were used to a minor degree: geochemistry, rock mechanics, and trigonometry.

Geologic Map Analysis

'Geologic map and section of the north ½' Confidence Hills quadrangle, Inyo County, California' Wright and Troxel (1984)

As described in the literature section, Wright and Troxel (1984) provided valuable geologic understanding of the Amargosa Chaos formation after Noble (1941). In this study, Wright and Troxel (1984) served as an invaluable field aid for learning the local variations of stratigraphic units and individual members. In the office, it provided reference for the structural patterns and cross-cutting populations of faults. Mapped bedding orientations of the sedimentary rocks were used qualitatively to detect and support orientation of the Chaos Syncline. Basement foliation measurements were quantitatively used to derive the orientation of the Desert Hound Anticline.

I have grouped the faults on this map into five overlapping domains based on orientations and relationships, shown in Figure 16: 1) a discontinuous set of low-angle faults dipping under “Ashford Ridge” (orange); 2) a set of high-angle north-south oriented faults throughout (blue); 3) a set of N70ºW high-angle faults in the 'South Hills' (pink), which appear to cross-cut 1) and 2). 4) Many “scoop-shaped, gravity-slide” faults

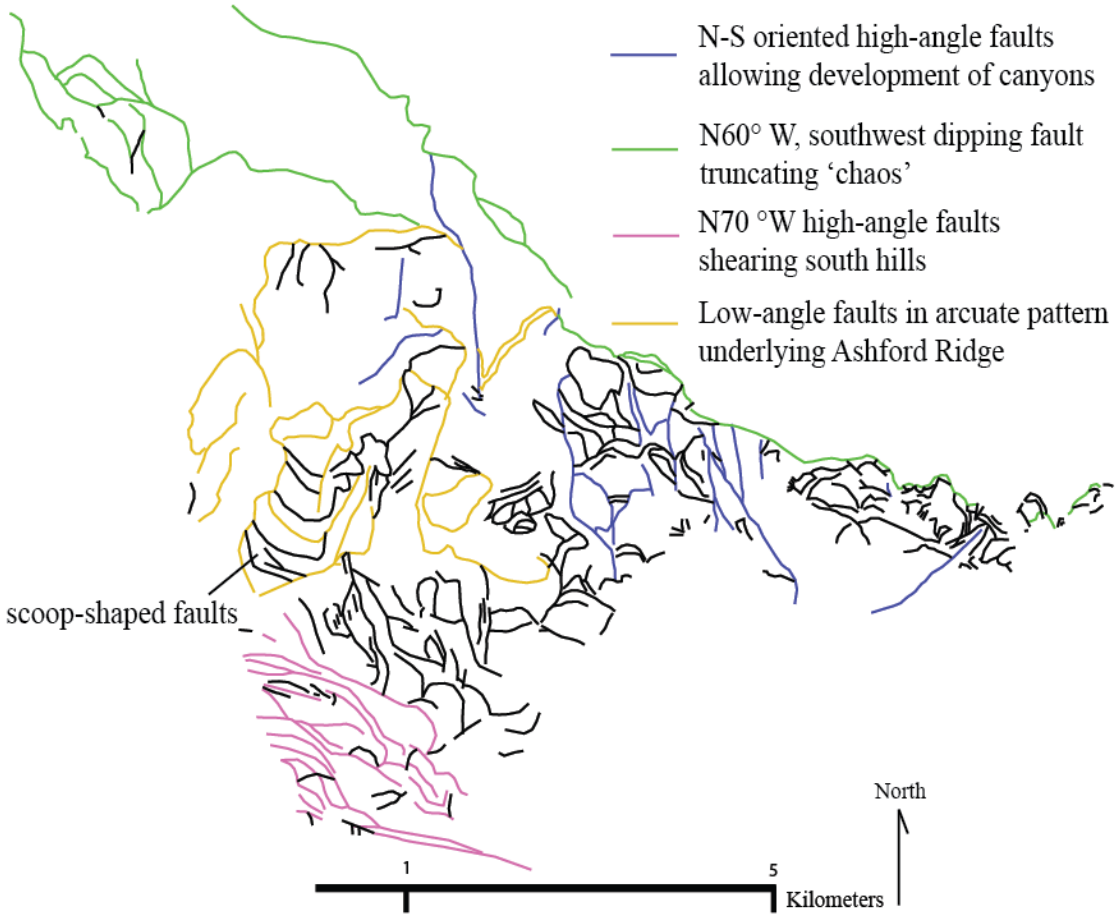

Figure 16: Line drawing of all Wright and Troxel (1984) faults. Emerging patters of strikes and cross cutting relationships are color coordinated. Four domains are recognized, though other populations occur.

(Troxel, personal communication) are mapped on the steep slopes (not colored).

5) Lastly, the prominent N60ºW oriented fault that borders the north side of the Chaos (green). These five domains account for ~75% of the faults mapped by Wright and Troxel (1984). Personally communicated by Troxel, the mapping pair depended heavily on aerial photographs to map the area surrounding Ashford Peak.

*Topping figures (*Topping, 1994; 2003*)*

Topping's published studies on the origin of the Jubilee Chaos and Funeral Formation assisted in placing the map area into a regional structural and stratigraphic reference frame. Figures from Topping (2003) were georeferenced, digitized, and modified for use in the final map and regional tectonic figures.

Unpublished geologic maps (Miller, Wright and Troxel, and Topping)

All unpublished data were acquired in the beginning stages of research for this project in 2011. Unpublished field maps from Wright and Troxel were obtained, at Troxels suggestion, from the Death Valley National Park Library where they can be viewed upon request. Copies of Topping's original field maps were acquired during the field season 2011. Some maps were digitized, georeferenced, and used for guidance while mapping the Jubilee and Funeral Formations. Unpublished fault mapping by Miller, the primary advisor of this study, depicts a complex geometry between the basal unconformity and the supposed Amargosa Fault. If a N60ºW directed slip on the fault is imposed, the relationship constrains the fault slip to <15 km (Miller, 2002). Miller suggested this relationship be explored and further investigation pursued (personal communication).

Field mapping for this study (Castonguay, Hornsby, and Miller)

A total of four expeditions for this project occurred between December 2010 and March 2013. I used forty-eight total days of data collection, with the bulk occurring in October-December 2011 with assistance from Kris Horsby and Dr. Marli Miller.

We employed traditional geologic mapping tools (topographic base map, compass, clinometer, notebook, rock hammer) and techniques (Low, 1957), while also focusing on the three non-material aspects of geologic data collection: hiking, seeing, and imagining. Topographic base maps produced in ArcMap were printed on 11”X17” paper sheets for field mapping.

Spatial Analysis using ArcGIS

Most major maps created and displayed in this manuscript were created with ArcGIS software. Digital mapping allows for precise geographic transfer from the field to office map and eases the ability to open-source the data. Digital mapping guidelines were published by the Federal Geographic Data Committee (FGDC, 2006) and were followed during compilation. The geographic reference frame for all maps is WGS 1984 Web Mercator Auxillary Sphere, chosen for compatibility at many scales.

Maps from previous published and unpublished data were digitized as shape files for spatial analysis. Some of the shapefiles were used in the final compilation. The tectonic reference frame map shown in Figure 4 is a compilation of 17 digitized maps, the sources to which appear in a separate list.

Stereonet Analysis

Stereonet projection methods are essential to analyzing three-dimensional structural data. Using the Stereonet8 program developed by Allmendinger *et al.* 2012,

selected orientation data was plotted to explore and support various hypotheses. The next section, Descriptions of Structures, includes many stereonets that were made to calculate relative angles between structures and characterize fault populations.

Geochemical Analysis

Three samples were chemically analyzed by Dr. Leah Minc using Instrumental Neutron Activation Analysis at the Oregon State University Radiation Center. Samples were bombarded with neutrons to convert isotopes from the stable to radioactive state. The amount and intensity of gamma radiation was measured. The radiation energy is particular to the radioisotope undergoing decay. This analysis was employed to investigate mineralization in the upper plate faults and fractures of the 'Crystal Fault'. Trace element abundance, particularly Uranium and Rare Earth Elements, is crucial to assess the hypothesis regarding the origin and classification of the mineralization.

Rock Mechanics

Rock strength experiments were conducted with Dr. John Logan of University of Oregon. These experiments were conducted to test a hypothesis that developed from a field observation: Local variations in gouge thickness on the Amargosa Fault are a function of pegmatite abundance in the footwall. Samples collected during the 2011 field season were cored and cut into either 1” diameter by 2” long cylinders or 1” by 1/2” thick disks. The disks were inserted individually into a point-load device for tensile strength tests. The cylinders are jacketed and inserted into a uniaxial compression device for vertical compression. Both procedures yield an ultimate strength and fracture pattern for each sample. The results were used qualitatively to support the field hypotheses.

Trigonometry

Trigonometric techniques can be useful for analyzing unknown lengths and angles. For example, if a map distance offset and angle of the off-setting plane are known, the sine function can be used to calculate the length of the fault surface between the offset marker beds.

CHAPTER III

DESCRIPTIONS OF STRUCTURES

The final map of this study illustrates the relationship between six generations of structures, referred to as D1-D6. Using principles of cross-cutting relationships, I have derived an inferred relative timing, which will be discussed in this section and followed by a summary. Also discussed here are field measurements and implications derived from those measurements, such as sense of slip and slip estimates. A simplified version of this study's final map that excludes rock units and most orientation data is offered in Figure 17 for reference while reading this section. This illustration accentuates the cross-cutting relationships.

D1: Imbricate Thrust Faults and Tight Folds

Tight Folds

The folds are generally small and tight with inclined axes that plunge southeast. Fold morphology is variable but the trends are consistent. The folds were first noted by Wright and Troxel (1984), but they were not discussed in any detail (p. 4). Figures 18 through 31 encapsulate the field observations and data, to document the structures and conduct spatial analysis. Each location is marked with a star that correlates to the map inlay. Figure 32 summarizes the orientation data with a density plot of all axial lines.

A symmetrical syncline, shown in Figure 18, developed in the well-bedded middle Stirling Quartzite Formation. Only 200 meters to the south is syncline with steep, box-like limbs, shown in Figure 20. A similar box-like morphology is exposed at location I in "Fault Gouge Canyon" (Figure 26). Notice the fold resides in the footwall

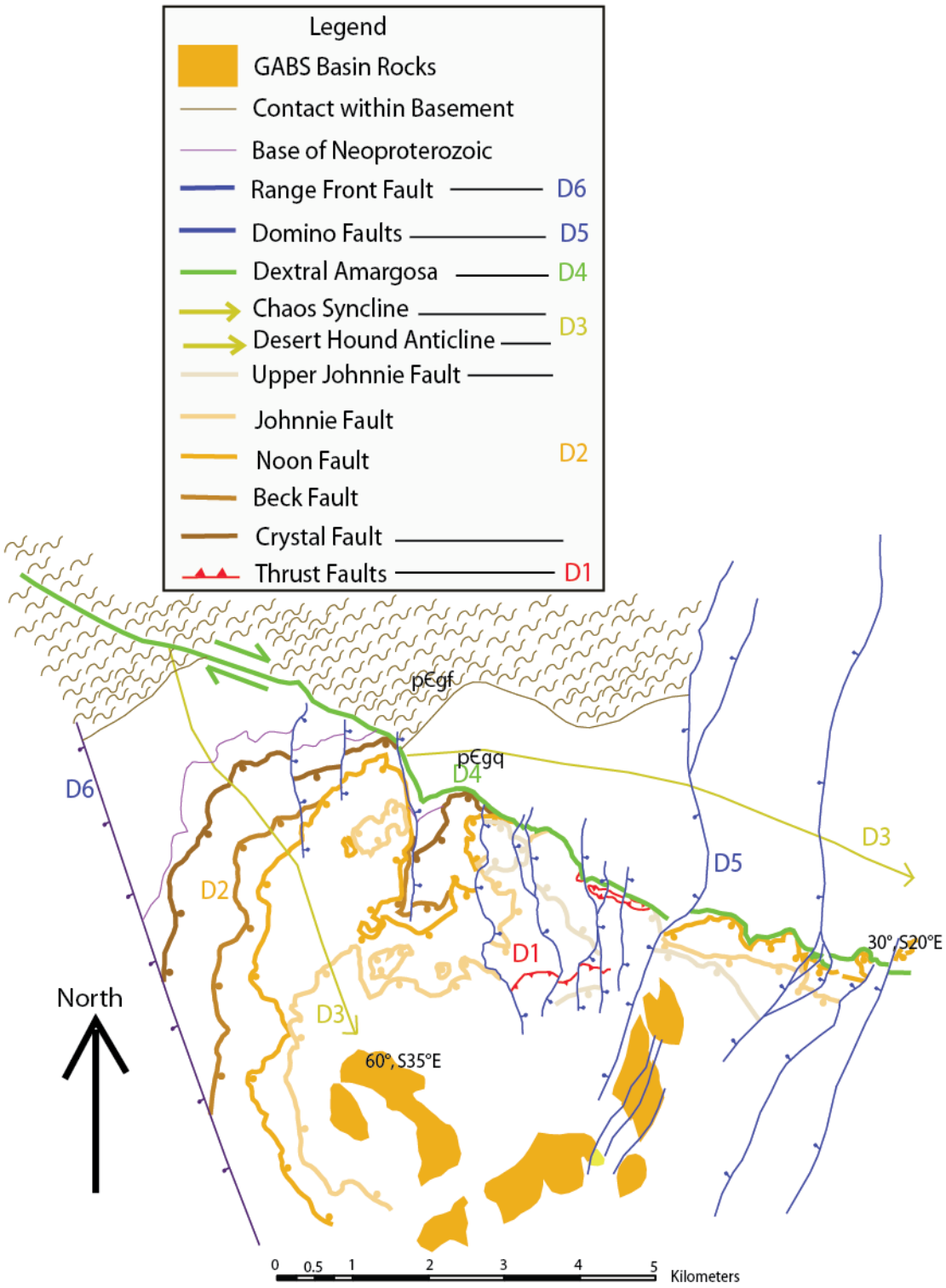

Figure 17: Simplified Chaos. This line drawing of the shows six major deformational populations, modified from the main map. Because lithology is removed, cross-cutting relationships are accentuated.

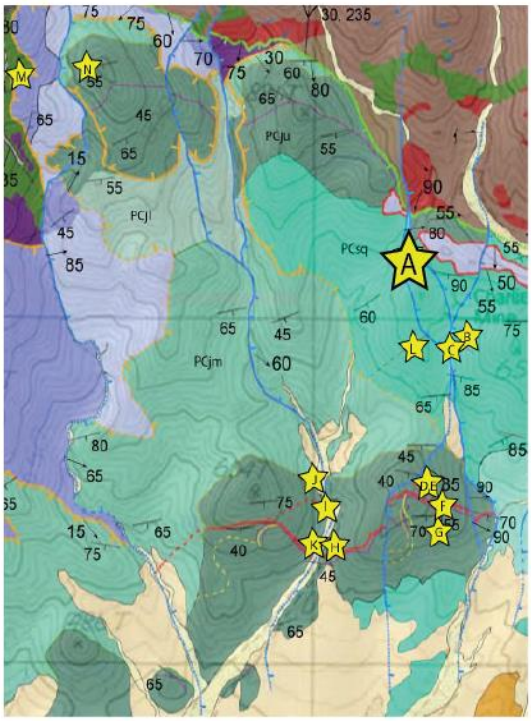

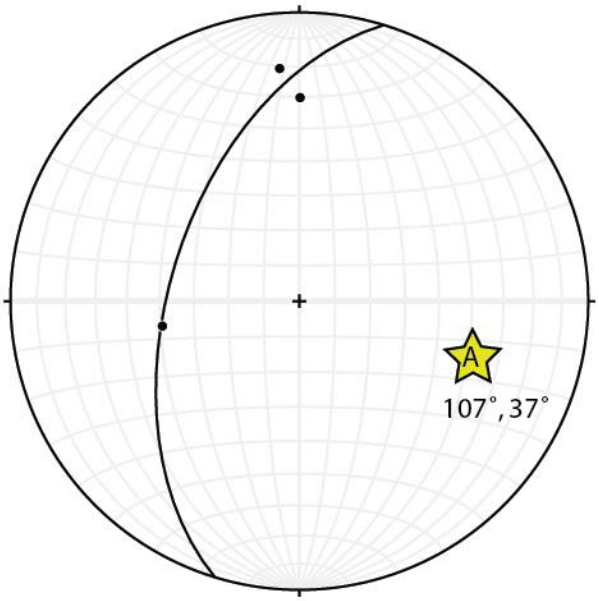

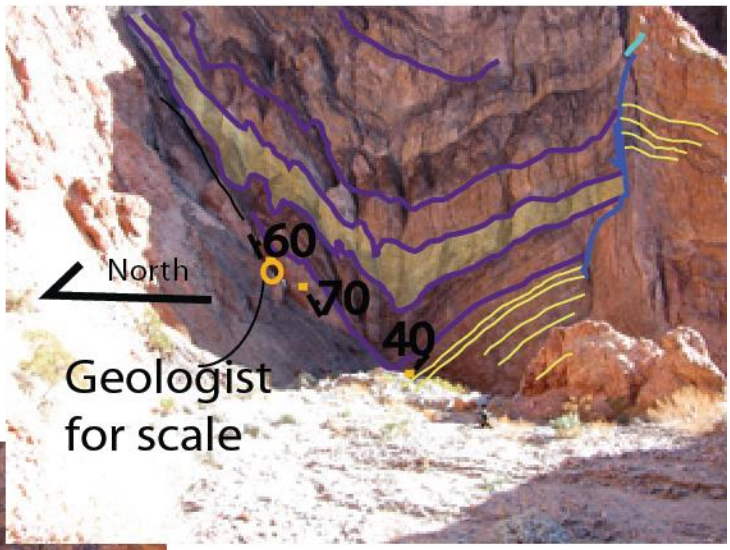

Figure 18: Syncline in Stirling Formation trends 107˚, and plunges 37˚.

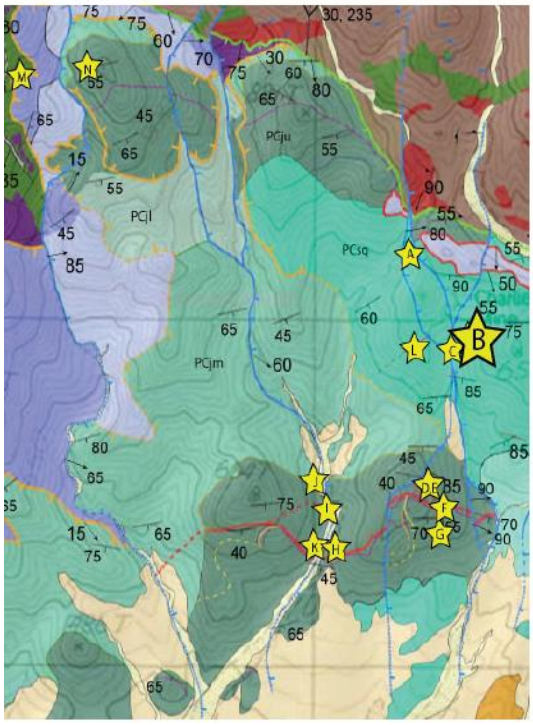

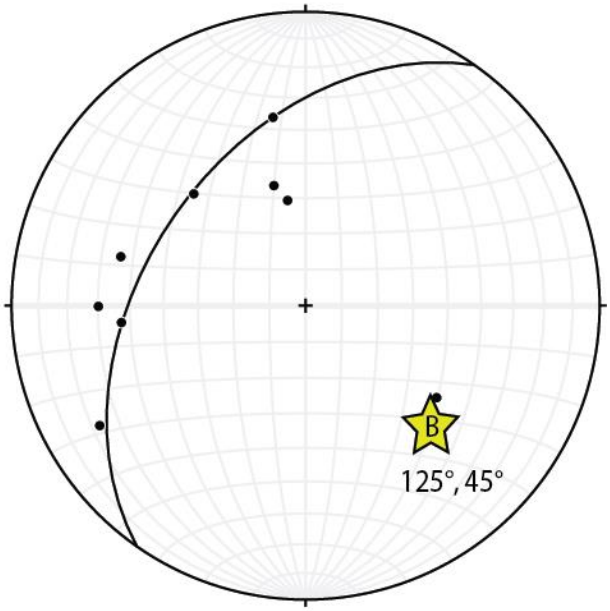

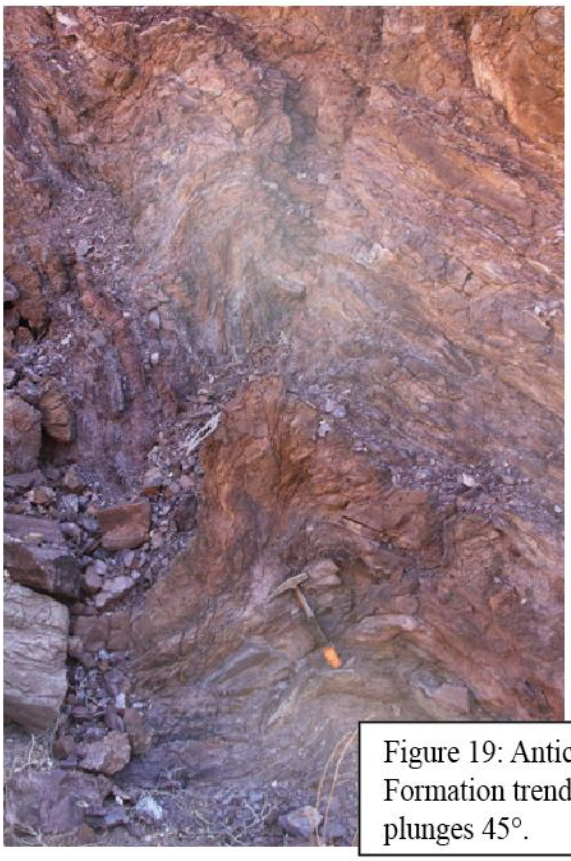

Figure 19: Anticline in Stirling Formation trends 125°, and plunges 45°.

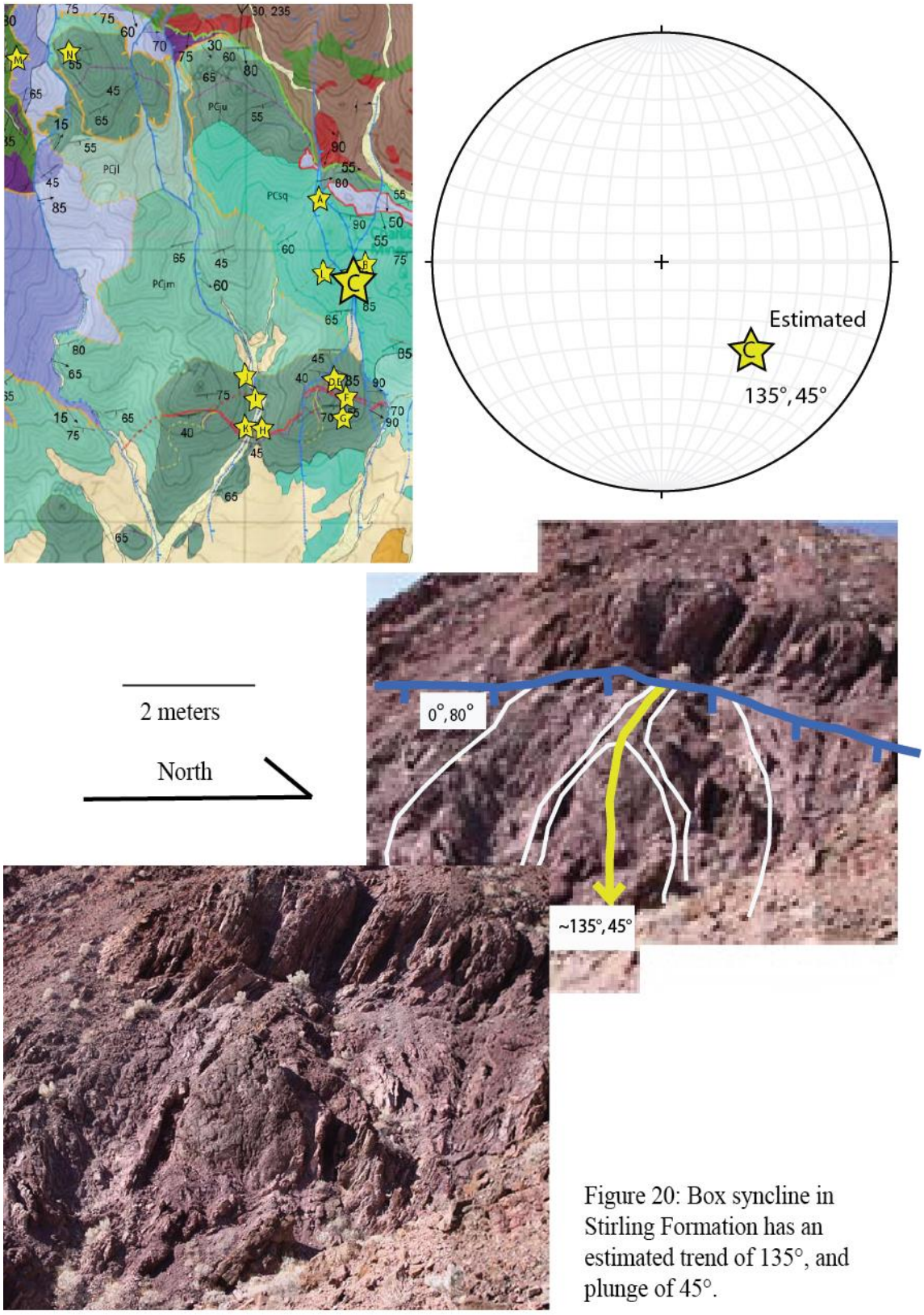

Figure 20: Box syncline in Stirling Formation has an estimated trend of 135°, and plunge of 45°.

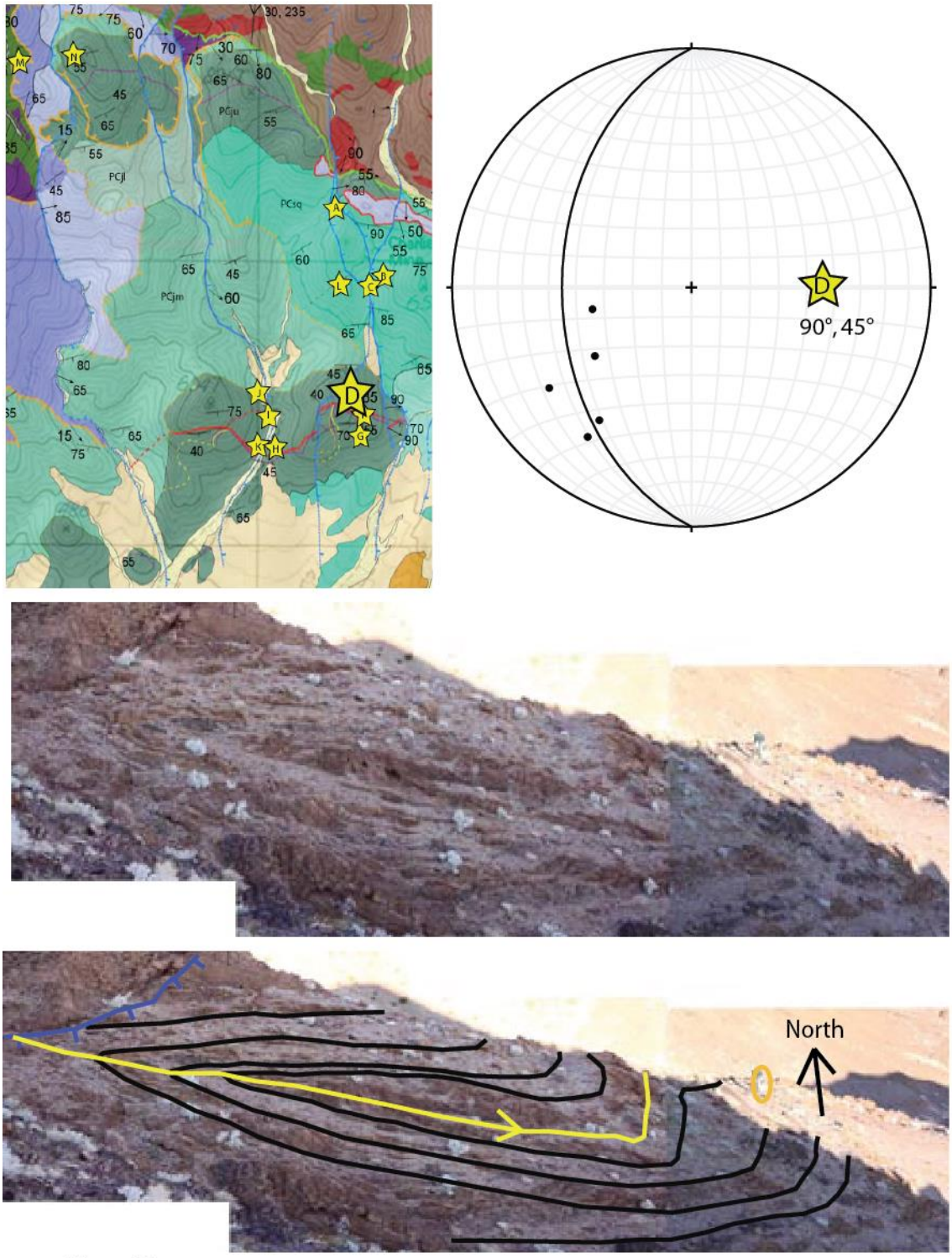

Figure 21:
Recumbent anticline in Johnnie Formation has a trend of 90° and plunge of 45°.

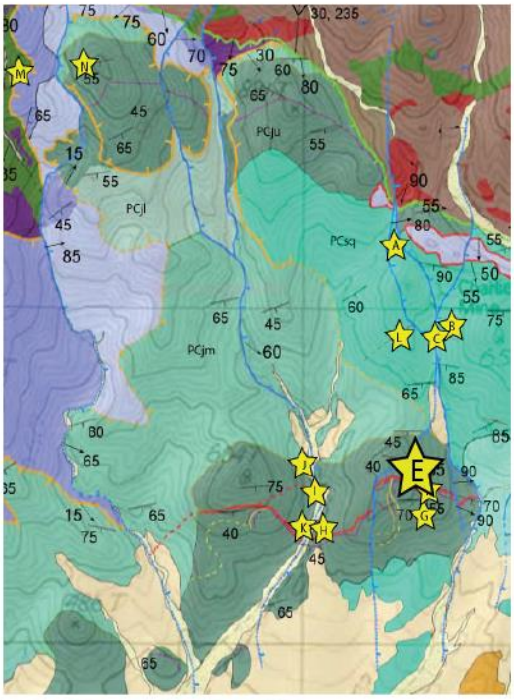

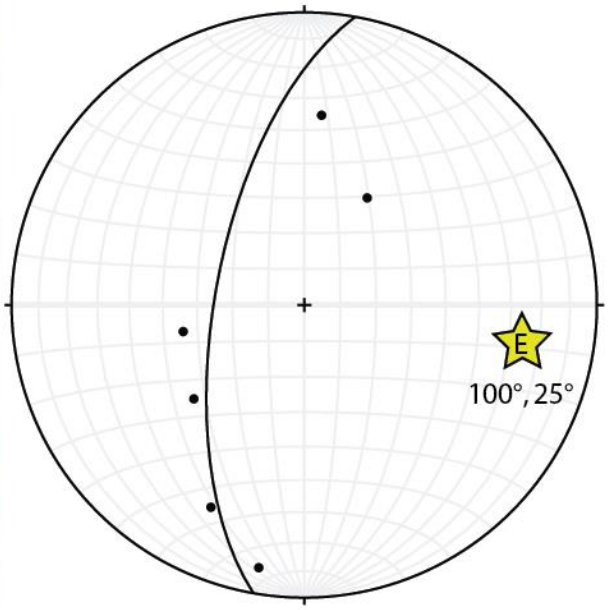

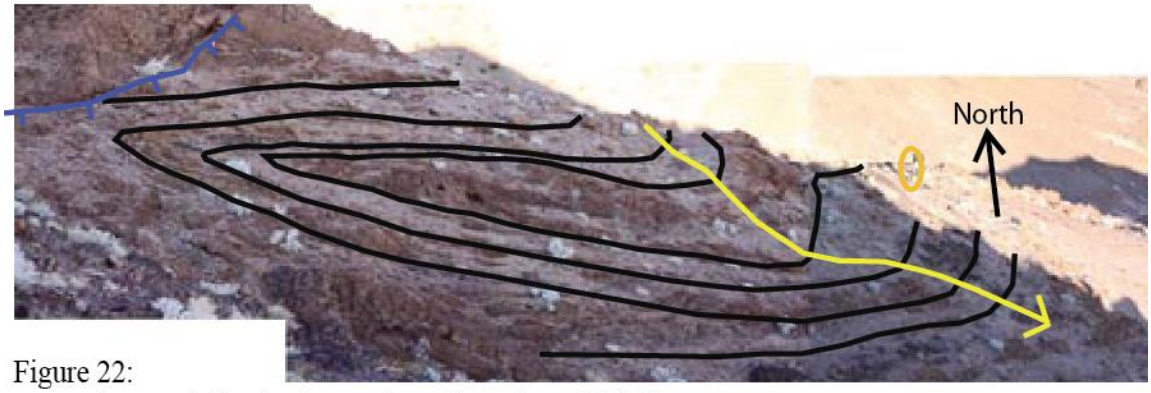

Figure 22:
Recumbent anticline in the previous figure is re-folded about a hinge trending 100° and plunging 25°.

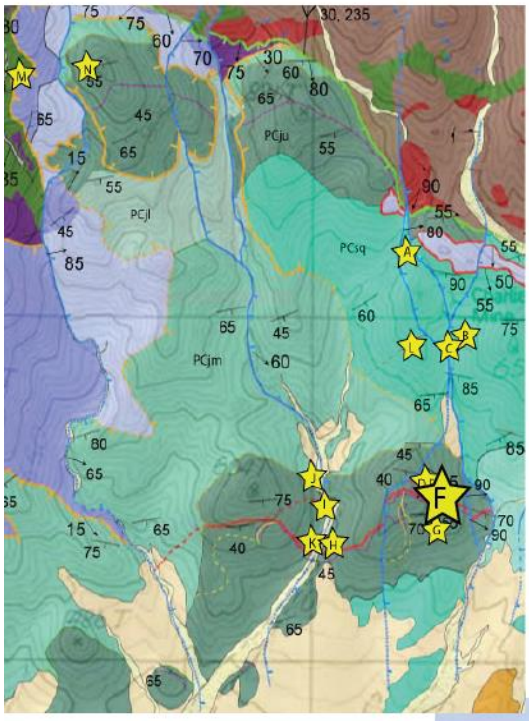

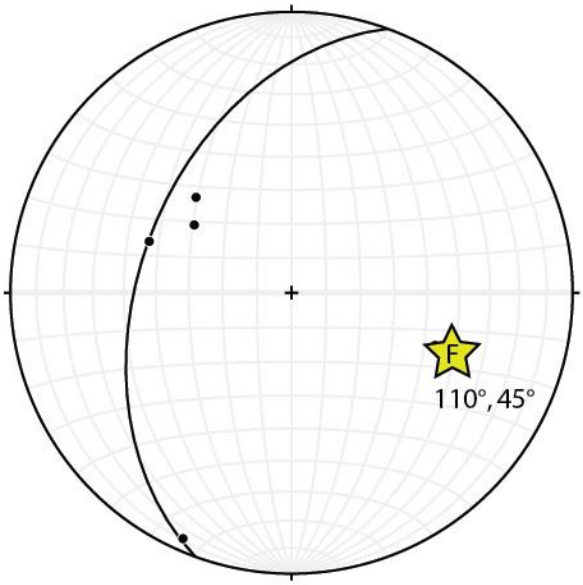

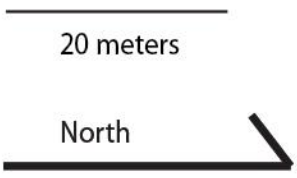

Figure 23: Anticline in hangingwall of imbricate thrust, trends 110° and plunges 45°.

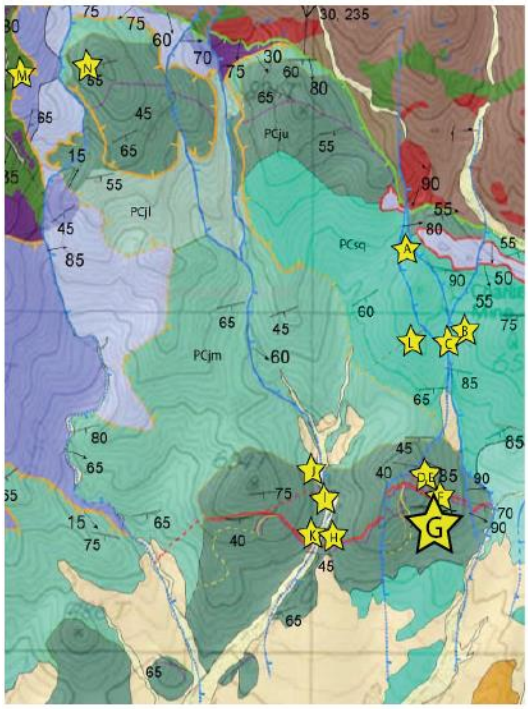

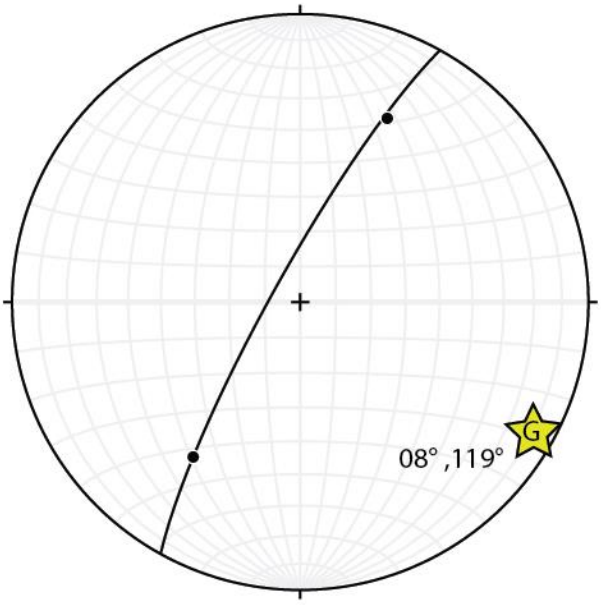

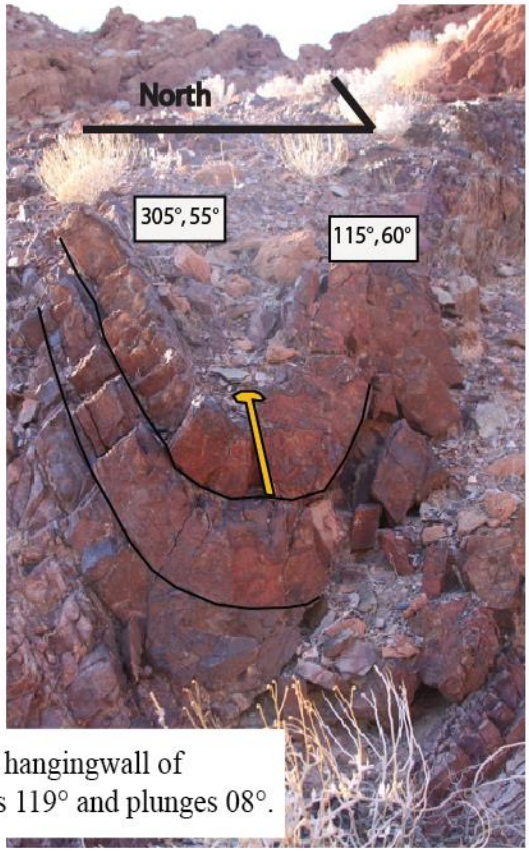

Figure 24: Syncline in hangingwall of imbricate thrust, trends 119° and plunges 08°.

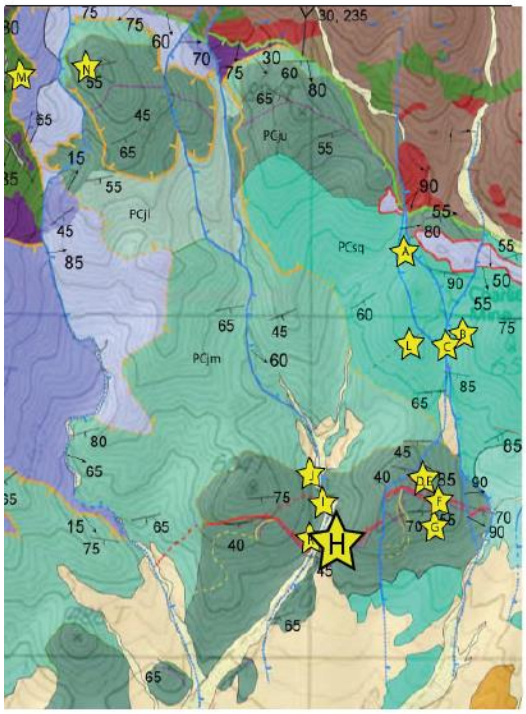

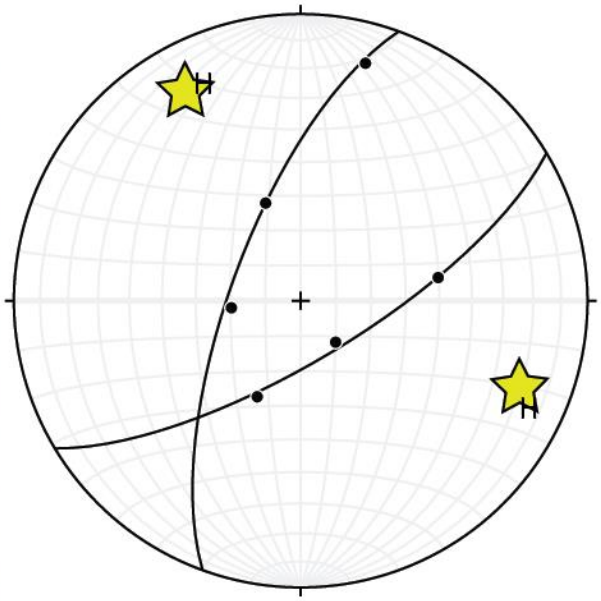

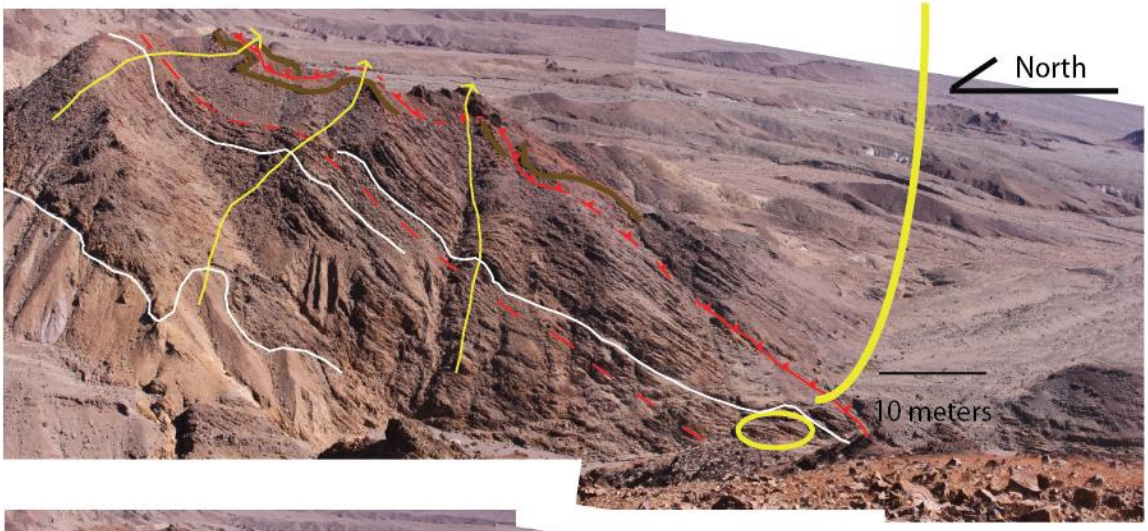

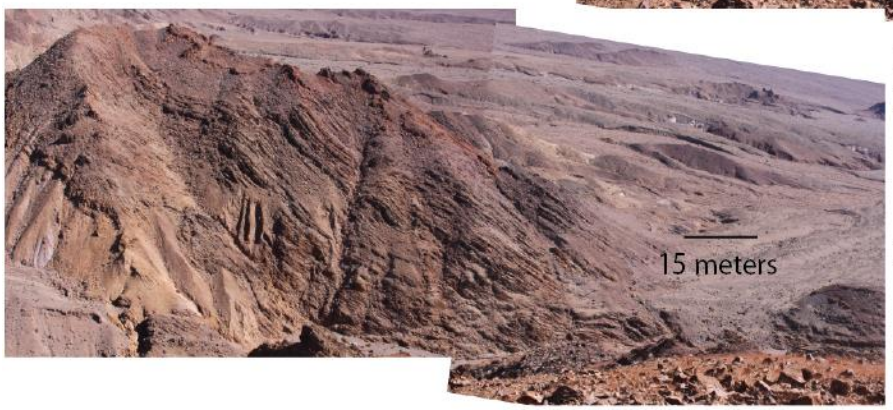

Figure 25: Mosaic of east 'Short Johnnie Hill' showing bedding and parasitic folds. Main folds are oriented ESE, and conjugate folds NNW.

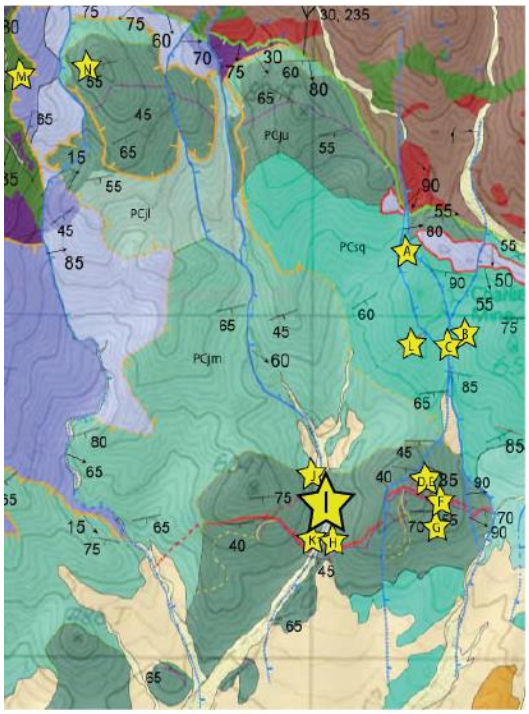

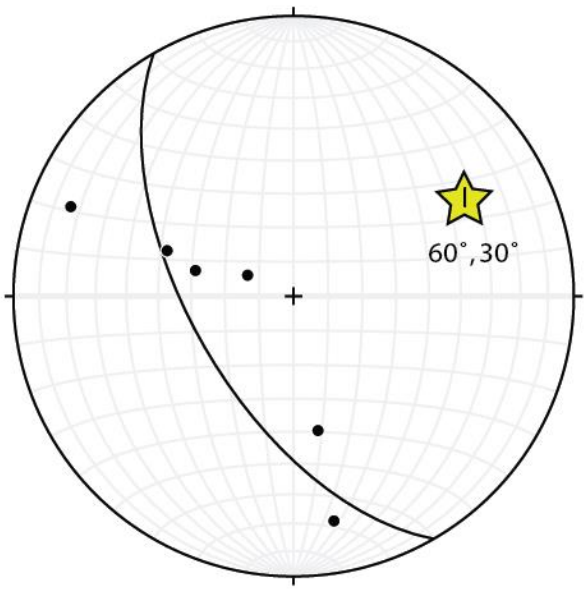

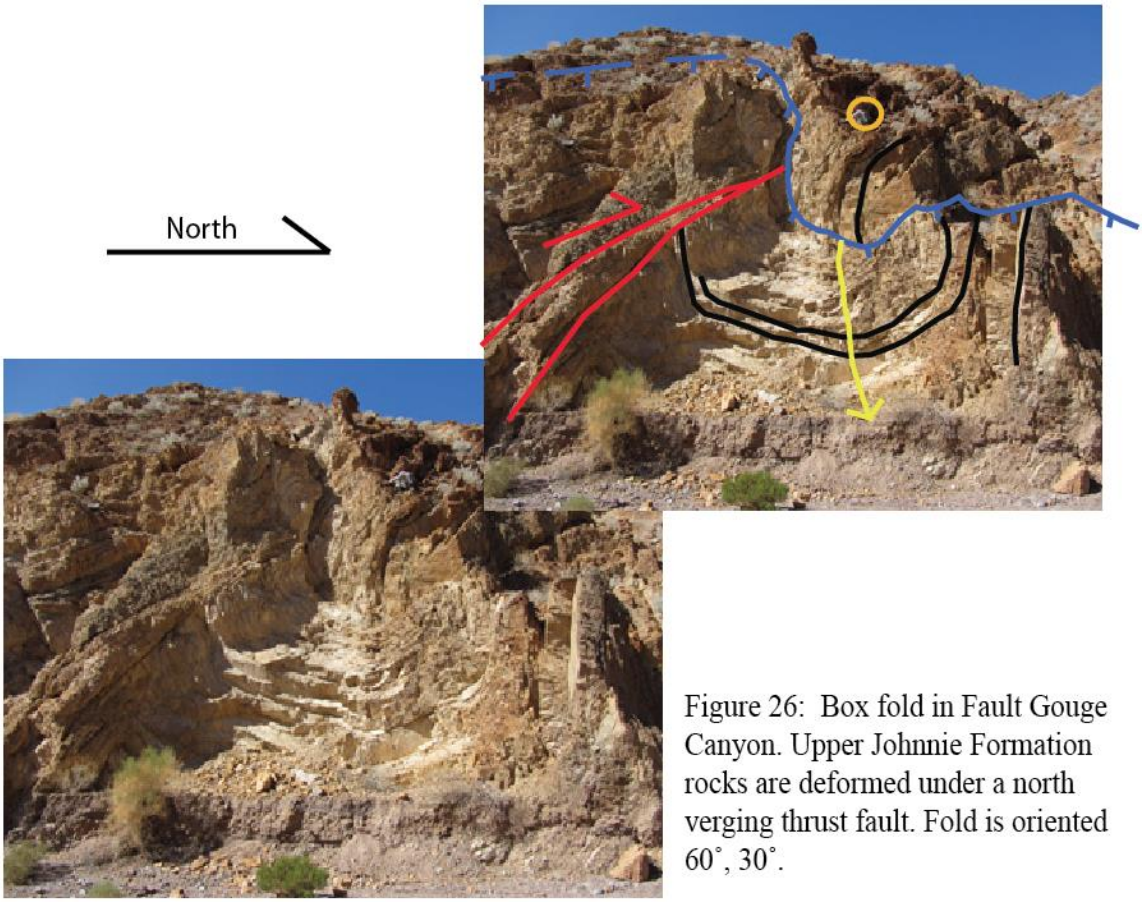

Figure 26: Box fold in Fault Gouge Canyon. Upper Johnnie Formation rocks are deformed under a north verging thrust fault. Fold is oriented 60˚, 30˚.

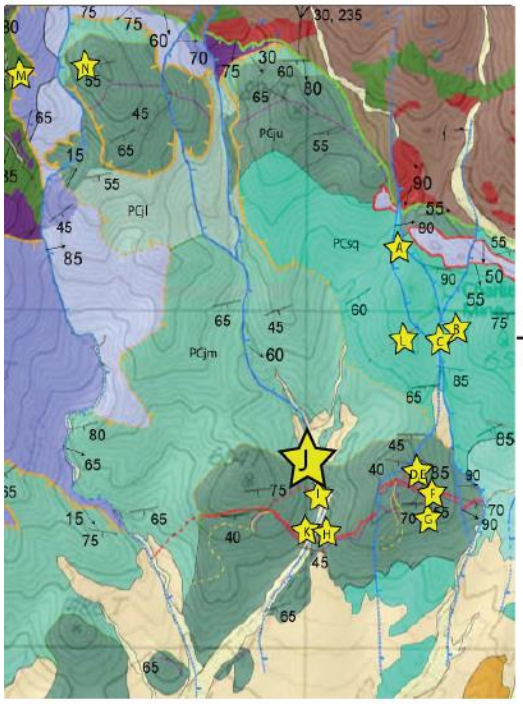

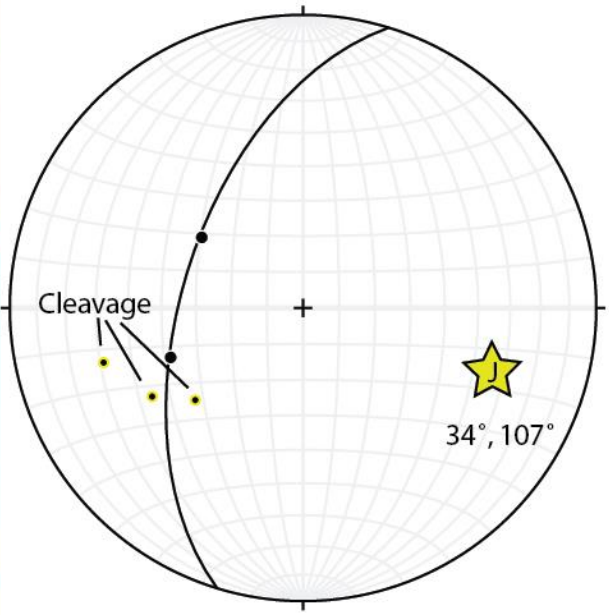

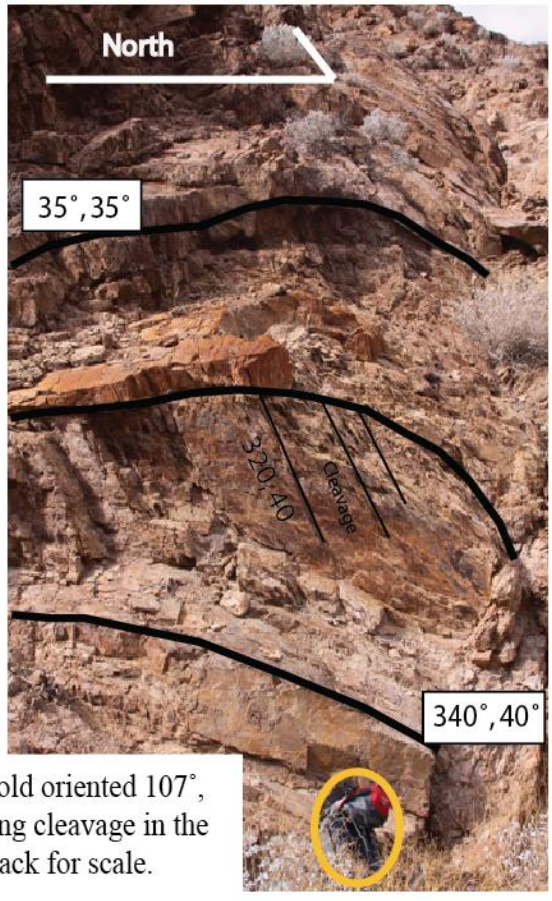

Figure 27: Fold oriented 107°, 34 °) exhibiting cleavage in the hinge. Backpack for scale.

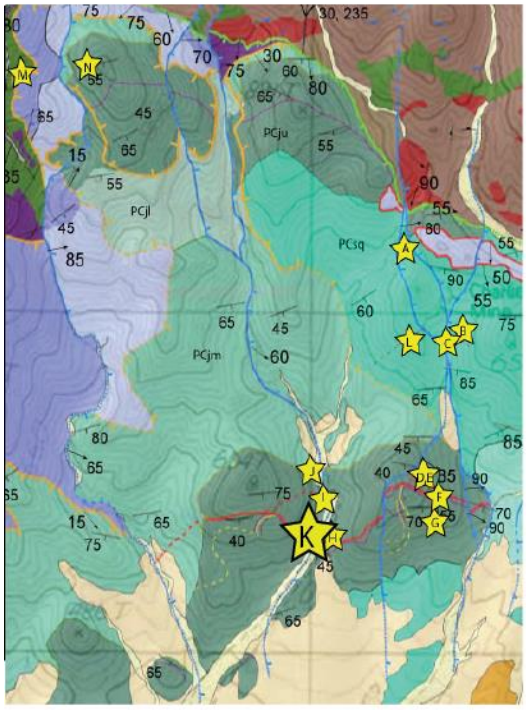

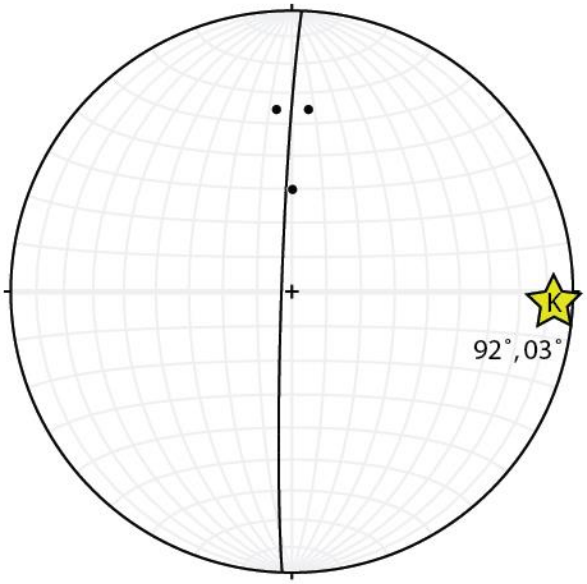

North

5 meters

Figure 28: Syncline in Johnnie Formation. The fold is in the footwall of the main thrust of the imbricate fault system. It is oriented 92˚, 03˚ and is oblique to the fault trace.

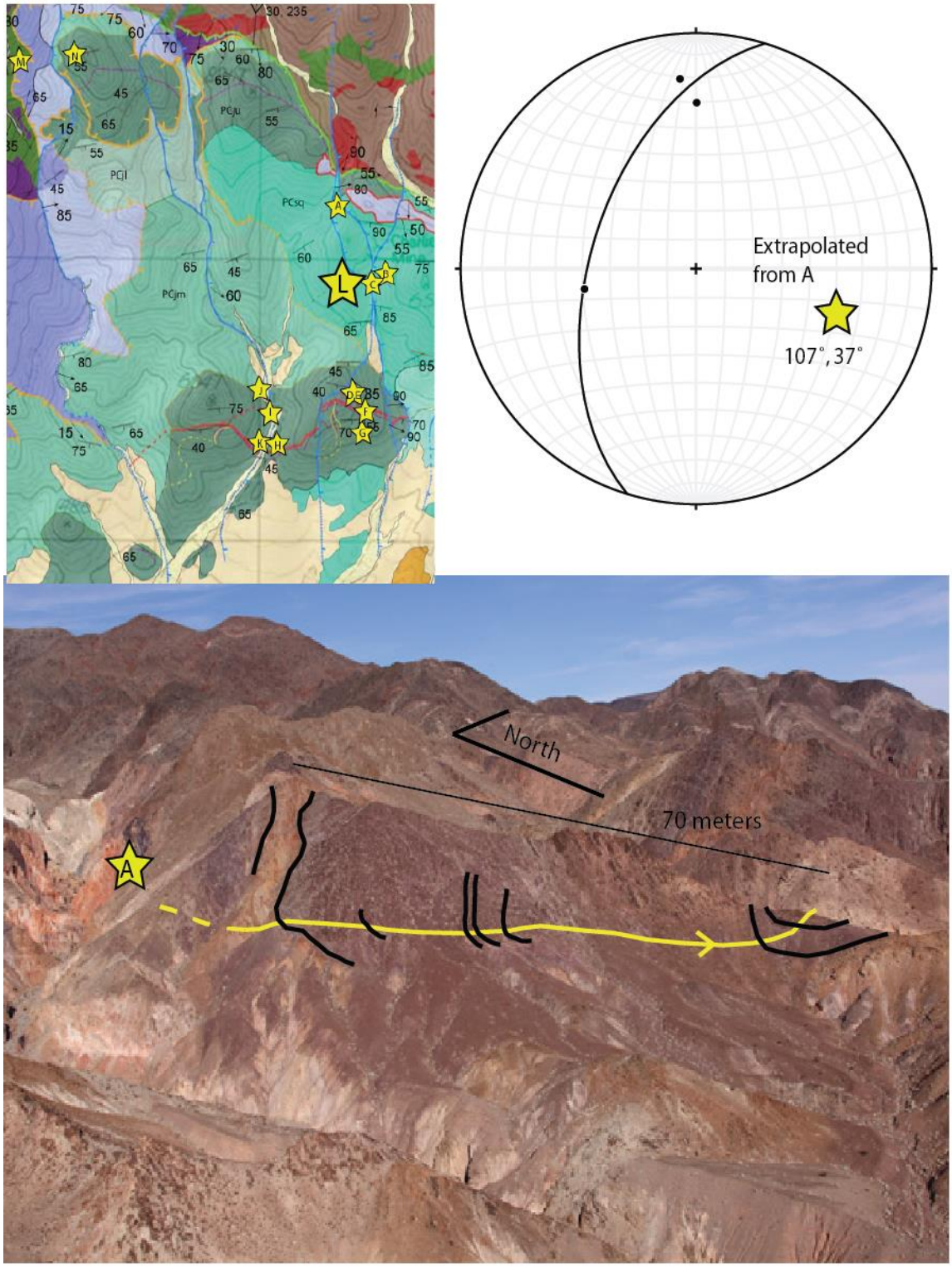

Figure 29: Sighting from peak 604T, a distant syncline can be seen in the Stirling formation. The fold appears to be similarly oriented and along stike with the fold at Location A.

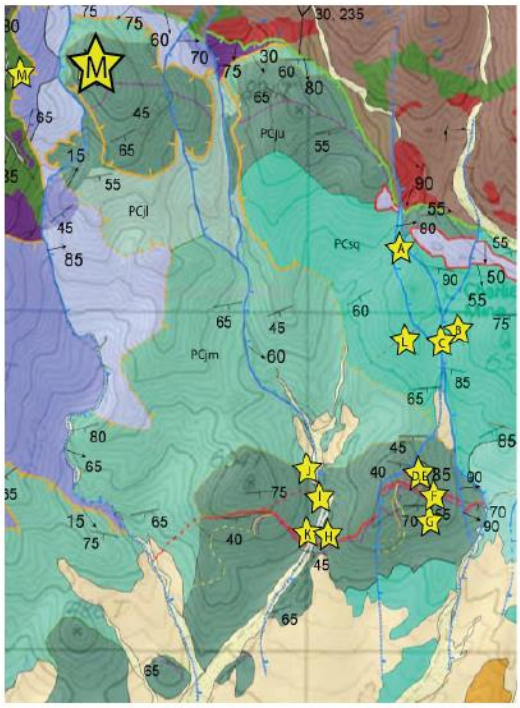

Figure 30: This mosaic of east 'Tall Johnnie Hill' shows bedding patterns of Upper Johnnie formation. The southeast plunging parasitic folds are very similar to those on the east 'Short Johnnie Hill', implying the two locations are offset along the low-angle D2. Upper Johnnie Fault. The imbricate thrust system is exposed on the short hills, but was not located on the tall hills.

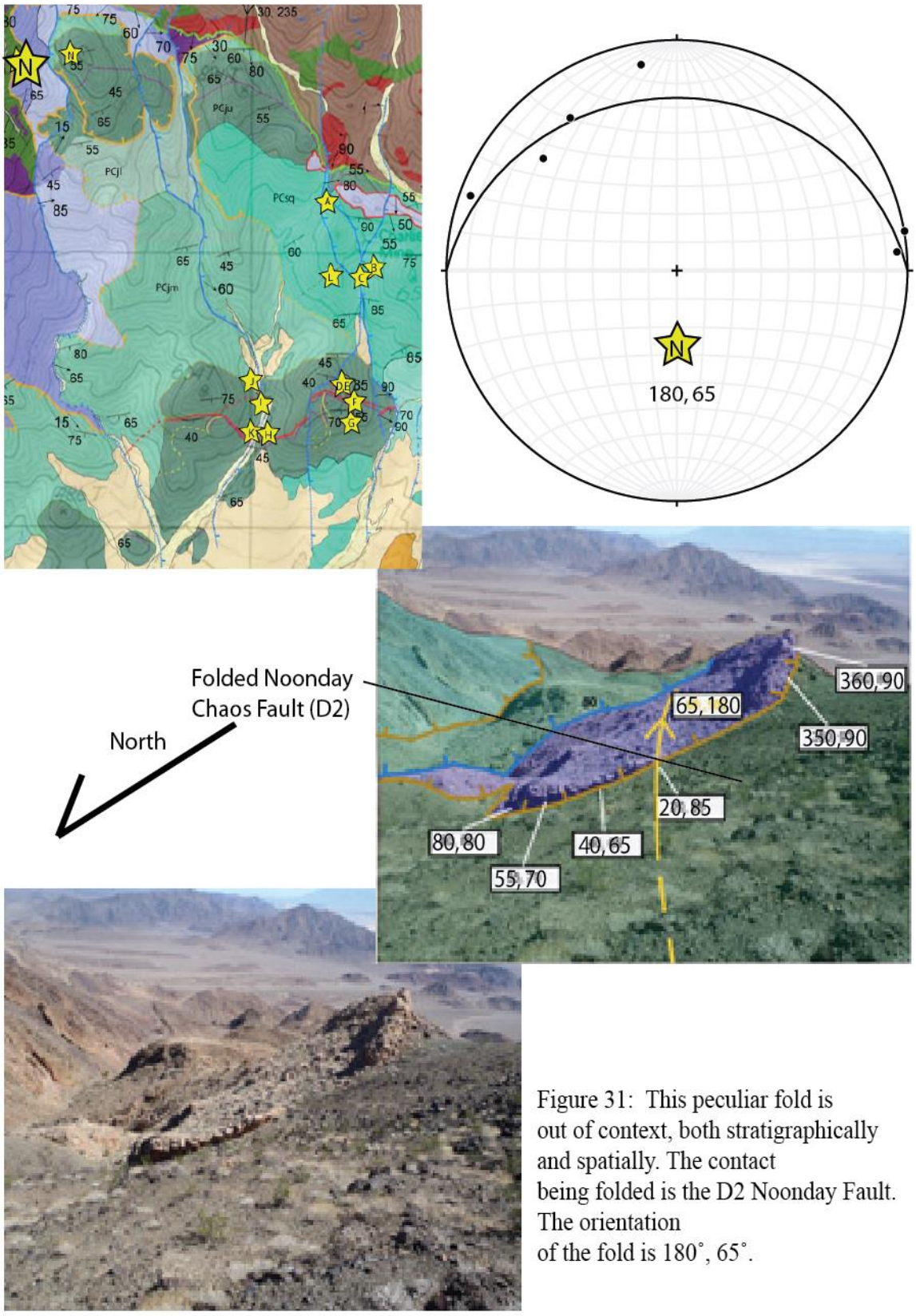

Figure 31: This peculiar fold is out of context, both stratigraphically and spatially. The contact being folded is the D2 Noonday Fault. The orientation of the fold is 180˚, 65˚.

of a thrust fault. Figure 21 depicts a tight recumbent fold in the footwall of a thrust, which was refolded about the axis shown in Figure 22. Figures 25 and 30 show the typical wavy geometry of the bedding exhibited by the upper Johnnie Formation on both sets of "Johnnie Hills", due to small parasitic folds.

At location M, I observed a folded fault. The fault places Noonday Dolomite above the diabase of the Crystal Springs Formation. This fault was then folded about the axis shown in Figure 31. I argue the fold is not kinematically related to the other folds because of the distance from the other folds, the much different trend and plunge, and the stratigraphic units involved. With the exception of the neighboring upper Johnnie Fault block, the fold in Figure 31 is nearly a kilometer apart from the others observed. The axial line plunges 65˚ southeast, which is ~30˚ from the a-m. Contextually, this fold involves deeper stratigraphy and resides in a deeper fault block.

The map pattern of these folds shows a common eastern trend (Figure 32). As shown in the accompanying figures, many of the folds are in the hangingwall for footwall of thrust faults. The amount of shortening accommodated is calculated by comparing pre-shortened to post-shortened lengths on the fold featured in Figure 18. This technique yields a shortening estimate of approximately 25%.

Imbricate Thrust Faults

Two major older-over-younger fault relationships occur in the field area: 1) the Imbricated Oolite (Figure 33) and 2) the Ibex Klippe (Figure 34). The imbricate system contains the tight folds, while no folds are observed near the 'Ibex Klippe'. The 'Ibex Klippe' is seemingly misplaced from any other kinematically related structures. The

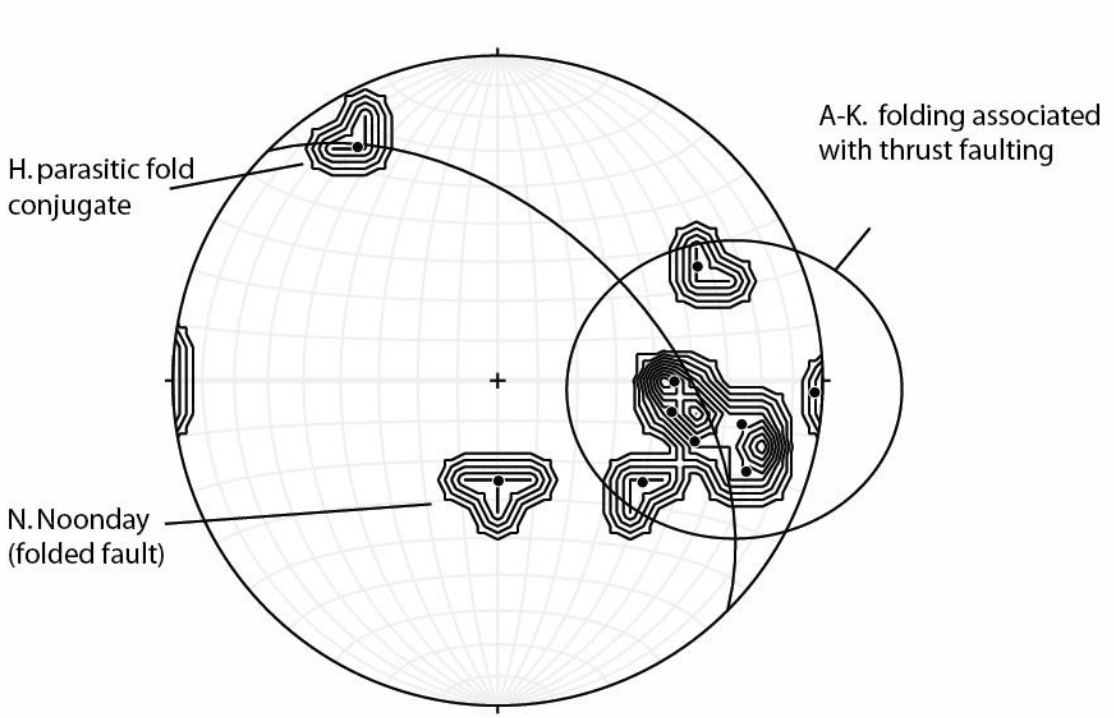

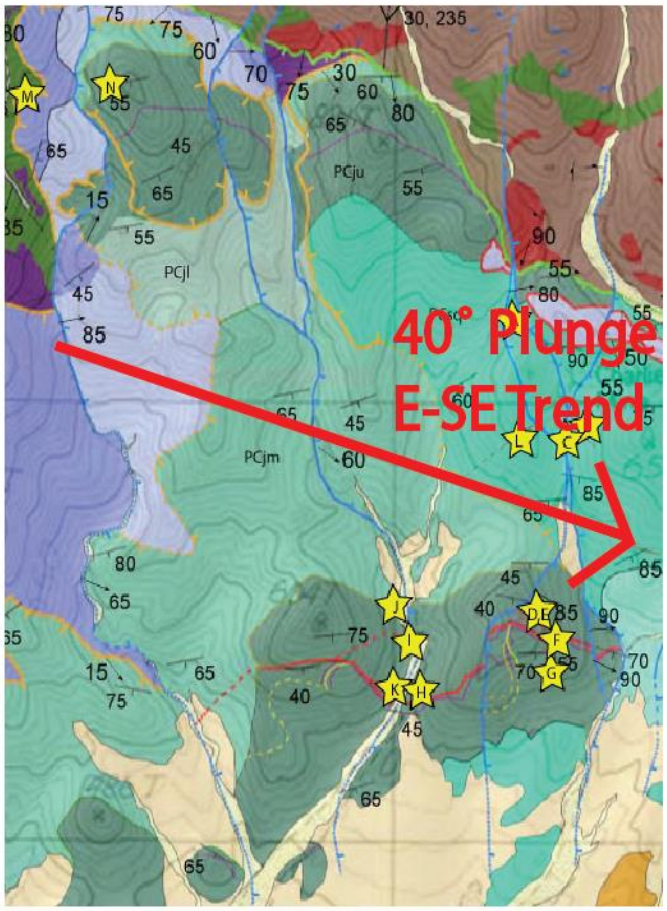

~25% Shortening

Figure 32: The stereonet above is a density plot of all the small fold axes. The average trend of the folds is east-southeast and plunging ~40˚. The shortening accomodated by these is estimated to be ~25%.

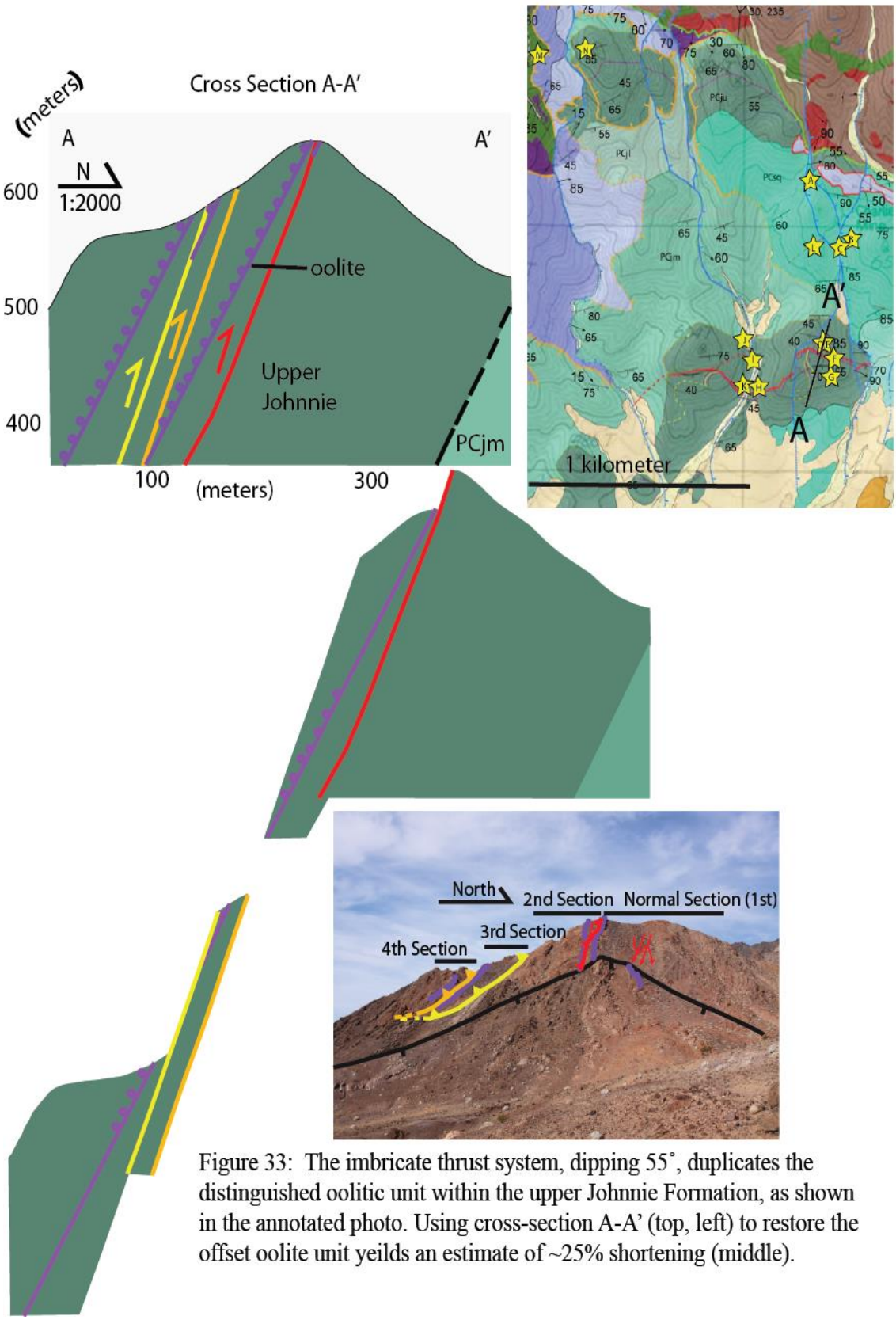

Figure 33: The imbricate thrust system, dipping 55˚, duplicates the distinguished oolitic unit within the upper Johnnie Formation, as shown in the annotated photo. Using cross-section A-A' (top, left) to restore the offset oolite unit yeilds an estimate of ~25% shortening (middle).

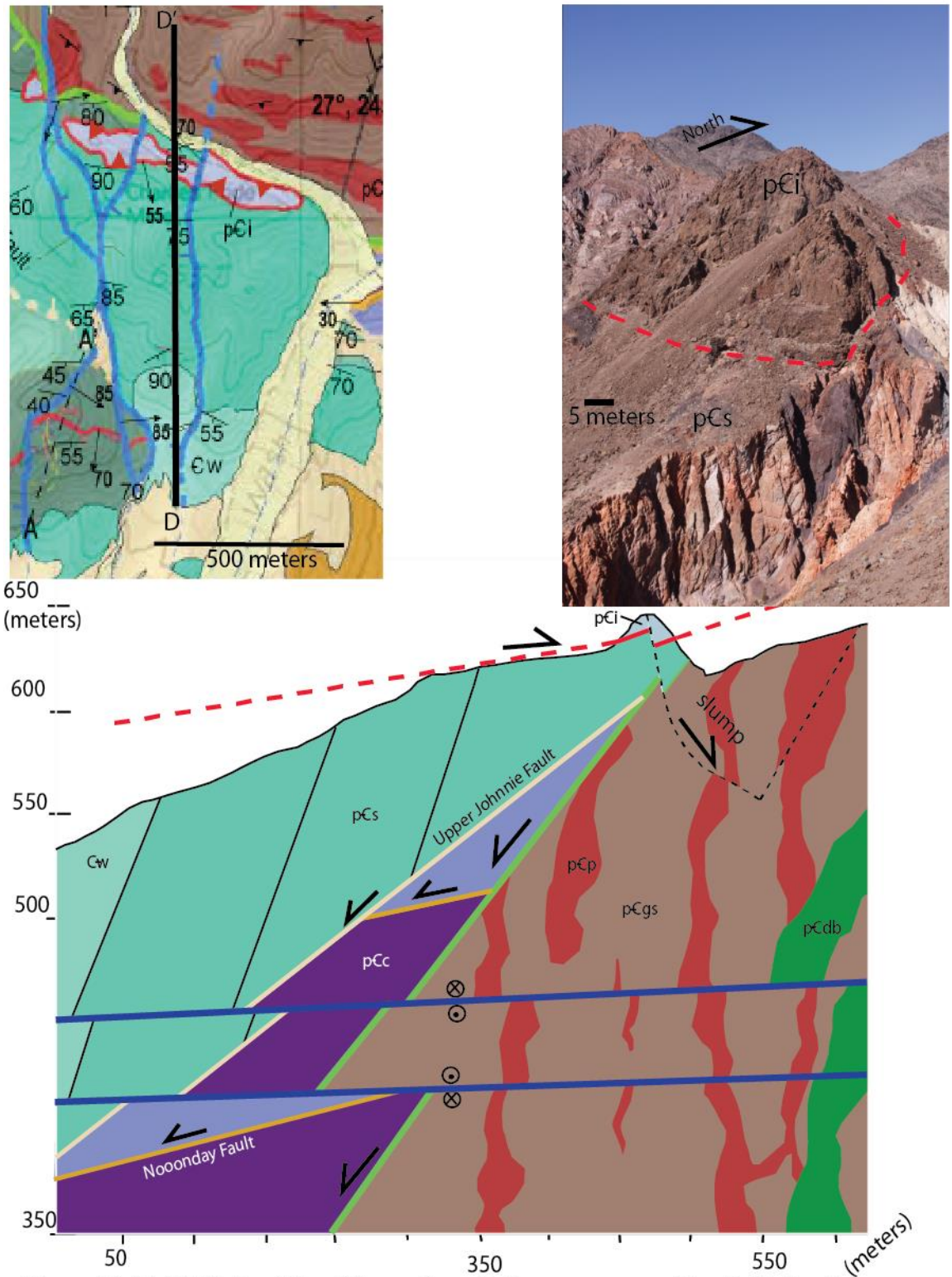

Figure 34: (right) Photo of Ibex Klippe, above fault gouge canyon. Map (left) showing D-D' through the klippe. The cross-section (bottom) shows the relationship between the klippe and the faults below.

klippe occupies a structurally higher block, indicating the Ibex Klippe thrust system is structurally higher than the Imbricated Oolite thrust system.

The Imbricated Oolite is best described as a structurally up-imbricating sequence involving three main thrusts and resulting in a quadrupling of the Johnnie Oolite marker bed. A shortening estimate is conducted by retrodeforming the cross-section in Figure 33. This process yields ~25% shortening accommodated by the structure at the most extremely shortened section. Because the Ibex Klippe has limited exposure and no offset marker beds were observed, no shortening estimate is suggested.

Together, the relative orientations of D1 structures show a past record of ~ 25% north-northwest directed shortening (Figure 35).

D2: Currently Low-Angle Shingle-Style Normal Faults

The shingle-style structures are the underlying cause of the attenuated stratigraphy of the Virgin Spring Chaos, so I refer to them collectively as the Chaos Fault System. Noble (1941) recognized a shingle-like attenuation structure to the stratigraphic blocks of the Virgin Spring phase of the Chaos. The D2 faults are essentially the bounding structures between what Noble (1941) called lozenge-shaped shingles.

When separated, these faults are named after the dominant rock type in the hangingwall slab. For example, the Noonday Fault consistently places Noonday Dolomite on various lower stratigraphic units. Similarly, the intervening rock slabs are named after the fault at its base. For example, the upper-plate of the Crystal Fault is the Crystal slab.

The faults are described in structural order from lowest to highest. Descriptions include the location(s) where the fault relationship can be observed and measured, the

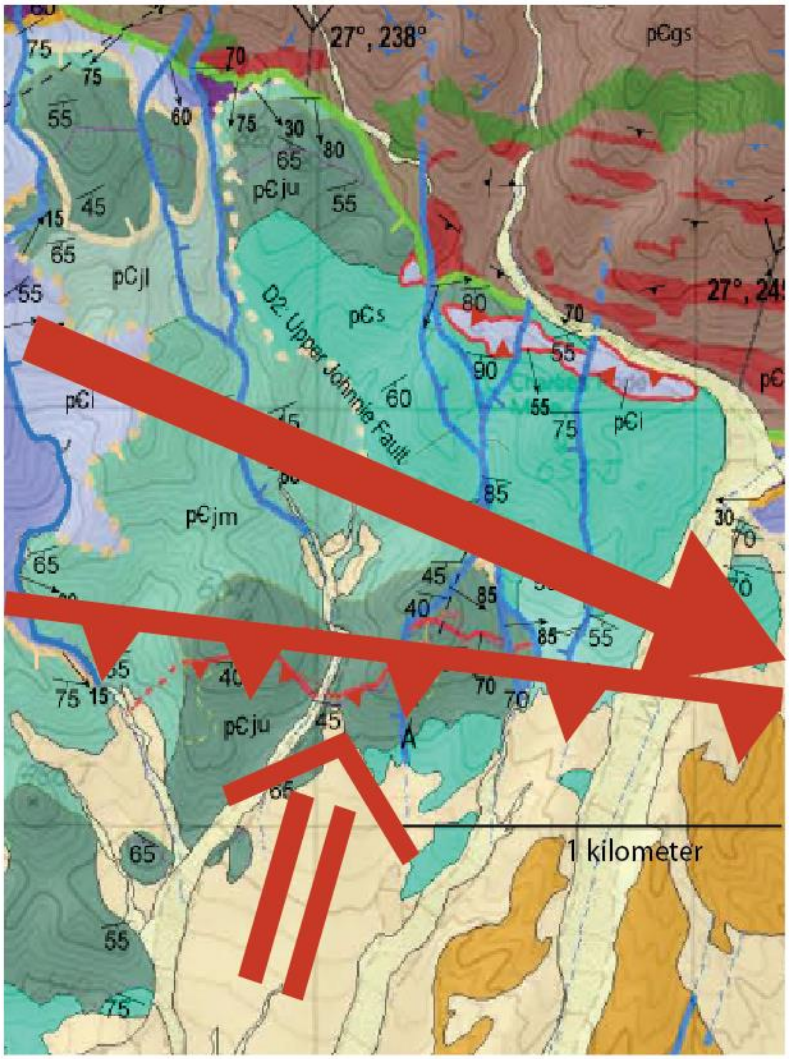

1) 40° southeast plunging folds
2) North verging thrust faults
3) ~25% shortening on faults and folds

Figure 35: The kinematic indicators of the D1 system suggest north-northwest directed shortening. Though the relationship is still unclear, it is hypothesized the 'Ibex Klippe' system is structurally above the 'Imbricated Oolite'. If correct, these structures could represent an unrecognized thrust system between the Panimint and Chicago Pass thrusts.

fault geometry, a description of the fault surface, the cross-cutting relationship to other Chaos Faults, and the process to estimate slip.

Assumptions Used while Calculating Slip Estimates

The slip estimates offered here were derived using five major assumptions. The assumptions are:

1) A generalized stratigraphic that does not account for local variation in unit thickness, lateral facies changes, or basin margins.
2) Either the hangingwall or footwall rocks were horizontal before faulting.
3) Each fault had a constant dip at depth before D3 deformation.
4) Slip on the fault was down dip.
5) Fault dips are based on outcroppings and average relative angles to bedding

Therefore, the rough calculations conducted here are only rough estimates and are not to be taken as minimum or maximum slip estimates. Though, in an attempt to compensate for assumption five, I have also conducted calculations using a standard normal fault dip of 60°. For consistency, I take the minimum calculation as the estimate. For example, if five numbers are derived (1020, 300, 450, 670, 420) I report the lowest value as my estimate (300). Results are highly variable because of the variable inputs and major assumptions. A better assessment of slip on the D2 faults is necessary, but this remains a solid first-order series of estimates.

D2.1: Crystal Fault

Depicted in burnt orange, the 'Crystal Fault' is best exposed on the east wall of “V Canyon”, and best viewed from “Grey Wizard Pass” (Figure 36). At this location, the

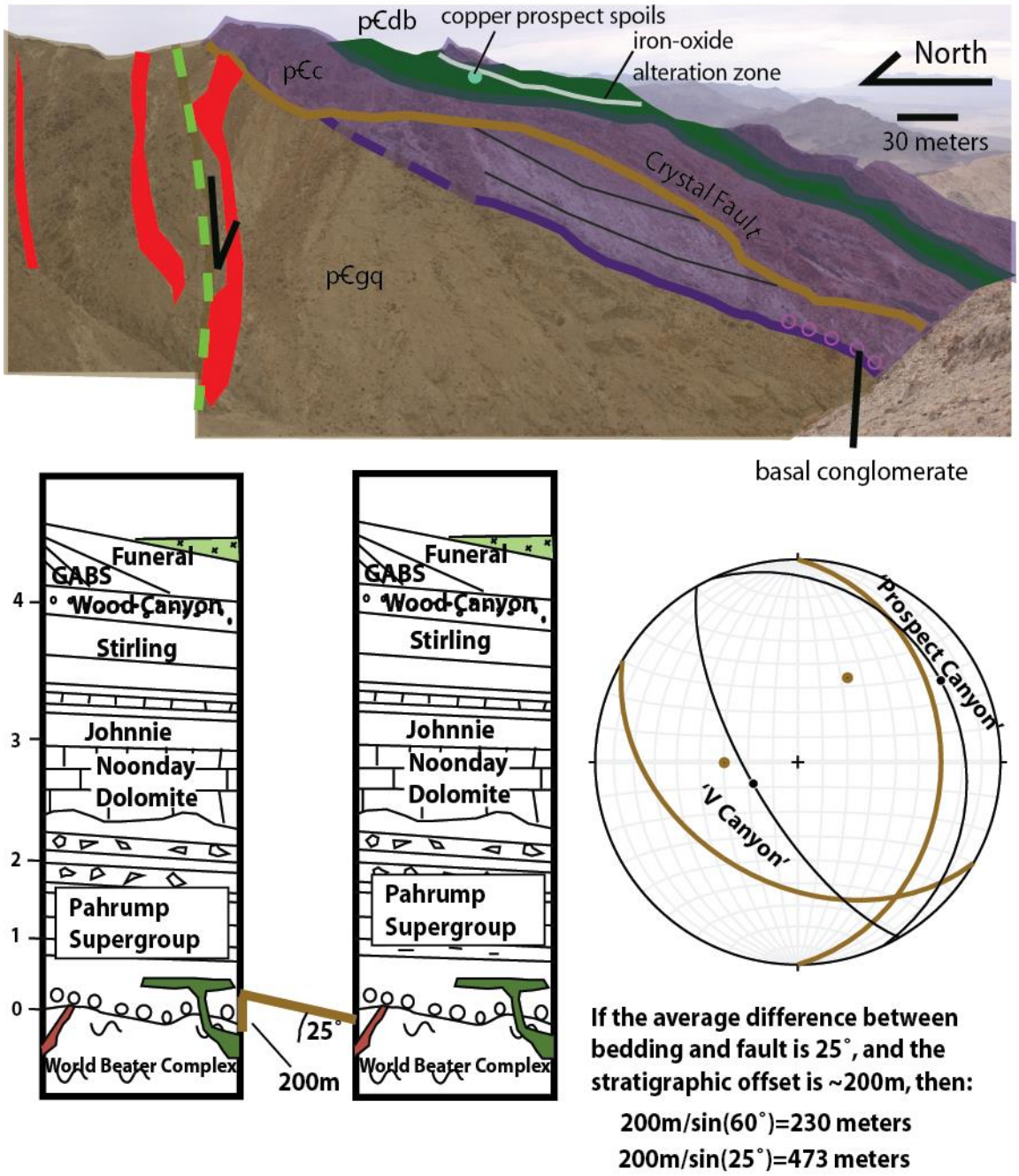

Figure 36: (top) From 'Grey Wizard Pass', the Crystal Fault can be seen truncating bedding of the white quartzite member of Crystal Springs. The base of the orange carbonate of the Crystal Springs defines the upper plate. Mineralization in the upper plate faults and fractures is thick in some zones. The fault intersects bedding here at ~37°, and at ~14° near prospect canyon (right). The stratigraphic offset is estimated at 200 meters between the carbonate and gneiss. I estimate minimum slip at ~470 meters.

“Crystal Fault” can be seen juxtaposing the orange carbonate member of the Crystal Springs Formation against the crystalline basement. The fault then cuts up section, to the southwest, through the unconformity, basal conglomerate, and lower clastic members of the Crystal Springs. Exposures in “V Canyon”, “Crystal Nipple Pass”, and “Prospect Canyon” reveal ~50 cm of talc gouge between the upper plate and lower plate. As observed at every exposure, the orange carbonate member of the Crystal Springs Formation is the first stratigraphic unit above the fault. Similarly, the diabase sills are exclusive in the upper plate of the 'Crystal Fault', though some vertical dikes are seen in the lower-plate.

Where observed and measured, this fault cuts hangingwall bedding at low-angles. In 'V Canyon', as shown in Figure 36, the fault (N75°E, 40°S) intersects bedding (N50°E, 70°S) at a ~30° angle. To the southwest, the fault is exposed the mouth of 'Prospect Canyon' as the contact between orange carbonate and basement. Two to ten meters of talc mineralization is exposed above the fault plane, some of which was removed commercially. Here the fault plane (N5W, 30°E) intersects bedding (N30W, 20°N) at ~14° angle. Using previously developed stratigraphic thickness estimates (Mahon, 2012), I estimate the observed maximum stratigraphic thickness missing across the fault at ~200 m. The average difference between the fault plane and bedding is about 20°. Using trigonometric principles, I figure the true offset as (200m)/SIN(20°), which yields 470 meters. Alternatively, if the fault was at 60°, then (200m)/SIN(60°), which yields 230 meters. 230 meters is my estimate for slip accommodated by this fault.

D2.2: Beck Fault

The fault plane is discrete, flat, and smooth with well-developed medium grain gouge below and well-cemented course tectonic breccia above (Figure 37). The 50-150 cm thick gouge zone below was developed in quartz-rich clastic sedimentary rocks and physical grain size reduction and grain rotation created what appears to be riedel shear fabrics. The upper- plate breccia is reversely graded. Near the fault plane, about 8 cm of fine-grained particles, the tectonic breccia grades upwards into a 50-100 cm thick zone of coarser grained clast-supported breccia. About one meter away from the fault the breccia grades into a tectonic fracture fabric with no observable rotation between blocks. Uniformly dipping laminations were recognized about 5 meters above the fault.

Though many cross-sectional exposures of the fault exist, the lateral exposure of the fault is limited because it is truncated by the structurally higher the Noonday Fault near Ashford Peak. As exposed, this fault does not interact with the structurally lower Crystal Fault. However, geometric constraints suggest the faults would intersect up dip, if both were not truncated. The cross-cutting relationship cannot be determined.

The Beck Fault is best exposed in the west wall of "V Canyon" below Ashford Peak and is best viewed from the adjacent "Knife Ridge". In this exposure, pictured in the photo at the top of Figure 37, the "Beck Fault" truncates bedding of the Crystal Springs Formation at a subtle angle and places steeply dipping Beck Springs Dolomite above moderately dipping upper Crystal Springs Formation. This fault relationship was inferred in other areas where a similar stratigraphic juxtaposition occurred.

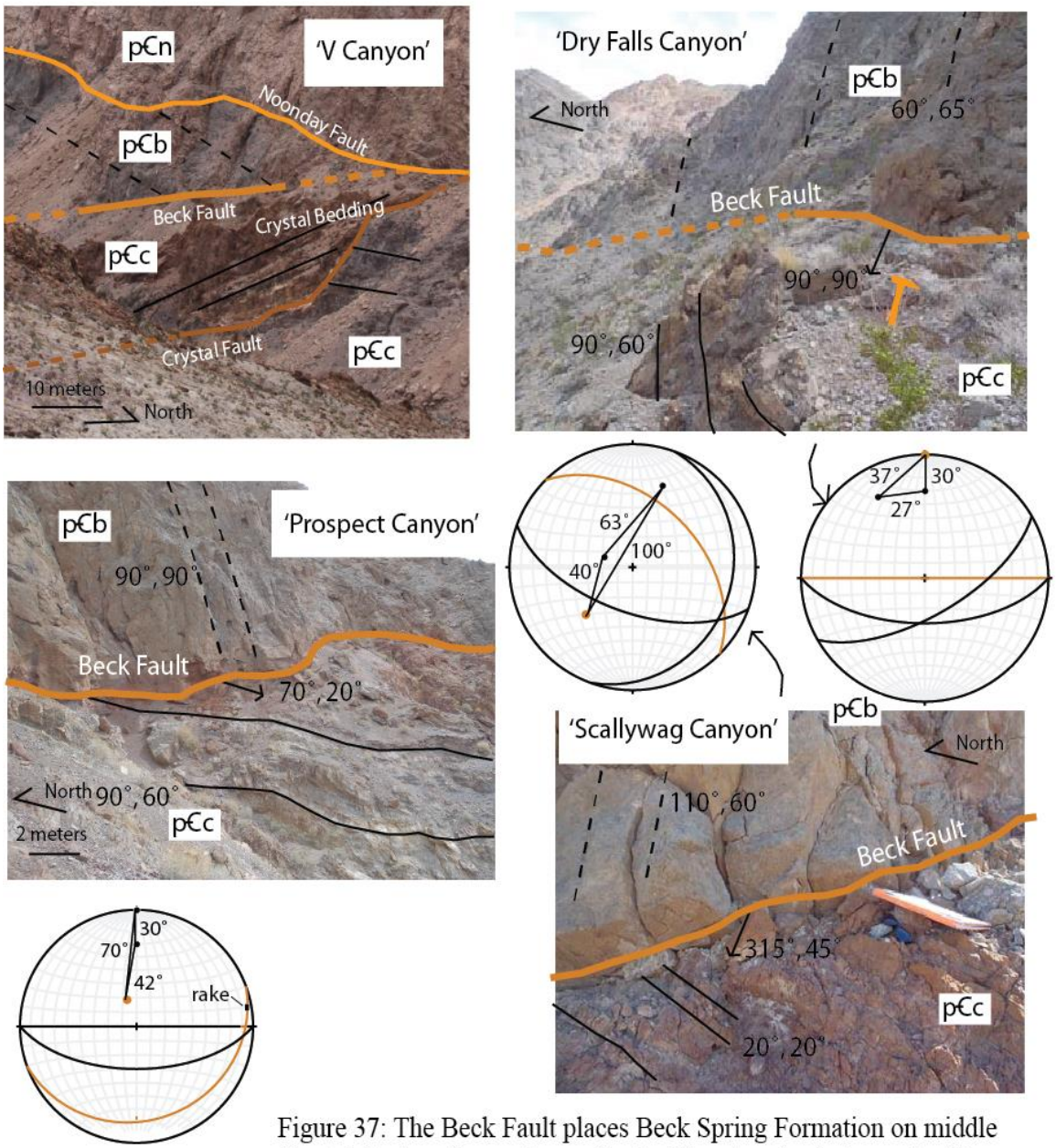

Figure 37: The Beck Fault places Beck Spring Formation on middle Crystal Springs Formation, with significant angles between bedding. In the stereonets, the pole to the Beck Fault is in orange. In 'V Canyon' (top, left) the cross-cutting relationships between three Chaos Faults can be seen. The Beck Fault cuts the Crystal Fault, and the Noonday Fault cuts both. (top, right) In 'Dry Falls Canyon' the Beck Fault is oriented 90˚,90˚. It makes a 30˚ and 37˚ angle with Crystal and Beck Spring bedding, respectivley. (bottom, left) In 'Prospect Canyon' the Beck Fault is oriented 70˚,20˚. It makes a 42˚ and 70˚ angle with Crystal and Beck Spring bedding, respectivley. (top, right) In 'Scallyway Canyon' the Beck Fault is oriented 315˚,45˚. It makes a 40˚ and 100˚ angle with Crystal and Beck Spring bedding, respectively.

Accessible exposures of the fault and adjacent bedding between “Scallywag Canyon” and “Dry Falls Canyon” were reached and measured. The fault plane is highly variable, as shown in the photos and stereonets in Figure 38. The observed variation is a manifestation of later phases of deformation, namely the Chaos Syncline of D3. It is difficult to resolve the original orientations of these planes without accounting for the later deformation, but an attempt is illustrated in Figure 38. A first order estimate of the slip on the fault is 470-1250 m.

D2.3: Noonday Fault

As the naming convention reveals, the hangingwall of this fault is dominated by the Noonday Dolomite. This dolomite is the platformal facies to the partially time-correlative Ibex Formation and both formations occupy sections of the upper plate. Though bedding, laminae, and algal features are recognizable sometimes, the overall structure of the upper-plate is broken into a field-scale, structurally isotropic breccia. This brecciation is pervasive throughout the mapping area

This fault is also best viewed from “Knife Ridge” (Figure 39), where it can be seen truncating the structurally lower Chaos Faults. This feature dominates the appearance of the western slopes of “V Canyon” as a low-angle fault contact running the length of the canyon wall. I speculate it is this feature that has inspired earlier geologists to discuss the Amargosa as a low-angle fault. From this vantage, the fault can be seen juxtaposing Noonday Dolomite against the crystalline basement rock, and to the south placing creamy-pink Noonday Dolomite over blue-gray Beck Springs Dolomite. The field area contains many such relationships and it is my observation that the Noonday

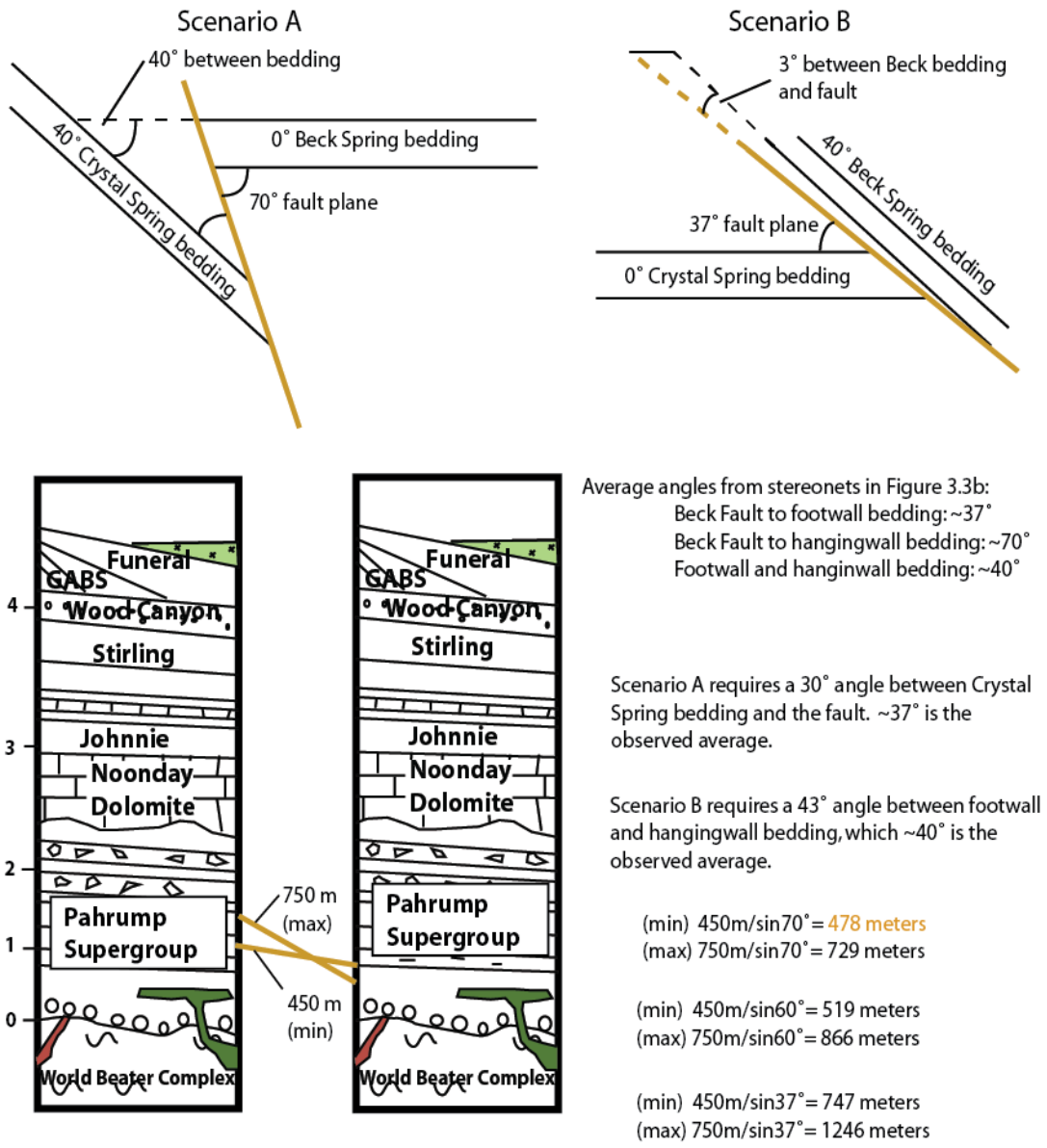

Figure 38: The estimated stratigraphic offset by the Beck fault is 750 meters (maximum) and 450 meters (minimum). If the differences between bedding and the fault are averaged, and we assume either the hangingwall or footwall rocks were horizontal at the time of faulting, an estimate for the minumum amount of slip can be calculated using trigonometry. The minumum value calculated is 478 meters, which is my estimate for minimum slip on the Beck Fault.

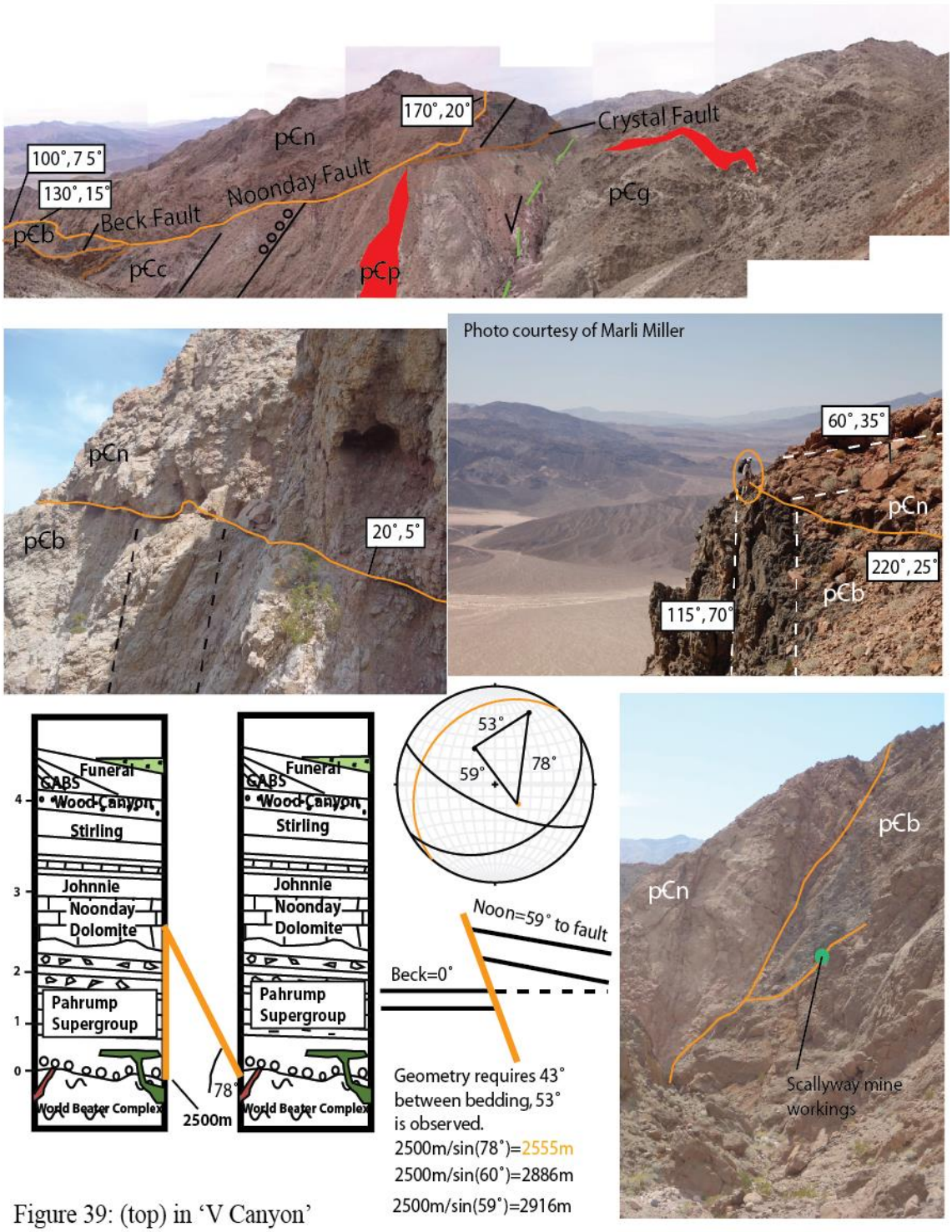

Figure 39: (top) in 'V Canyon' the Noonday Fault cut the lower Chaos Faults and places Noonday Formation in fault contact with the cyrstalline basement. In 'Dry Falls Canyon'and near 'Scallyway Canyon' the fault (middle left and right, respectivley) the fault places Noonday against steeply dipping Beck Spring Dolomite. This horizon was exploited by the Scallywag Mine (lower right). Given the angle of the fault and stratigraphic offset, I estimate the minimum slip at ~2555 m.

Dolomite is everywhere in fault contact with the rocks below it. Sections of this fault were mapped using satellite imagery from ArcMAP and inferring the above observation.

Exposures of this fault on the south face of 'Dry Falls Canyon' below 'Ashford Ridge' offer close-up observation of the fault surface and zone. Similar to the 'Beck Fault', the fault plane is flat, smooth, and discrete, but the gouge zones above and below the fault differ. The lower plate, composed of Beck Springs Dolomite at this location, is altered to a red, hematite rich, and fine-grained gouge with occasional secondary calcite mineralization. This zone has been scavenged for extractable resources and is riddled with cavernously weathered prospect pits. The upper-plate is brecciated, but to a lesser degree than seen above the Beck Fault.

Bedding is unreliable in the upper plate, due to the pervasive tectonic brecciation. Because of this limitation, the geometric relationships between the fault and bedding are not well measured. The fault exposures show a wide range of orientations: in “V Canyon” the fault plane is oriented N80°W, 75°S. To the northeast the orientation is N50°W, 15°SW. At “Ashford Ridge” the plane is oriented N20°E, 5°E, and north of “Scallywag Canyon” the fault is oriented N60°E, 25°N. In the last location, the Noonday contains three orange carbonate marker beds with intact bedding measured at N60°E, 35°S. These beds lay at a ~38° angle with Beck Springs laminations, which are consistently measured near N65°W, 70°S. The fault plane makes a 70° angle with Beck Springs laminae and 60° angle with the Noonday bedding. These relationships are used in Figure 39 to estimate the faults offset. I estimate the minimum slip accommodated by the Noonday Fault as approximately 2500-3000 meters.

D2.4: Johnnie Fault

This fault is best exhibited as the several Johnnie Formation klippen on the south slopes of the "Noonday Bulb" and Ashford Peak. The eastern-most of these klippen is the best example of the general relationship between Johnnie Formation and Noonday Dolomite, and the relationship was inferred in the rest of the field area (Figure 40).

The physical fault plane is not well exposed and the fault zone generally does not contain gouge, but bedding in the hangingwall meets bedding of the footwall at a high angle. The upper plate bedding is oriented at N55°W, 65°SE. The N30°E, 5°E fault cuts bedding at 60°. The Johnnie klippe on the southern flank of Ashford Peak has bedding oriented N80°E, 50°S with the basal fault oriented much steeper, at N65°W, 70°S.

In other locations, the following relationships are observed: Johnnie fault measured at N65°W, 55°SW and Noonday Dolomite bedding above the fault is oriented N45°E, 85°SE, 77° to fault, while the Johnnie Formation beds below are oriented N80°W, 70°S, 51° to fault. Thus, the hangingwall bedding makes a 55° angle to footwall bedding;

elsewhere the fault steepens to N80°E, 85°S or is overturned to N75°E, 75°N, where Johnnie bedding contacts the fault at ~90° angle (Figure 40, lower right).

Stratigraphically, this fault places middle Johnnie Formation over Noonday Dolomite. This juxtaposition represents ~600 meters of missing stratigraphy. The observed angle of the fault yields an estimate of 900 meters, while a 60° fault would require 700 meters of slip to produce the stratigraphic offset.

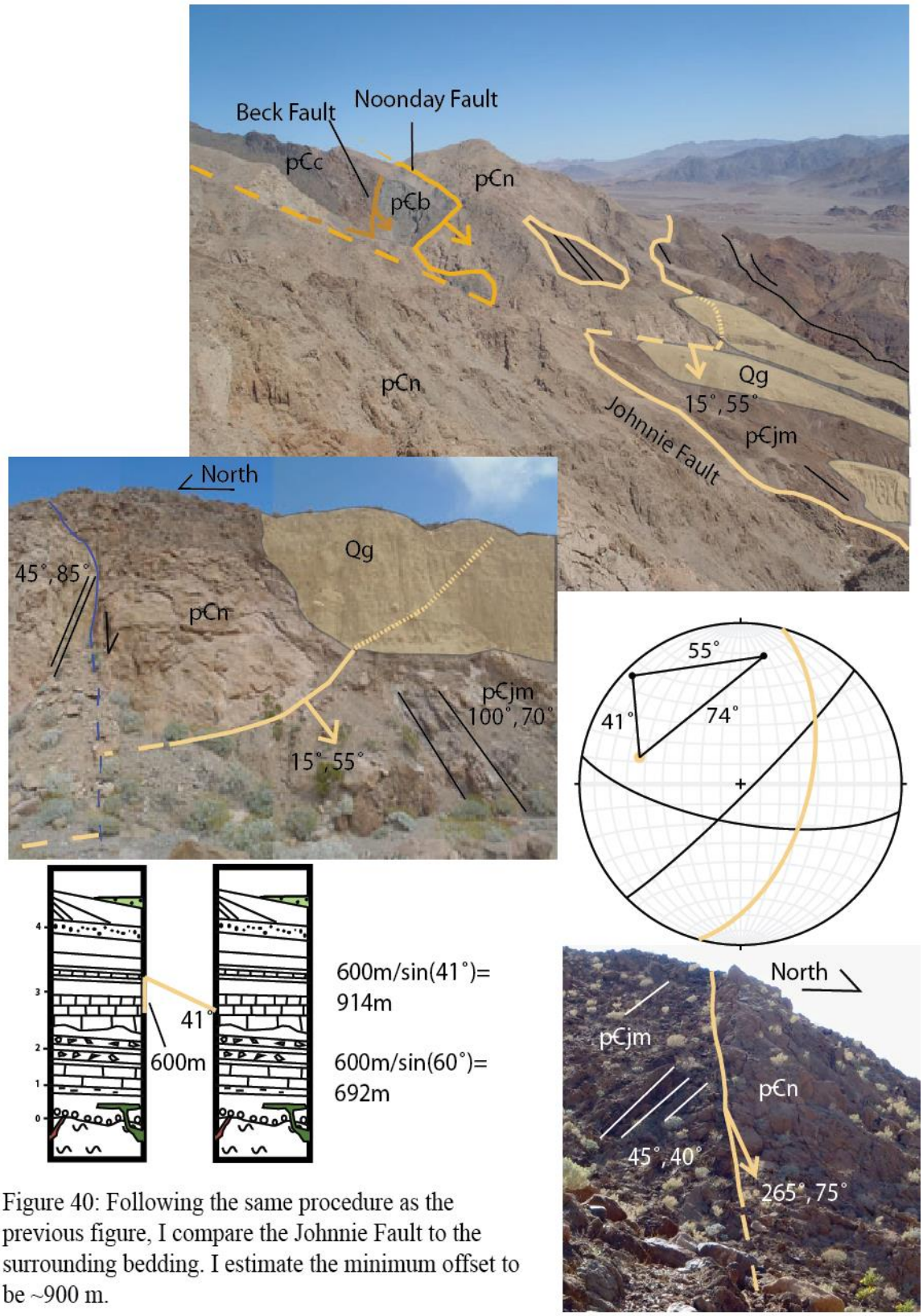

Figure 40: Following the same procedure as the previous figure, I compare the Johnnie Fault to the surrounding bedding. I estimate the minimum offset to be ~900 m.

D2.5: Upper Johnnie Fault

This fault is most clearly observed on the east face of west “Tall Johnnie Hill”, as viewed from the east “Tall Johnnie Hill” (Figure 41, top). At this location, the fault exhibits a flat and discrete plane with very little brecciation in the fault zone. This observed relationship is extrapolated to similar stratigraphic juxtapositions in the field. This structure is the least understood of the 'Chaos Faults' and also has the fewest measurements for geometrical control. Between the two 'Tall Johnnie Hill', I mapped this fault cross-cutting the structurally lower 'Johnnie Fault'. This relationship is not exposed anywhere else and needs to be explored further. On the south flank of the western 'Tall Johnnie hill' is a good accessible exposure of the fault plane, oriented N50°W, 15°N. This makes ~47° angle with the upper plate Johnnie Formation bedding.

Using the geometric relationships described above, the minimum slip estimated is approximately 400 meters. If a 60° dip is used for the fault, the slip is 340m. But, the Johhnie Oolite can be used as a piercing plane between the 'Tall' and 'Short Johnnie Hills'. The shortest map distance drawn between the offset oolite beds yields a length of 1.6 km and a N10°W direction. I derive an estimate of 2300 m= 1600m/COS(47).

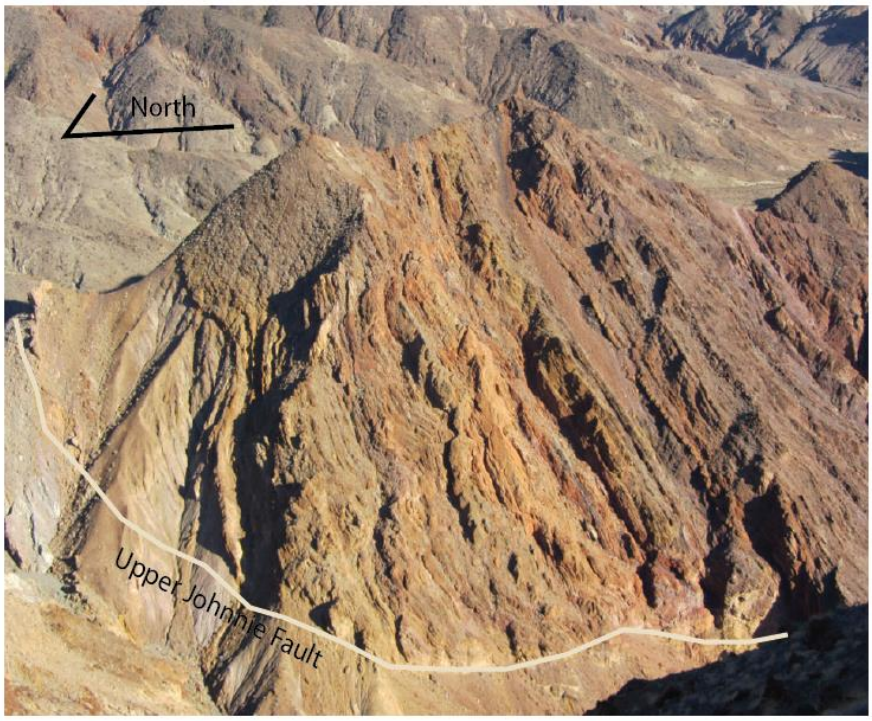

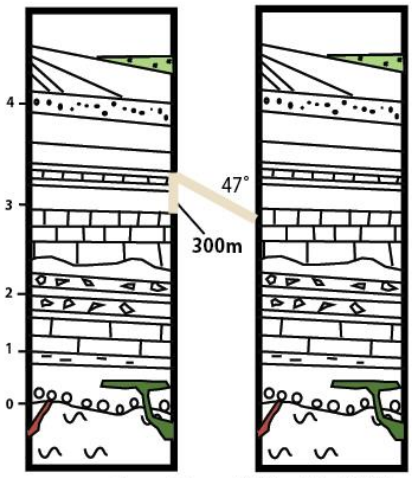

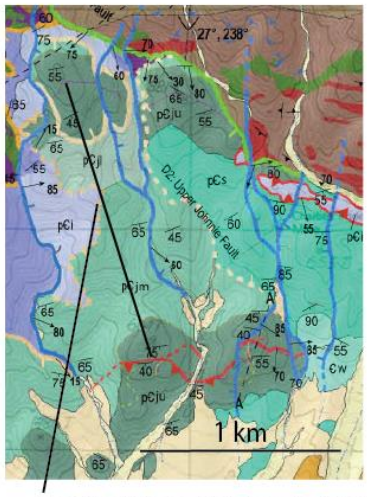

Using stratigraphic offset: 300m/sin(47°)= 410m
300m/sin(60°)= 340m

Using map offset: 1600m/cos(47°)= 2,300m
1600m/cos(60°)= 3,200m

Shortest map distance between offset oolite marker bed: 1.6 km

Figure 41: The Upper Johnnie Fault juxtoposes upper Johhnie Formation against Noonday Dolomite and lower Johnnie Formation. The only measurement of the fault (N50˚W, 15˚N) makes a 47˚ angle with the hangingwall bedding. The geometry and stratigraphic offset combined suggests ~400 m slip. The map distance offset between oolite marker beds is 1,600 m, which requires ~2,300 m of slip.

Chaos Fault Orientations

Essentially, the Chaos is composed of large, lozenge-shaped slabs of rock, separated by a system of shingle-style faults. The fault system is here named the Chaos Fault system. Figure 42 is a compilation of stereonets showing fault orientations and estimated slips. The sum of all slip estimates totals to ~4.25 km. All the Chaos Faults appear to be folded about similarly oriented axes, which will be described next. Notice the upper Johnnie Fault has a different geometry.

D3: Broad, East-Southeast Plunging Fold Pair

The overall map pattern depicts a southeast-trending fold pair that includes the basement cored Desert Hound Anticline and a syncline cored by the Virgin Spring Chaos that is here named the Chaos Syncline (Figure 43, top). The map shows the fold pair offset and the hinges are not oriented parallel. Stereonet analysis shows the Desert Hound Anticline (DHA) trends east-southeast, while the Chaos Syncline (CS) trends southeast. If the two were originally sub-parallel, the CS has been rotated clockwise.

Desert Hound Anticline

The map pattern suggests this fold is generally shallowly plunging and trending east-southeast. Foliation of the local Paleoproterozoic gneiss is well characterized and documented in Wright and Troxel (1984). I conducted the analysis using their measurements. Patterns in foliation suggested the presence of multiple fold hinges in an oblique superposition to one another (Figure 44). Using the analytical method from Turner and Weiss (1963), called the “Analysis of a Superimposed Fold System”, I have calculated a more accurate estimate of the trend and plunge: 30°, S70°E.

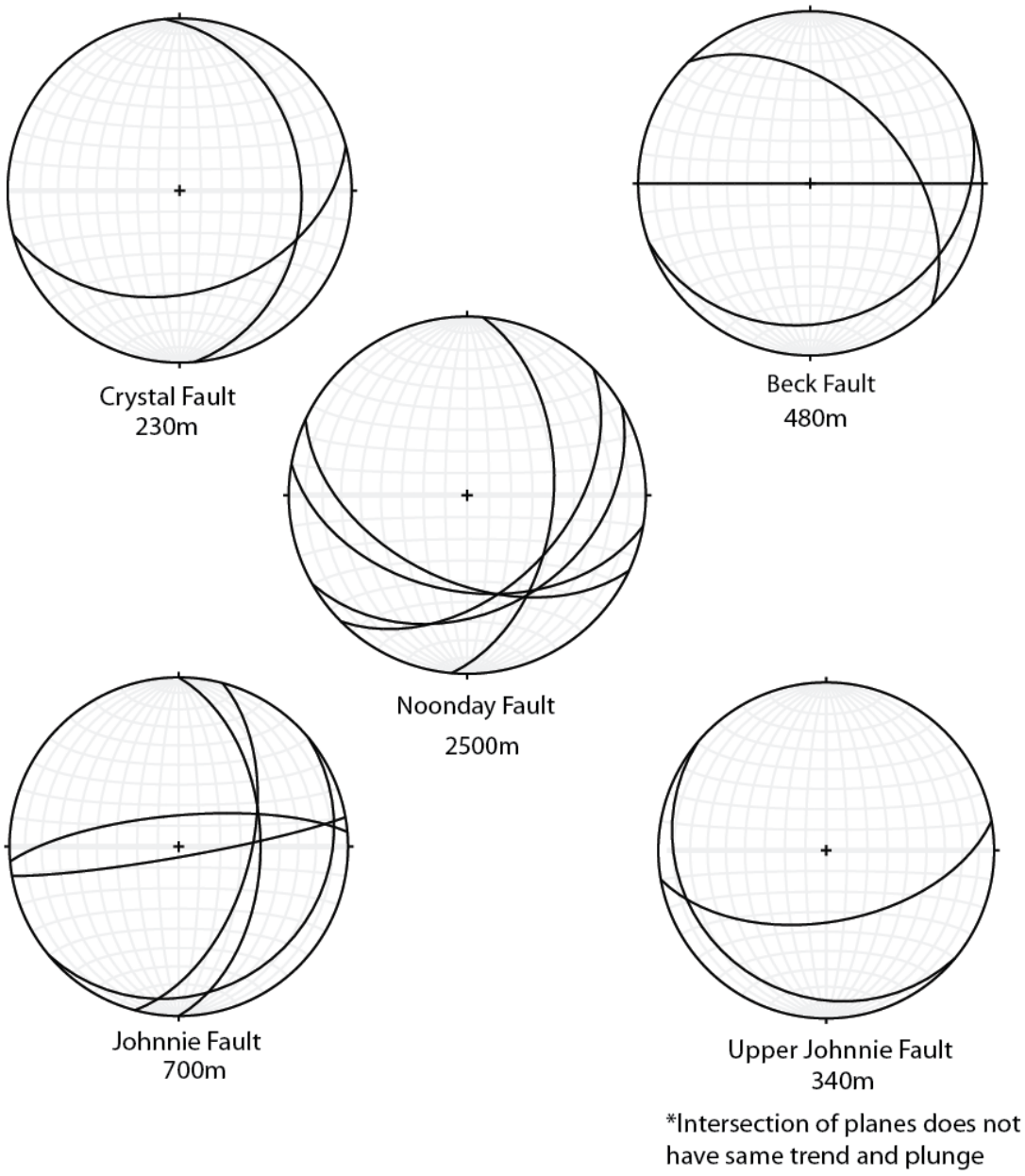

Figure 42: These stereonets show the variable geometry of the Chaos Faults as they are folded about an east-southeast plunging axis. Minimum slip values were calculated in 2-D. The system is collectivley responsible for an estimated 4.25-8.7 km of extensional slip.

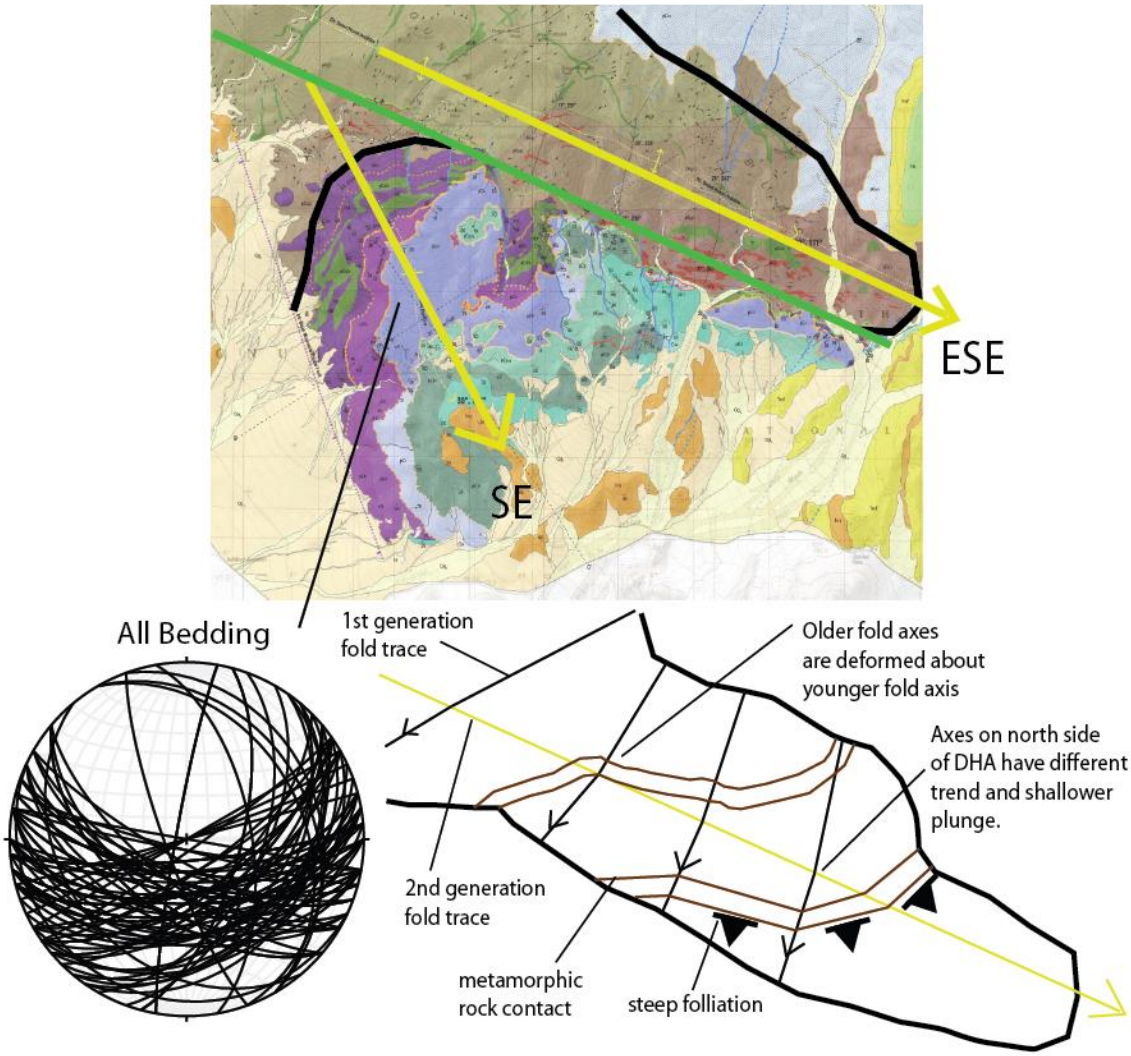

Figure 43: (top) The map pattern of the contact between basement gneiss and Proterozoic sedimentary rocks suggests a fold pair, with the nose of the anticline pointing in the direction of plunge. The fold axes are offset along the Amargosa Fault and are not parallel. The stereonet shows planes of all bedding, again showing a geometric pattern of a fold. The schematic illustrates the hypothetical relationships between steeply orientied basement folliation, metamorphic rock contacts, and generations of folding.

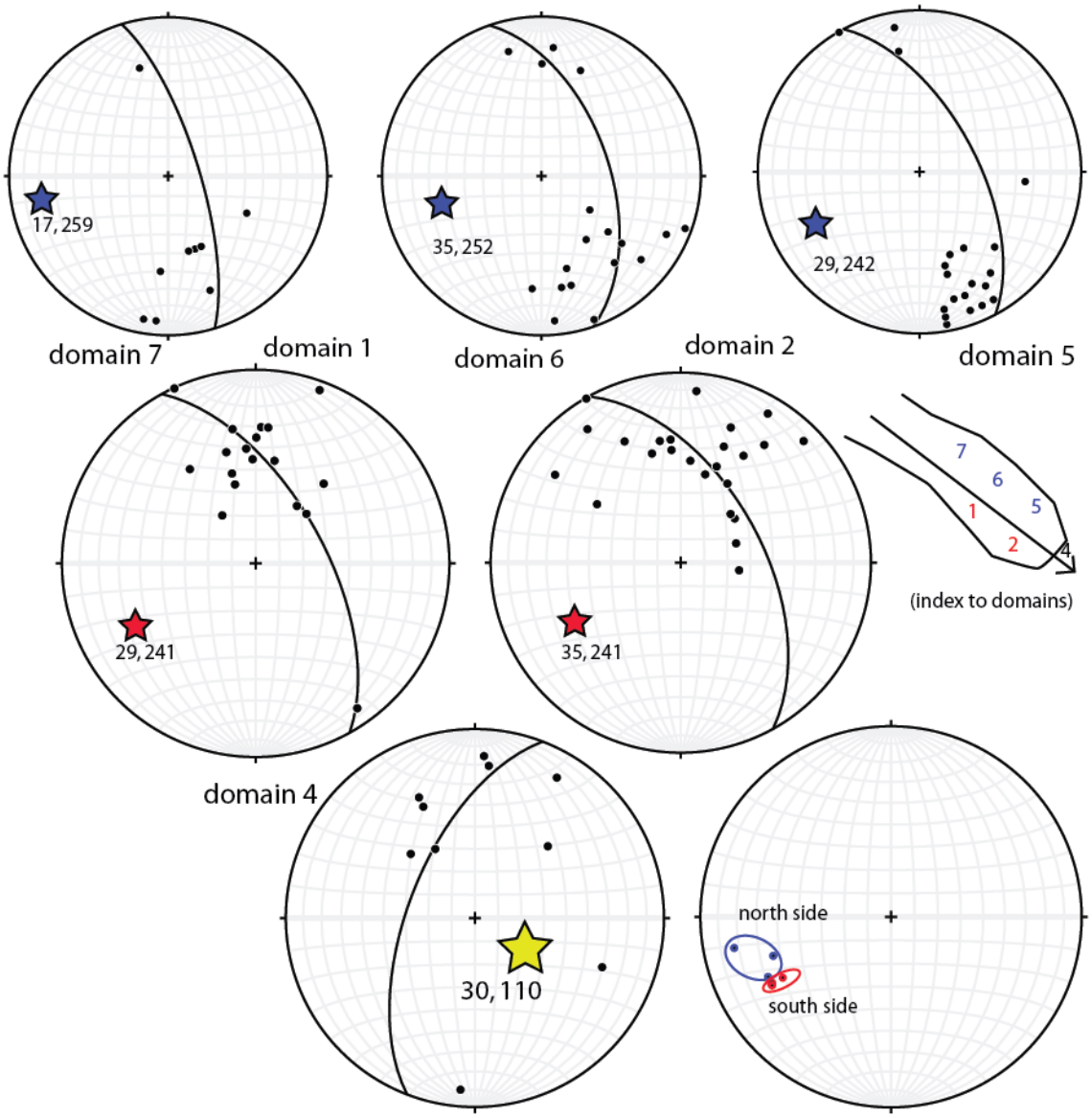

Figure 44: Superimposed fold assesment:
The top stereonets represent domains chosen to characterize the first generation fold axes. These correspond to the blue symbols on the map. See text for explaination on designating domains. Domain one and two are south of the second generation hinge, while domain five, six, and seven are on the north side, as shown in the index to the right. Domain four, the red symbols on the map, characterizes the second generation fold axis, known as the Desert Hound Anticline. The lower right stereonet shows the orientation of all first generation fold axes. The first generation fold axes appear to change orientation with respect to the hinge of the anticline.

In accordance with the method, domains were chosen and color coded on the map. Foliation chosen from the limbs of 1st generation of folds characterized the trend and plunge of that generation. These domains are colored blue. Foliation chosen from the intersection of both the 2nd generation and the 1st generation characterized the trend and plunge of the 2nd generation. This domain is colored red. The conceptual relationship is illustrated in Figure 43 (bottom), showing both sets of folds interacting with steep foliation, while the orientation data of the domains is shown in Figure 44.

When the blue domains were plotted, patterns revealed two sets of fold axes. The folds on the south side of Desert Hound Anticline are generally steeper and trend more southerly. While the folds on the north side progressively shallow and trend more westerly up-plunge (northwest). Plotting of the foliations of the red domain reveal patterns that suggest the axis of the Desert Hound Anticline is oriented 30°, S70°E. This analysis suggests the east-southeast plunging Desert Hound Anticline is superimposed over older southwest plunging folds. The first generation of folds was deformed differentially about the second axis of folding, giving rise to the radial pattern of the axes.

Chaos Syncline

The map pattern and field data indicate this syncline is trending south to southeast. This syncline was represented by Wright and Troxel (1984), both in map pattern and cross-section. Figure 45 shows a steronet plot of selected field data to characterize the fold. The approximate orientation of the fold is ~60°, S35°E.

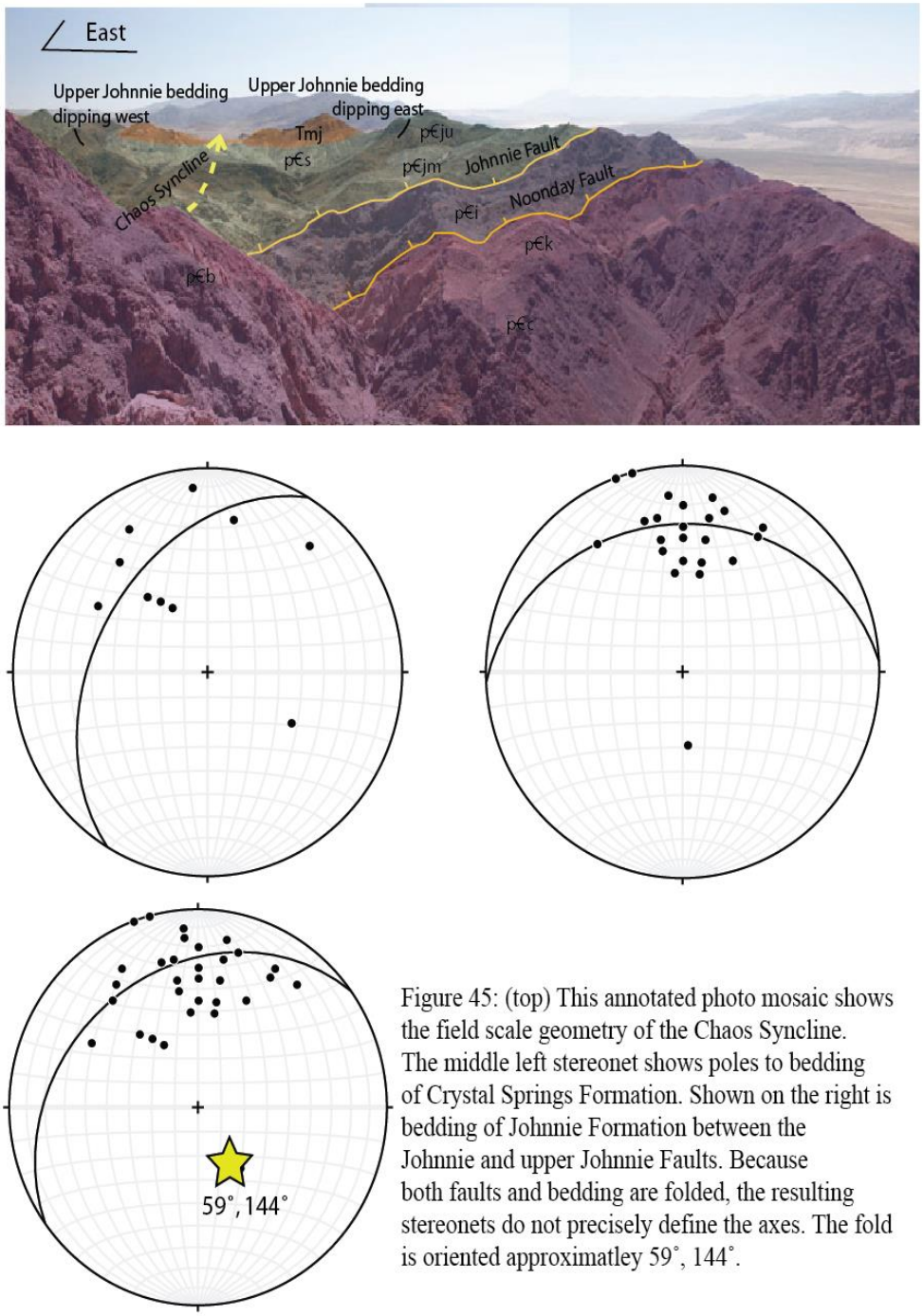

Figure 45: (top) This annotated photo mosaic shows the field scale geometry of the Chaos Syncline. The middle left stereonet shows poles to bedding of Crystal Springs Formation. Shown on the right is bedding of Johnnie Formation between the Johnnie and upper Johnnie Faults. Because both faults and bedding are folded, the resulting stereonets do not precisely define the axes. The fold is oriented approximatley 59˚, 144˚.

As established, the area is composed of rock slabs separated by the shingled Chaos Faults. However, more detailed analysis is required and this orientation is not a precise estimate. The planes composing each of the first generation of structures have been folded differentially about the primary axis of folding. I have simply estimated the axis by lumping together all the slabs. To be more precise, each slab should be plotted separately and the collective axes from each slab should be analyzed for a pattern. For example, the difference between the Crystal slab and Johnnie slab fold axis is shown in the middle set of stereonets of Figure 45. However, the current amount of bedding orientation data is not dense enough in most slabs to complete such an analysis.

D4: Dextral Oblique Normal Fault (Amargosa Fault)

This section of Amargosa Chaos is bound on the north, against the Desert Hound Anticline, by a prominent N60°W trending fault that has classically been defined as the Amargosa Fault. As defined, this fault here juxtaposes Paleoproterozoic basement rock against Meso-Neoproterozoic sedimentary rock in an up-to-the-northwest sense. My mapping more completely defines this fault and suggests an estimate for the amount of slip accommodated by the structure.

The consistent strike and dip of the Amargosa Fault, N50°W and N85°E, and dips 70-60°is highlighted in the map and stereonet of Figure 46. Northwest of “Grey Wizard Pass”, Wright and Troxel (1984) show three splays of the fault. I have refined this to show the main trace on strike with the southeast segment. I have not observed the Proterozoic sedimentary rocks in the footwall of the Amargosa Fault. Also, the fault is high-angle, brittle, and within the basement rock.

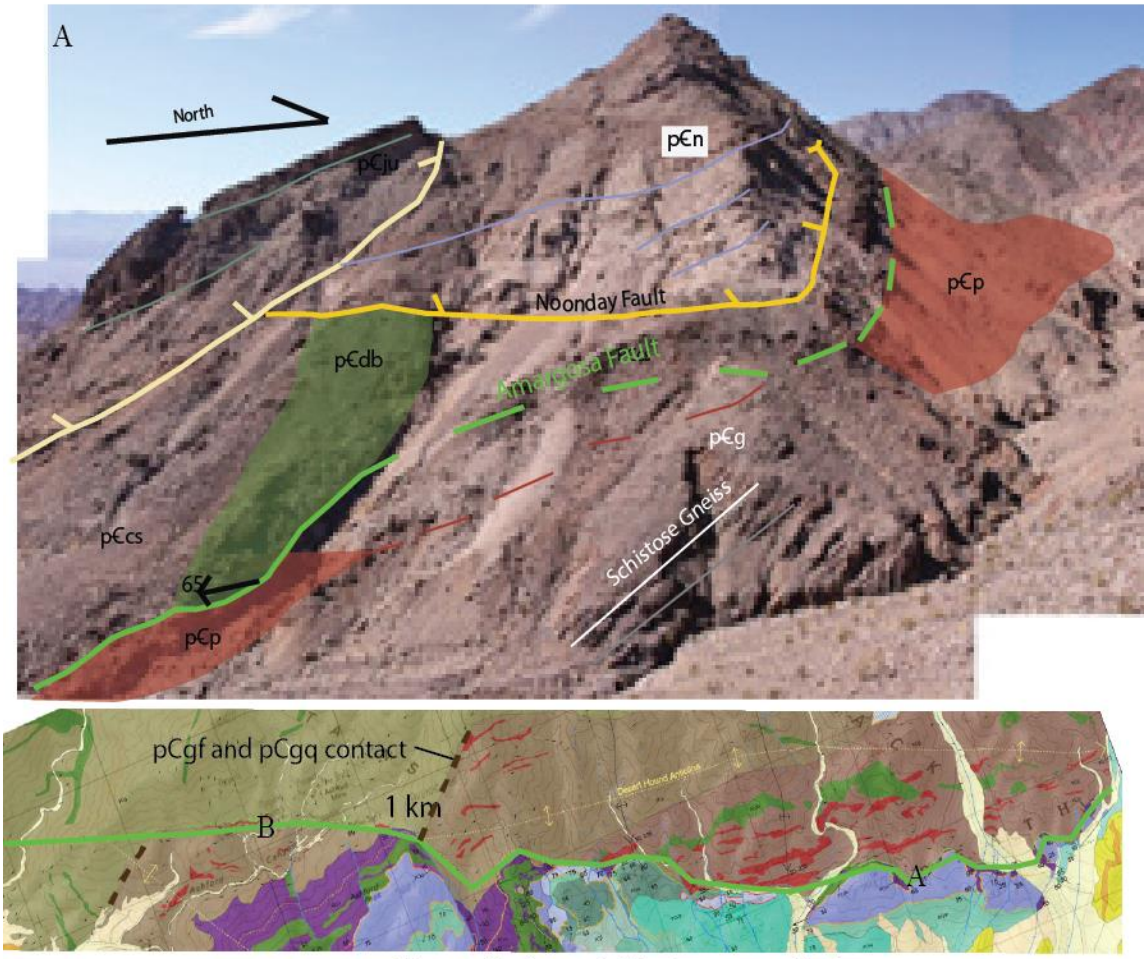

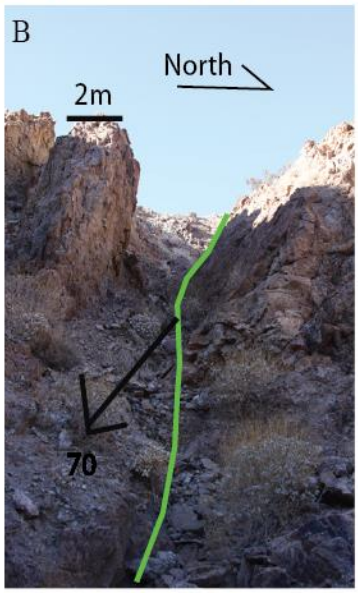

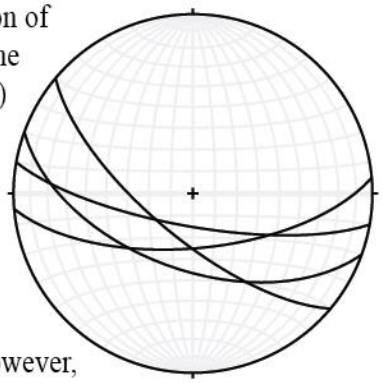

Figure 46: (center) The Amargosa Fault exhibits a consistent orientation of ~N60˚W, 65˚ SW, shown on the stereonet. In the field, (photos) the fault contacts the basement gneiss and Neoproterozoic were not observed in the footwall. Thick gouge zones have led others to suggest the fault accomodated 10's km slip. However, my investigation of the rock strengths suggest the thick gouge zones are produced by the quick physical reduction of mineral grains of the pegmatite in the fault zone. A metamorphic contact is offset by the fault and is used to estimate slip in the next two figures.

To assess slip on the fault, I use the lithologic contact between the Precambrian gneiss unit pЄgf and pЄgq, which is offset 2,800 meters right-laterally (Figure 47). The contact is diffusive and deformed, so some error occurs when using this contact as a piercing plane. This contact is dipping steeply toward the south-southeast, assuming the contact is sub-parallel to foliation. To estimate pure dip-slip, the gneiss contact must be projected into the fault plane (Figure 48). In Scenario A, a predictable folded geometry is assumed based on previously discussed basement folds. In Scenario B, no correction is made for folding and the contact is assumed to be planar. I favor Scenario A, therefore I estimate the amount of slip on this fault as approximately 8,500 meters. Scenario B produces ~14,000 meters of slip, which is approaching previous estimates for the maximum amount of slip by a different method (Miller, 2002). Miller estimate slip by imposing a N60W slip direction and using the basal conglomerate as a piercing plane.

Slickenlines and other kinematic indicators are present at fault exposures, but are widely variable and so are not used here to constrain sense of slip. The fault could be pure strike-slip or pure dip-slip, but it is most likely somewhere in between. The above estimates incorporate both end members.

D5: Domino Faults

These sub-parallel high-angle faults cut the previously described structures. The faults are generally north-northeast striking and have normal displacement. They have been described as features that accommodate the intervening rock-blocks like dominoes: the faults are synchronously offset and rotate the blocks (Wright and Troxel, 1977). This

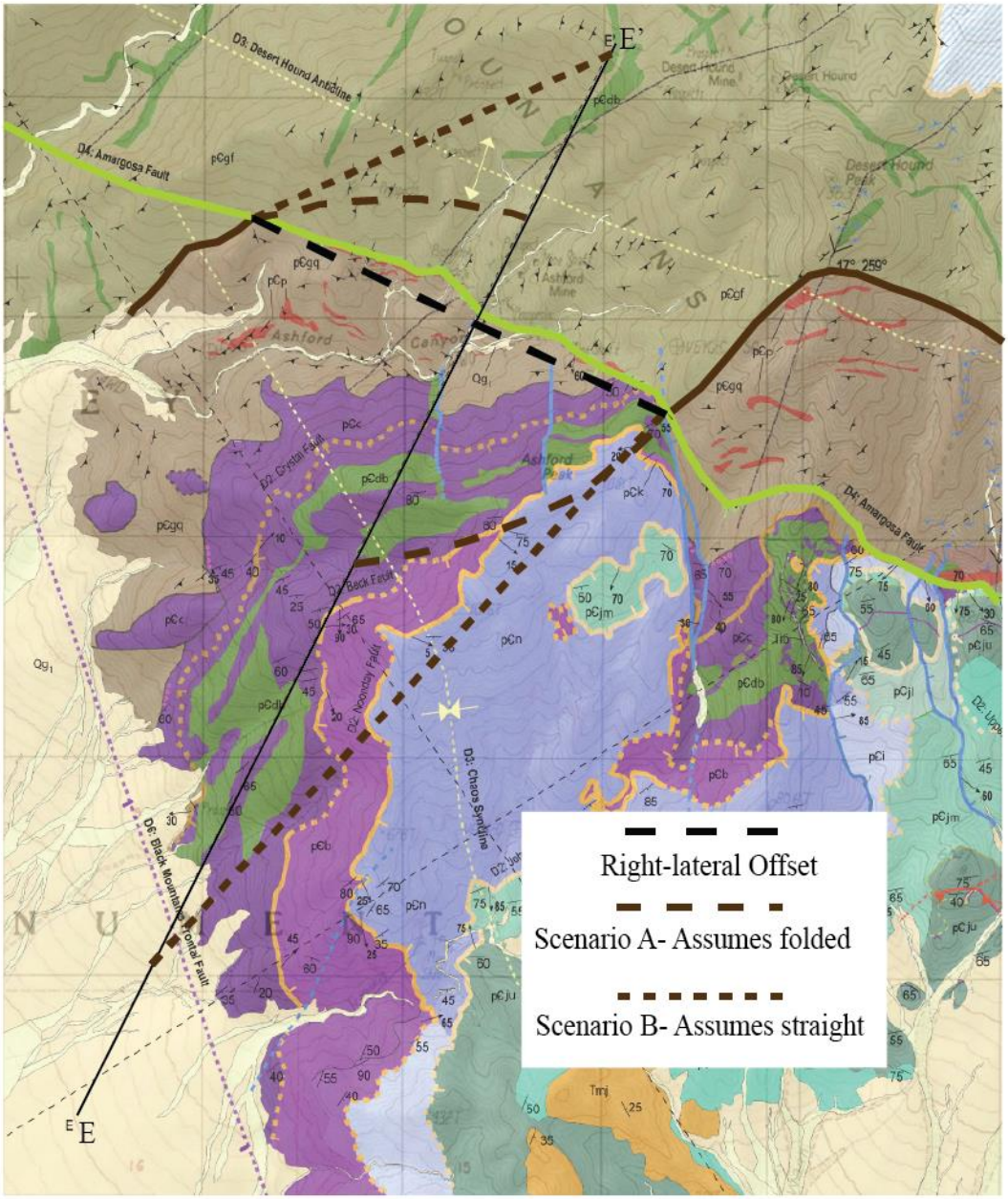

Figure 47: The Amargosa Fault offset the contact between pCgf and pCgq. The offset is 2.8 km in a pure right-lateral sense, but observed slickenlines show a vertical component. To analyze the pure dip-slip motion required to create the offset, I must make an assumption about the subsurface geometry of the metamorphic contact. In Scenario A, I assume the contact has a folded geometry similar to the exposed section. In Scenario B, I project the contact straight and assume no curvature. Because the folded geomety is exposed locally, I prefer Scenario A. The measured map distance of the offset metamorphic contact can now be used to assess the offset down the fault plane.

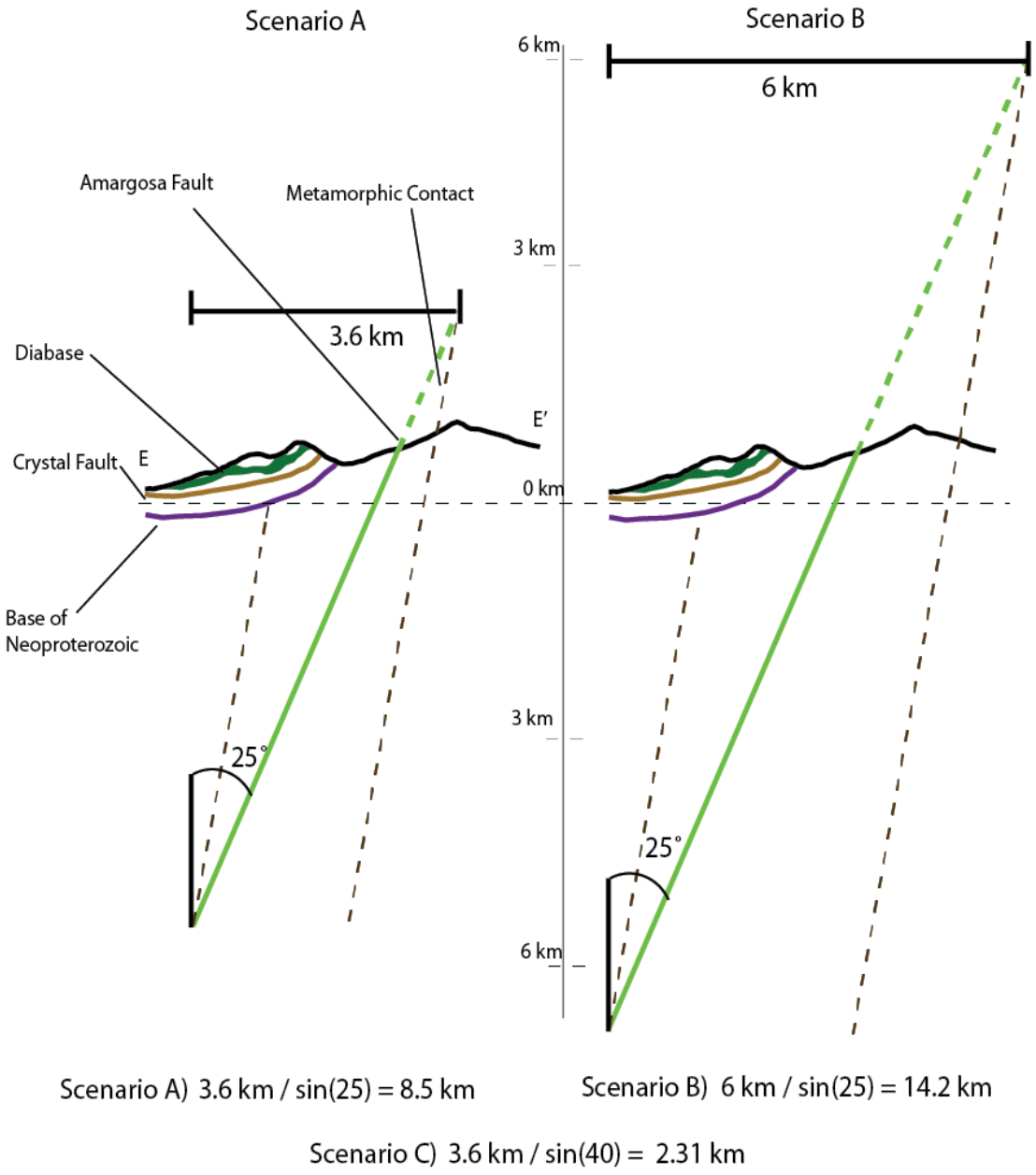

Figure 48: The Amargosa Fault dips consistently 75˚, while the metamorphic contact dips ~80˚. The map distance measured in Scenario A is 3.6 km. The resulting length between the offset metamorphic contacts is ~8.5 km. The map distance measure for Scenario B is 6 km, and the resulting length is ~14.2 km. My esimate of the Amargosa Fault slip is ~8-14 km if the sense was pure normal and ~3 km if pure strike-slip.

pattern of blocks requires multiple faults and encourages a "distributed faulting" view of local tectonics.

The D5 faults cut across widely varying orientations of contacts, which yields various apparent offsets post-faulting. For example, the D5 fault running the length of Virgin Spring Wash is down-to-the-east, but the apparent offset in the north and south is opposite, right-laterally and left-laterally respectively. In the north, the major structure is dipping north, producing a left-lateral apparent offset. The Amargosa fault is offset right-laterally <10 meters by most splays of the same fault.

These faults generally have poorly developed fault planes. Instead, the trace of these faults is most prominently marked by the major drainage pattern of the area. In many canyons, the walls simply do not match rock type or major faults do not project across the fault. Fault planes of these features were occasionally observed and measured; orientations are shown in the stereonet of Figure 49. Notice the change in trend of these faults from east to west in the map area.

D6: Black Mountains Frontal Fault

In aerial view (Figure 50, lower right), it is quite clear that a fault is responsible for creating the bedrock composed topographic rise with wine glass canyons and steep alluvial fan slop. This fault is not responsible for any of the Chaos assembly, but essentially exposed the Chaos enabling observation. This range-bounding fault has been called the Black Mountains Frontal Fault by Holm *et al*. (1994). Noble (1941) and Brogan *et al*. (1991) mapped fault scarps in alluvial fans in the immediate area. The fault was not directly observed or measured in the field, but was mapped by general

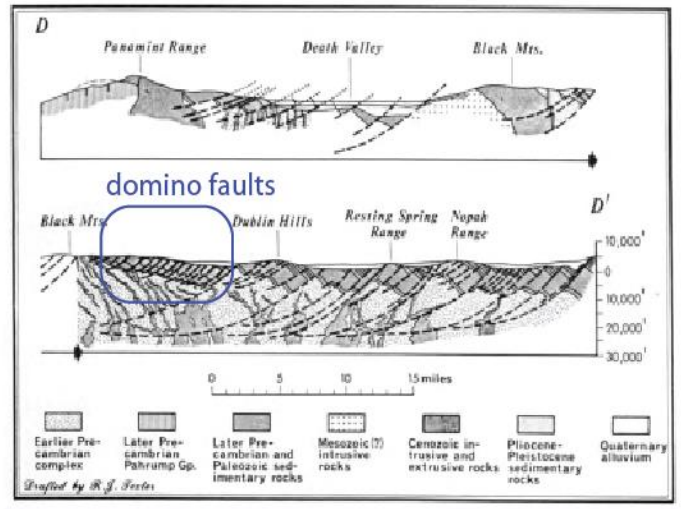

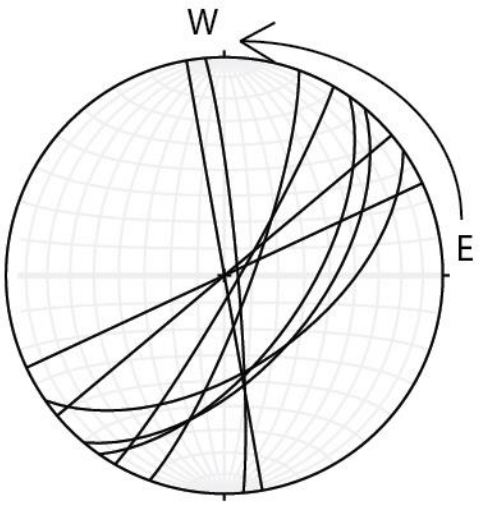

Figure 49: (diagram at top) This Wright and Troxel (1973) figure represents what is referred to as "domino faulting" or "distributed faulting". The blue box was added to draw focus to the domino faults. These faults are sub-parallel and the blocks behave like dominos. Fault attitudes change spatially: in the east of the map area the faults have moderate dips and east-northeast strikes, but orientations progressively become steeper and strike north-northwest toward the west.

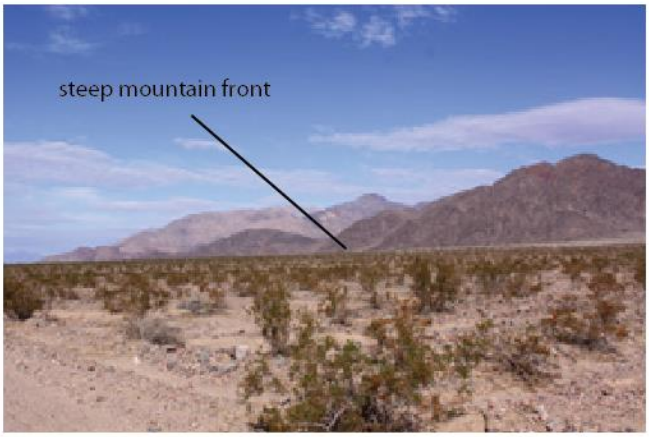

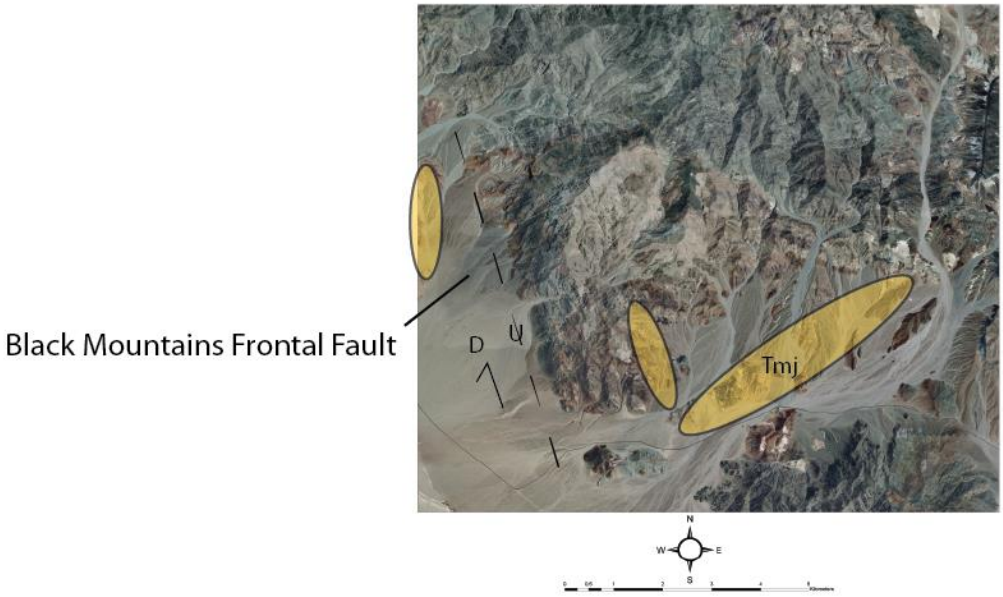

Figure 50: The Black Mountains Frontal Fault is well documented and Quaternary fault scarps were previously mapped between Ashford mill and Mormon Point. The fault creates the steep mountain front that can be observed from the ground (below) or aerially (right). The fault is significant to this study for exposing the Chaos, but did not form any part. This fault drops the Jubilee Chaos formation down and right-laterally relative to other outcrops, but no stratigraphic correlation exists. This offset is consistent with a N60W transport direction.

geomorphic expressions. The Qg_1 fans show an increase in slope approximately 200-1000 m from the bedrock range front. The increase in slope is indicative of the hangingwall fan gravels dropping down on the fault.

Summary of Inferred Relative Timing

Cross-cutting relationships observed in the field, which are represented and color coded on the map, suggest the following inferred relative timing: D1) north-northwest directed shortening on faults and folds (Imbricated Oolite System in red); D2) stratigraphic attenuation on five presently low-angle shingle-style normal faults (Chaos Fault System in orange); D3) Long wavelength, broad folds called the Desert Hound Anticline and Chaos Syncline, both of which plunge shallowly to moderately southeast (yellow); D4) dextral-oblique shear on a prominent high-angle fault that borders the assemblage (Amargosa Fault in green); D5) east-west extension on brittle high angle domino-style faults (blue); D6) extension on the Black Mountain Frontal fault (purple).

CHAPTER IV

ADDITIONAL OBSERVATIONS AND ANALYSES

Pegmatite Yields Thick Gouge

I conducted rock mechanic experiments to test the field hypotheses that the local variations in gouge thickness on the Amargosa Fault can be attributed to pegmatite abundance in the footwall. Figure 51 illustrates the spatial correlation between areas of thick gouge and amount of pegmatite in the footwall. The schematic diagram at the bottom of the Figure 51 shows, conceptually, how the amount of pegmatite in the footwall can affect the thickness of gouge. The experimental result generally support the hypothesis, but more tests need to be conducted for more robust support of the hypothesis.

The rock disks featured at the top of Figure 52 were fractured using a point-load device. The force required to fracture the rock is proportional to the maximum tensile strength of the rock. The results show the gneiss rock strength reached the maximum capacity of the rig, while the pegmatite consistently fractured. These results suggest the gneiss has higher tensile strengths.

The graphs represent the results from the uniaxial compression tests and show displacement as a function of yield strength; the peaks represent the ultimate strength yield strength of the rock type. The pegmatite has the greatest compressive yield strength, but consistently fractures under tensile stress. The pegmatite also has the widest maximum fracture zone, which is up to five times wider that the quartz-feldspar-biotite unit of gneiss. This is the lab result, but the same relationship is observed in the field.

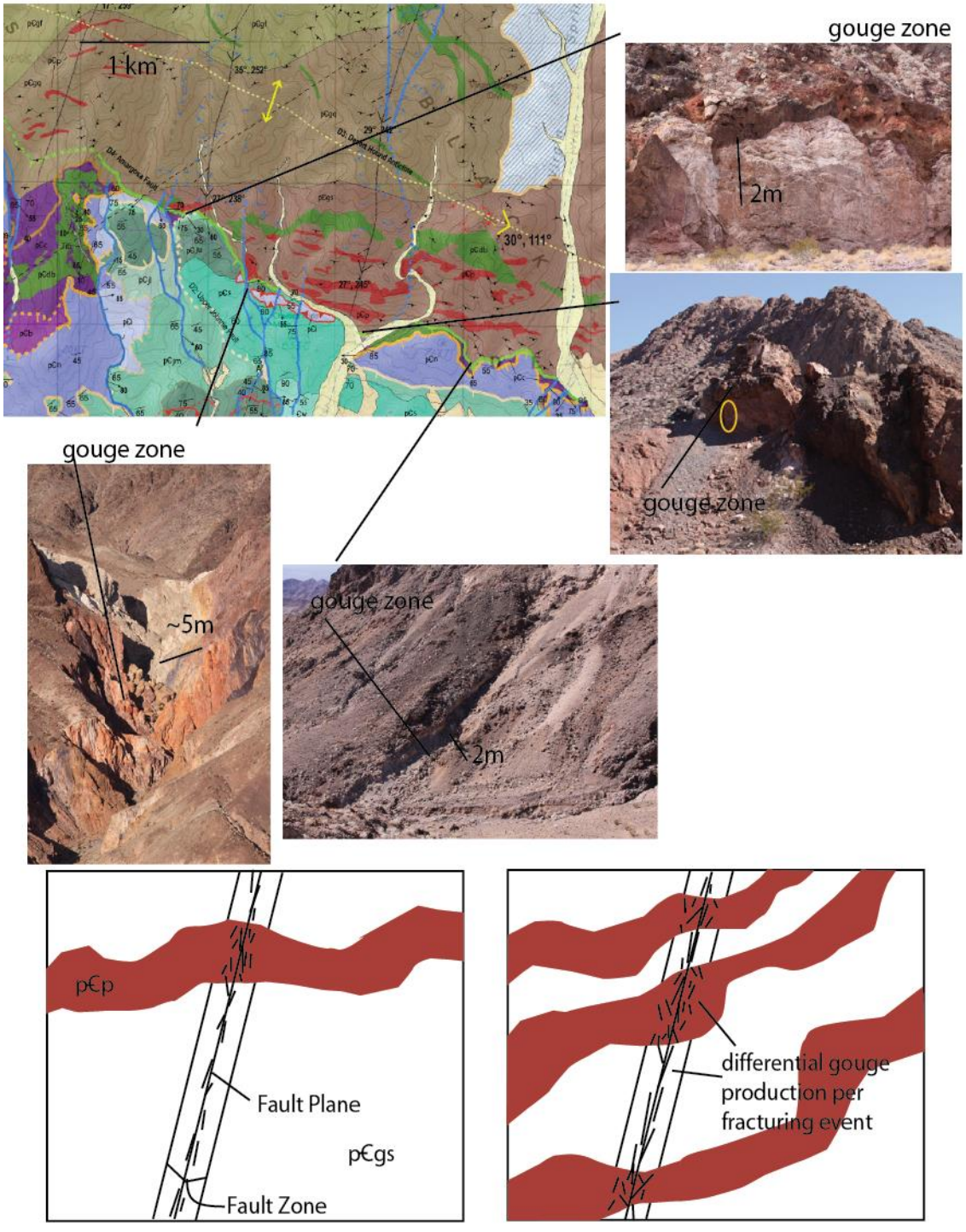

Figure 51: In the field, the Amargosa Fault has a thick accumulation of fault gouge only on the eastern segment of the fault. The exposures of thick gouge are associated with the presence of pegmatite.This observation led to the field hypothesis that fault gouge thickness is a function of pegmatite area in the fault plane. The conceptual illustration below shows how the amount of pegmatite in the fault zone can affect the thickness of gouge.

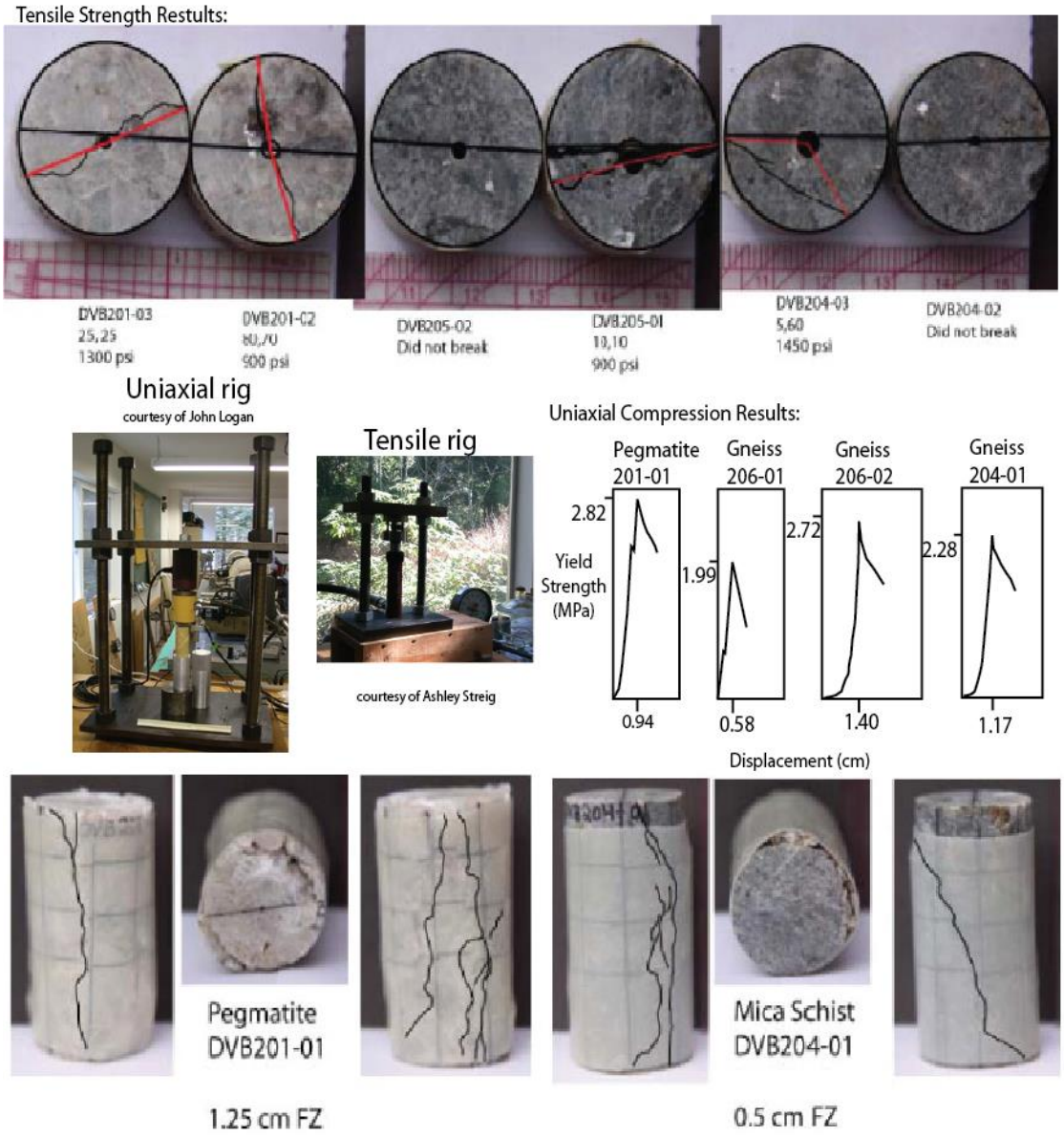

Figure 52: Tensile strength tests (above) and uniaxial compression tests were conducted. The results (graph) reveal the pegmatite has the highest rock strength and the widest fracture zone (FZ). This strengthens the field hypothsis that gouge thickness is a function the physical grain size reduction rate. The hypothesis is not robust and needs more testing.

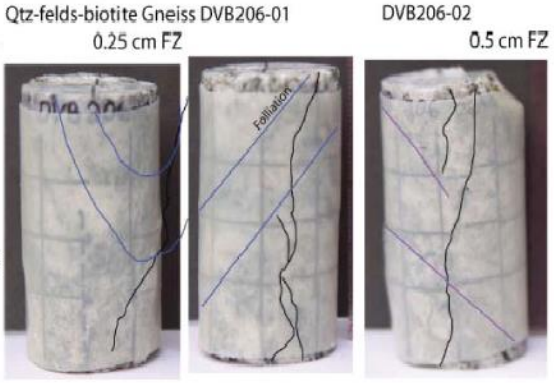

It is necessary to expand on this concept with a thought experiment that incorporates the field and laboratory observations. Experimental results show the fracture zone that develops in pegmatite is generally wider than that in gneiss. This is a qualitative observation, but likely results from the coarse crystalline structure of the pegmatite. Give this result, if a fault breaks through gneiss and also breaks through one pegmatite dike, the fracture zone in the pegmatite will be wider. By definition, the fracture zone is shattered rock and consists of smaller rock particles than before fracturing. When the fault ruptures again, the same relationship should hold. The pegmatite will again fracture more than the gneiss and the grain sizes in the fracture zone will again be reduced. By this process of re-fracturing, fault gouge is produced. If the pegmatite fractures twice as wide as the gneiss and the first rupture produces 2 cm of fracture zone in the pegmatite to 1 cm in the gneiss. During the second rupture, the fracture zone may or may not widen, but the width of grain size reduction will surely be wider in the pegmatite. Therefore, in this scenario, the pegmatite has the potential to create twice the amount of fault gouge as the gneiss. Furthermore, if the fault breaks through five dikes instead of one over the same fault area, there will be ten times more fault gouge produced. Though, this though experiment is supported by both field and laboratory observations, it remains qualitative and more tests should be conducted to strengthen the hypothesis.

Mineral Assemblages and Geochemistry in Upper-Plate of Crystal Fault

The mineral assemblage and occurrence is described in detail in Appendix B where it is hypothesized that the geochemical system responsible for this assemblage was most like an Iron-Oxide-Copper-Gold (IOCG) system. The field relationships show this mineralization is limited to the upper-plate faults and fractures of the Crystal Fault, which

was probably the local source of the mineral rich fluids. Four samples were chosen for geochemical analysis to test the field hypothesis. The chosen samples are highlighted in Figure 53 and highlighted results in Figure 54. The full results are shown in Appendix B.

The chemical trend of these rocks is strongly indicative of an IOCG deposit mainly because of the iron-oxides (hematite and magnetite), the small amount of chalcopytrite, and the relatively high concentration of Uranium and Light Rare Earth Elements in sample 325. The iron-oxide rich samples also contain other metallic elements, such as Titanium, Zinc, and Chromium, which is a similar assemblage of elements reported by Dupris and Beaudoin (2011) as a signature of IOCG deposits.

Barton and Johnson (1996) suggested an essential component of the IOCG systems is the fault's interaction with evaporite source rocks at depth. The diagram at the bottom of Figure 53 shows the theoretical relationship between the Crystal Fault and the fluids. Theoretically, meteoric waters interact with evaporite rocks and pick up salinity and decrease pH. The fluid is heated up at depth and then rises through fractures or faults and accumulates cations in solution by dissolving wall rock. When this saline solution interacts with carbonate rocks, the pH is increased and minerals stable at the new pH will precipitate out, which is commonly iron-oxides at high salinities. Though, no evaporite containing units are known in the Paleoproterozoic gneiss, it is likely that meteoric waters originally transported evaporite components from the playa to depth.

Other IOCG deposits exist throughout the Mojave, such as the Picacho gold deposit that formed in an Oligocene detachment fault (Losh *et al*., 2005). These systems

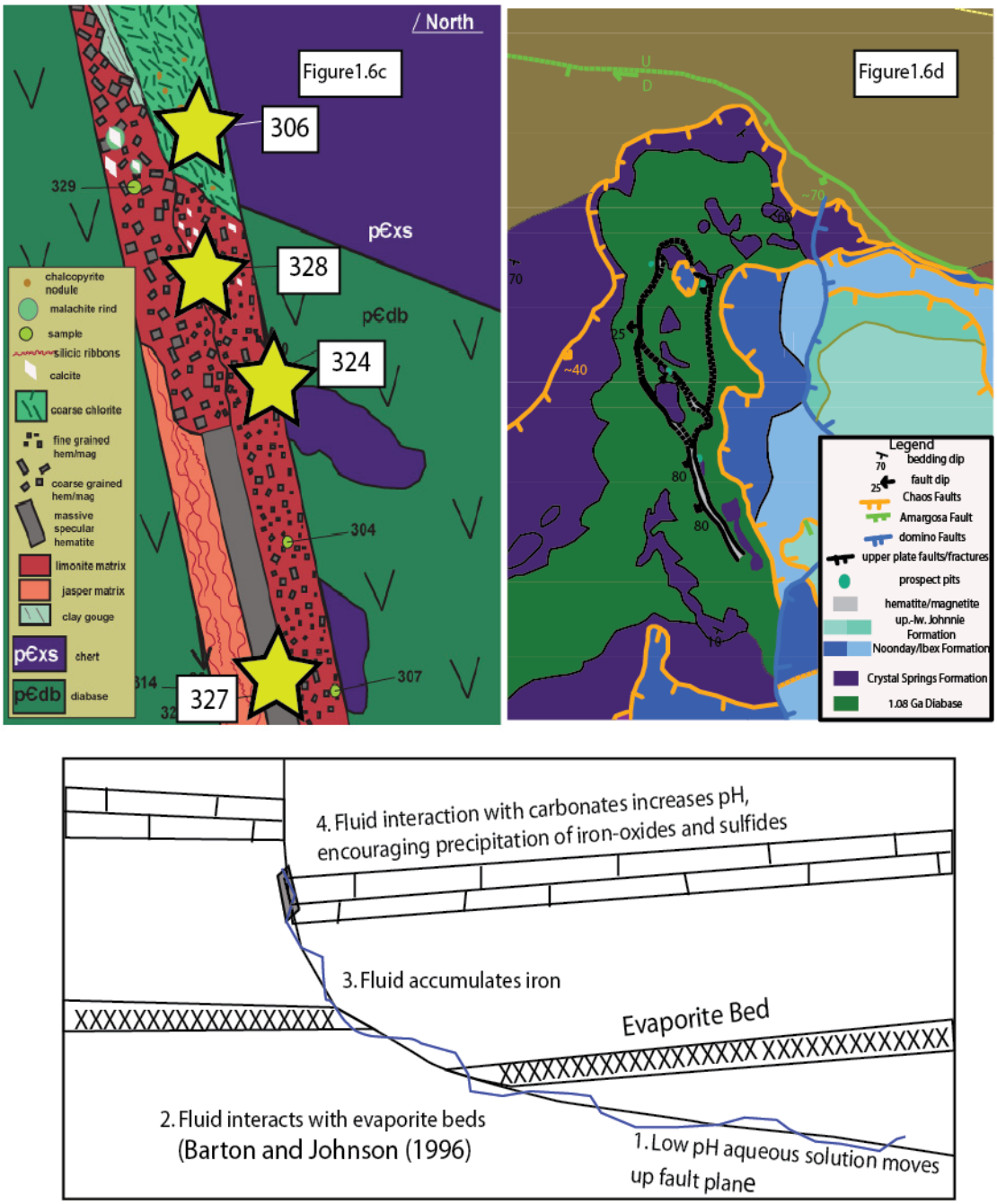

Figure 53: The mineralization assemblage is unique and required saline and low pH fluid to precipitate specular hematite. I hypothosize this assemblage represents an Iron-Oxide-Copper-Gold system. Field relationships (map) suggest the system the mineralization is exclusive to the hangingwall of the Crystal Fault. The schematic below is the hypothetical situation under which this mineralization occurred. To test the hypothesis, four samples (starred locations in schematic) were analyzed for trace element geochemistry.
Since IOCG systems are also high in both Uranium and Rare Earth Elements, a high abundance of these elements in the samples is supportive of the hypothesis.

Sample ID	CaO		Fe2O3		Ti		Cr		Mn	
	%	± 1 σ	%	± 1 σ	ppm	± 1 σ	ppm	± 1 σ	ppm	± 1 σ
DUH306-1	1.50	0.11	66.50	0.80	1663.16	282.27	7.41	1.88	936.12	24.64
DUH306-2	1.60	0.11	64.86	0.78	1311.09	284.20	8.75	1.94	966.72	25.44
DUH304-1	18.00	0.50	41.91	0.50	374.81	241.24	6.18	1.28	2666.56	69.92
DUH304-2	18.48	0.51	42.19	0.51	655.16	243.29	8.30	1.40	2685.24	70.41
DUH324-1	8.03	0.27	66.92	0.80	780.63	235.24	-4.59	0.08	1450.18	38.09
DUH324-2	7.59	0.27	65.48	0.78	999.86	237.35	7.02	1.70	1451.34	38.12
DUH327-1	4.72	0.20	64.23	0.77	1627.99	257.64	50.33	2.52	1571.33	41.26
DUH327-2	5.23	0.21	64.26	0.77	1421.77	255.94	49.53	2.56	1480.00	38.87

Sample ID	La		Ce		Sm		As		Th	
	ppm	± 1 σ	ppm	± 1 σ	ppm	± 1 σ	ppm	± 1 σ	ppm	± 1 σ
DUH306-1	2.07	0.04	-2.44	0.02	0.87	0.01	6.47	0.33	-0.38	0.00
DUH306-2	1.91	0.04	-2.38	0.02	0.83	0.01	6.48	0.31	-0.37	0.00
DUH304-1	3.64	0.05	6.08	0.69	0.96	0.01	14.91	0.29	0.14	0.10
DUH304-2	3.66	0.05	6.80	0.75	1.00	0.01	14.74	0.29	0.28	0.10
DUH324-1	6.56	0.07	12.39	0.95	2.31	0.02	1.29	0.19	10.49	0.23
DUH324-2	6.60	0.07	12.57	0.94	2.26	0.02	1.02	0.19	10.53	0.23
DUH327-1	1.54	0.05	-2.46	0.02	0.91	0.01	13.39	0.45	0.83	0.14
DUH327-2	1.66	0.05	-2.51	0.02	0.92	0.01	13.89	0.42	1.01	0.15

	Ba		U	
	ppm	± 1 σ	ppm	± 1 σ
DUH306	1106.79	73.47	1.23	0.41
DUH306	1019.92	71.02	0.82	0.31
DUH304	-80.82	3.24	1.39	0.26
DUH304	-80.24	3.22	1.08	0.23
DUH324	102.46	34.12	5.54	0.42
DUH324	85.36	31.84	5.75	0.45
DUH327	226.48	49.25	0.79	0.33
DUH327	150.05	47.25	0.78	0.30

Enriched Samples:

Sample 306 Ti, Ba
Sample 304 Ca, Mn, As
Sample 324 La, Ce, Sm, Th, U, Mn
Sample 327 Ti, Cr, As

Figure 54: The geochemical results show an elevated Uranium and Rare Earth Element abundance, which supports the hypothesis that the observed mineralization is indeed IOCG type system. The spatial relations between the mineralized zone and the Crystal Fault suggest the main fault was the main source of local hydrothermal fluid. These systems are not rare throughout the Mojave and typically occur in the Oligocene.

are highly variable in their ore genesis (Barton *et al*., 2011), but it is possible this deposit formed in a similar time and mode as the Picacho deposit. This temporal correlation is certainly not enough to suggest the age of the structures as Oligocene, but it opens the possibility. The Uranium rich rocks occur at a particular horizon and it is possible to isolate uraninite or Uranium from within the calcite to obtain an absolute age using U-Pb radiometric dating, but this analysis was not attempted here.

Geologic Cross-Sections

Four geologic cross-sections allow the projection of surface mapping to depth. Cross-sections A-A', D-D', and E-E' were made specifically for the discussion Section 3.2 and Section 3.5 are displayed at increased scales. Discussed here, cross-sections B-B' and C-C' were created at the same scale as the map, but page-size replicas are presented for this section as Figure 55 and Figure 56.

Cross-section B-B'

This section line cuts NNW-SSE across Chaos Syncline, Desert Hound Anticline, the Amargosa Fault, and the Chaos Fault system. The section line is similar to that chosen by Wright and Troxel (1984), so it can be qualitatively compared to their A-A'. Figure 55 is a reduced copy of B-B'.

The cross-section shows the fold pair offset up-on-the-northwest by the Amargosa Fault. The apparent offset of the quartz-feldspar-biotitie is ~2 kilometers in the cross-section. I have exaggerated elements of the basement to emphasize the theoretical interactions at depth between foliation, the 1st generation fold axes, and the 2nd generation. The basal geometry of the Chaos Syncline is the most accurate because the

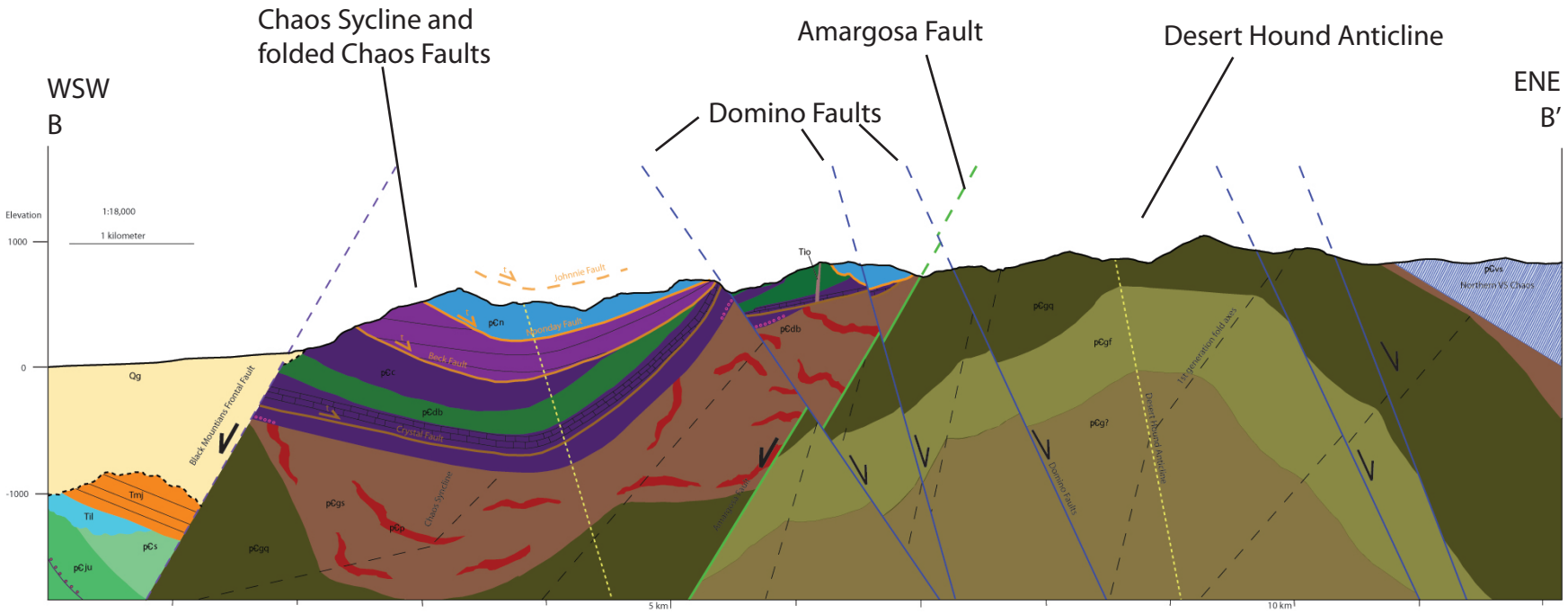

Figure 55: This figure contains a reduced-scale cross-section of the line B-B'. Most obvious is the fold pair--The Chaos Syncline and Desert Hound Anticline. These features are offset in a normal sense by the prominent Amargosa Fault, estimated here between 3-15 km. The axial trace of the Chaos Syncline is truncated by the Amargosa Fault. The Chaos Fault system is folded about Chaos Syncline axis, but generally appears to converge and slip toward the southeast. The Desert Hound Anticline exposes the lowest basement rock in the up-plunge core, while the Chaos Sycline exposes the structurally highest basement rock. The contacts between basement rock types are here assumed to be folded about a series of southwest plunging folds and this geometry is slightly exaggerated in the cross-section.

up-plunge section is exposed on the surface. The internal geometry of the Chaos Syncline is less accurate, but shows the general relationships between structures and bedding.

The Chaos Fault System is clearly folded about the axis of the Chaos Syncline. Because each of these faults had a distinct geometry pre-folding, each folded fault is expressed differentially as the cross-section depicts. Because each Chaos fault had a different initial geometry, each fault has a different folded geometry but all faults converge toward the east. The stacking geometry of the slabs is reminiscent of structural stacking along thrust faults, like nappes or duplexes. The slabs were offset in a normal sense and younger units are down against older units. Kinematic indicators on the fault plane of the Beck Fault suggest the upper plate moved east. I infer this is the sense of the whole Chaos Fault System.

The Black Mountains Frontal Fault is clearly expressed on the west side of this cross-section. This fault drops Jubilee Chaos Formation down, based on projecting the outcrops from the north of the section line. At the mouth of Ashford Canyon is the GABS basin basal unconformity with the Ashford latite (~13 Ma). Assuming the Johnnie Formation is below the Ashford latite, which is the relationship elsewhere, the Johnnie Fault must also exist below the down-dropped section of Jubilee Chaos. The theoretical location of the Johnnie Fault is shown. When this is compared to the theoretical location in the hangingwall the apparent offset is ~3 km.

Cross-section C-C'

This line of section was drawn sub-parallel to the axis of the Chaos Syncline. The geometry of the shingle fault system and intervening slabs is best portrayed in this cross-section (Figure 56). Notice the steep bedding in each of the slabs, which are juxtaposed by the Chaos Faults. The Chaos Faults converge to the southeast and are interpreted to be down-to-the-northeast. The differential folding about the Chaos Syncline can be seen in this cross-section. For example, the Johnnie slab and Johnnie Fault are folded into a more east-southeasterly trending syncline, while the folded Beck Fault is trending south-southeast. Similarly, the folded GABS unconformity seems to rest at a different orientation.

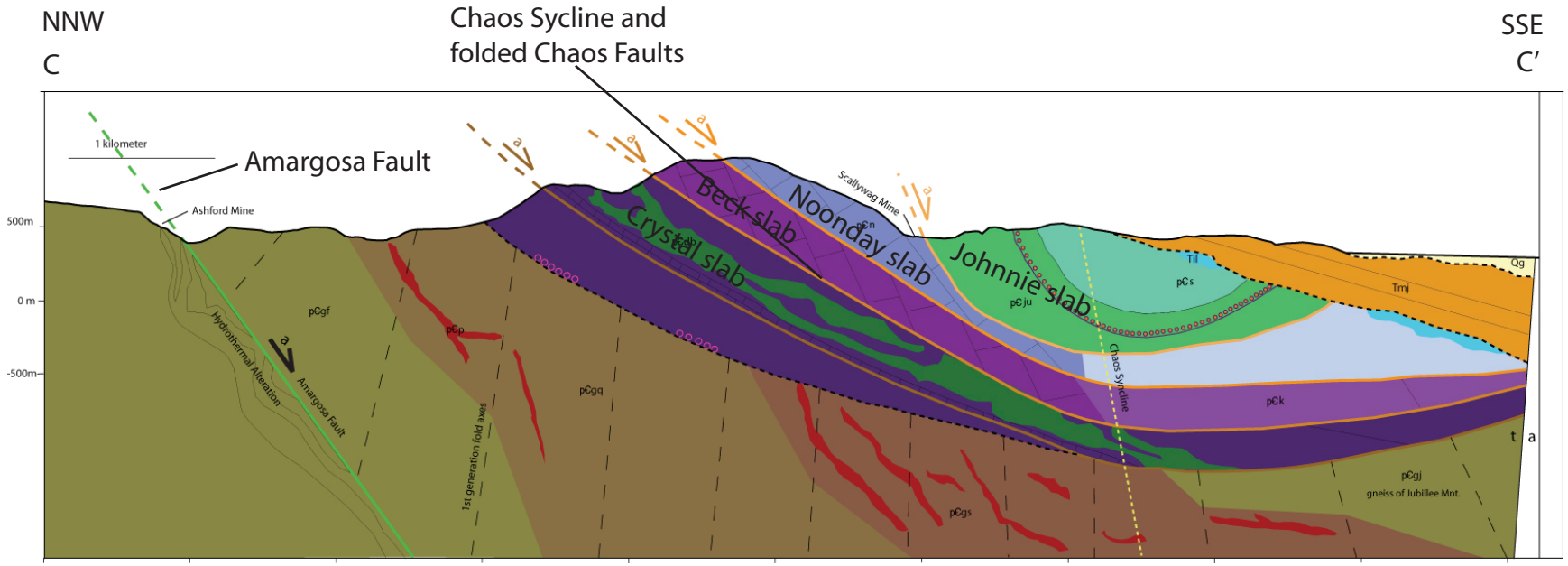

Figure 56: This cross section illuminates the down plunge geometry of the Chaos Syncline. The Chaos Fault System accommodated normal slip between thin slabs of rock that converged to the south-southeast. Each slab and basal fault has a unique geometry, e.g. the internal bedding of each slab varies, the upper plate of the Johnnie Fault is more folded, and the faults cut stratigraphy at different angles. The Amargosa Fault is excluded to the crystalline rocks and offsets the south facing limb of the Deserd Hound Anticline. The contacts, folds, dikes, and alteration within the basement are slightly exaggerated. Section line does not intersect upper Johnnie Fault.

CHAPTER V

INTERPRETATIONS OF STRUCTURES

D1: Shortening

As indicated in Figure 35, the trend and vergence of these structures indicates the Johnnie slab and upper Johnnie slab underwent significant (currently) north-directed shortening. Many folds in the area are upright, but a few–A, C, D–verge to the north-northwest. The south-dipping imbricate system also suggests north-directed shortening. In both styles of deformation, approximately 25% is the estimated amount of shortening across the field area (Figure 35).

The Ibex Klippe system occupies the upper Johnnie slab of the Chaos. The upper Johnnie slab was dropped down by a normal fault against the Johnnie slab that contains the Imbricated Oolite system. This geometry suggests the Ibex Klippe system was structurally above the 'Imbricated Oolite' system pre-Chaos Fault system. I suggest the 'Ibex Klippe' represents a higher imbrication of the Imbricated Oolite System and the two share a common basal thrust. Figure 57 illustrates this concept.

D2: Extensional Nappes

The faults are shingle-like surfaces between which are slabs of broken-up hangingwall rocks, which is exactly as Noble (1941) originally described them. The slabs are thoroughly fractured, faulted, and/or brecciated and include pervasive to localized hydrothermal alteration. While the structures provide the framework for Chaos, the internal structures within the slabs create the attenuated appearance. The Chaos Fault System is the primary structure responsible for assembling the Virgin Spring Chaos. The

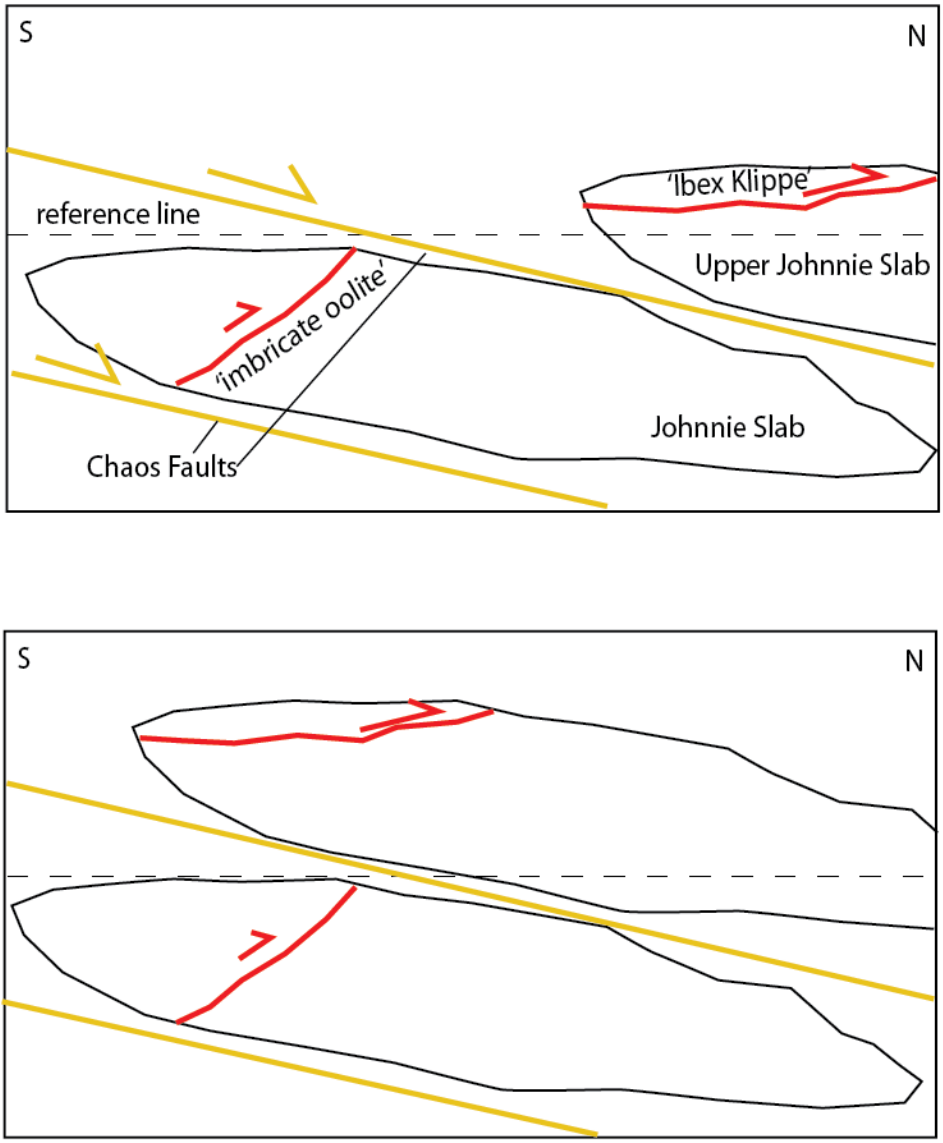

Figure 57: This schematic illustration shows the theoretical relationship between the shortening structures observed in the study area. The lozenge shaped slabs are offset along low-angle normal faults (top). If the slip is reversed (bottom) and the upper Johnnie slab is replaced above the Johnnie slab, the 'Ibex Klippe' system is structurally above the 'Imbricate Oolite' system. I suggest the two converged to a common basal structure, in the west, and were once an imbricate thrust system involved in thin skinned deformation.

outcrop pattern is a manifestation of D3 deformation. Adding estimates of the minimum amount of slip on each fault yields a system-sum of ~4.5 km.

Cross-cutting relations show the structurally-lower faults are cut by the structurally-higher faults. I suggest this system, in its active arrangement, was rooted into a detachment at depth. Two models are offered in Figure 58. The upper diagrams, created by the author, show a system that is antithetic to the main fault and younger faults form at lower angles to counteract hangingwall rotation. However, this geometry is not previously documented and requires a main fault that is unknown. In the lower diagram from Wernicke (1981), extensional nappes form synchronously, but differentially–by sliding along a low-angle basal detachment at mid-crustal levels. This model does not show the faults making high angles to bedding, which is observed at each fault in the system. Both models contain elements of the system, but neither model sufficiently describes it.

It is difficult to assess the timing and duration of these faults. The geochemical results from the mineralization in the Crystal slab further suggest an IOCG +/- REE and U deposit, which appear region wide during Oligocene detachment faulting. It is weak to temporally correlate the Chaos Fault system based on this mineralization, but identifying the Uranium rich rocks can provide material for absolute dating in later studies. The Chaos faults are all folded about the Chaos syncline and so must pre-date the folding, but it is also unclear when the folding began or ended.

The Crystal fault has a peculiar spatial relationship to the talc deposit horizon. The two primary locations at which the fault was directly observed have talc mineralization in

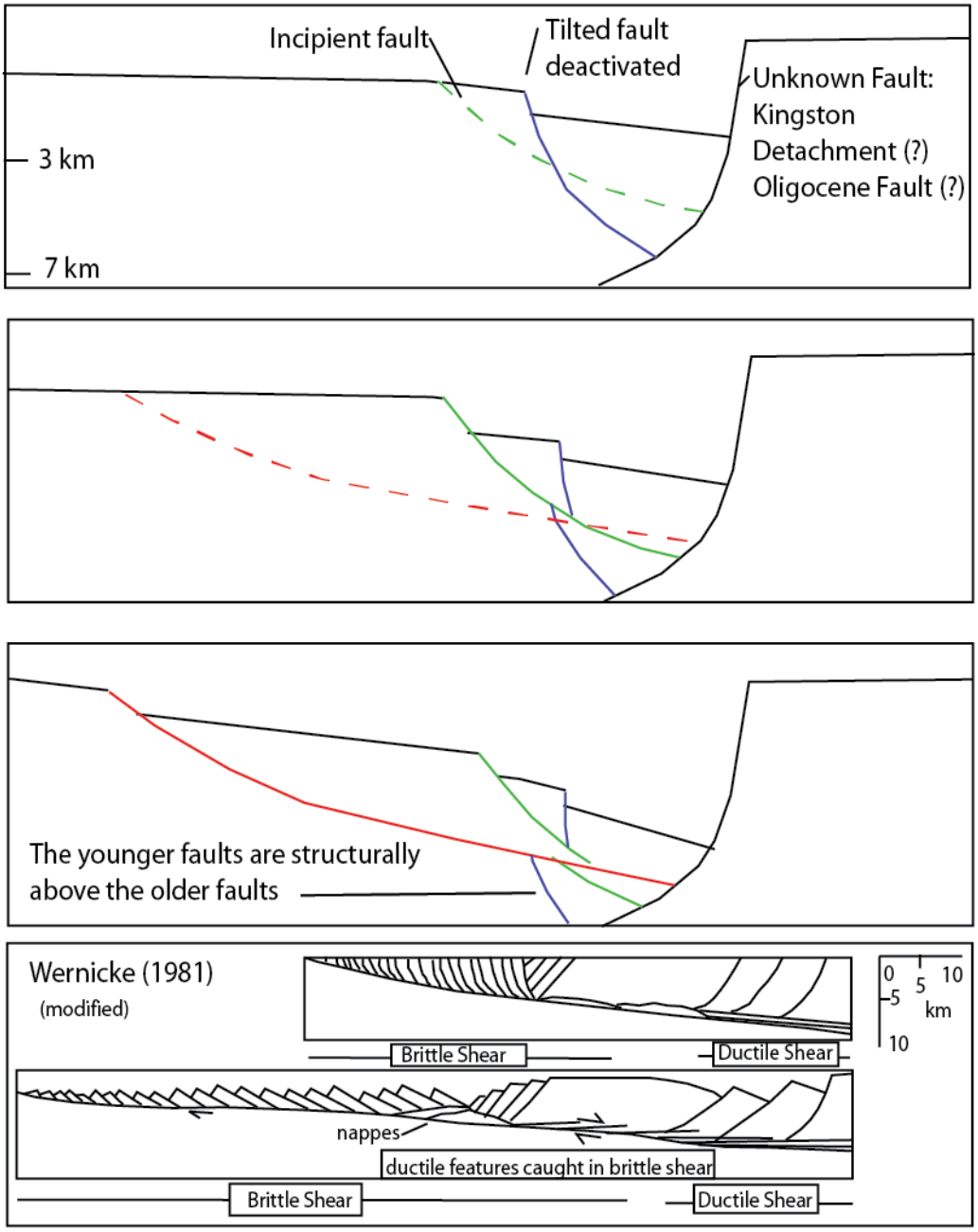

Figure 58: The three steps above represent one possible evolution of the Chaos Fault System. The spatial relationships and geometries are exaggerated to highlight the cross-cutting relationships. Incipient faults form when active faults become too high-angle after hangingwall rotation. The new fault forms at a lower angle, but eventually is rotated to higher angles. This faulting precession would create a system of cross-cutting faults that converge in one direction with the younger faults structurally higher. The lower figure is modified from Wernicke (1981). The system depicted reproduces a similar geometry. Notice the nappe slabs created by extensional processes. Either of these models can explain the modern geometric of the Chaos Fault System, but neither model completely describes the process to create the geometry.

the hangingwall. A similar relationship can be found at the Kingston Detachment in Crystal Springs Canyon where the detachment fault cuts through the talc mineralization at the Crystal Spring talc mine. It is possible the lubricating properties of the mineral influenced the mechanics of faulting and the talc zone once acted as a region-wide décollement-like surface on which early extension occurred. The relationship between low-strength minerals and fault surface development has been recognized in thrust fault systems (Davis and Engelder, 1985) and normal fault systems (Trudgill and Cartwright, 1994).

D3: Regional Folding

The Desert Hound Anticline and Chaos Syncline have different orientations, 30º, S70ºE and 60º, S35ºE, respectively. The trace of each hinge is truncated by the younger Amargosa Fault, which appears to have truncated and rotated the axial line of the syncline in the hangingwall, and juxtaposed down-plunge and up-plunge portions of the fold. This relation is illustrated in the top of Figure 59.

Topping (2003) hypothesized this syncline is an up-plunge portion of the syncline occupying the northeastern Ibex Hills. In this hypothesis, the syncline was offset vertically and left-laterally by the Sheephead-Jubilee fault, of which the Chaos Syncline mapped syncline occupied the hangingwall. If this extrapolation can be made, the geometry of the syncline in the Ibex Hills is a closer representation of the pre-faulted geometry. Shown in cartoon format at the bottom of Figure 59 is how the Sheephead-Jubilee fault may have affected the geometry of the fold axis. This offset of the axial

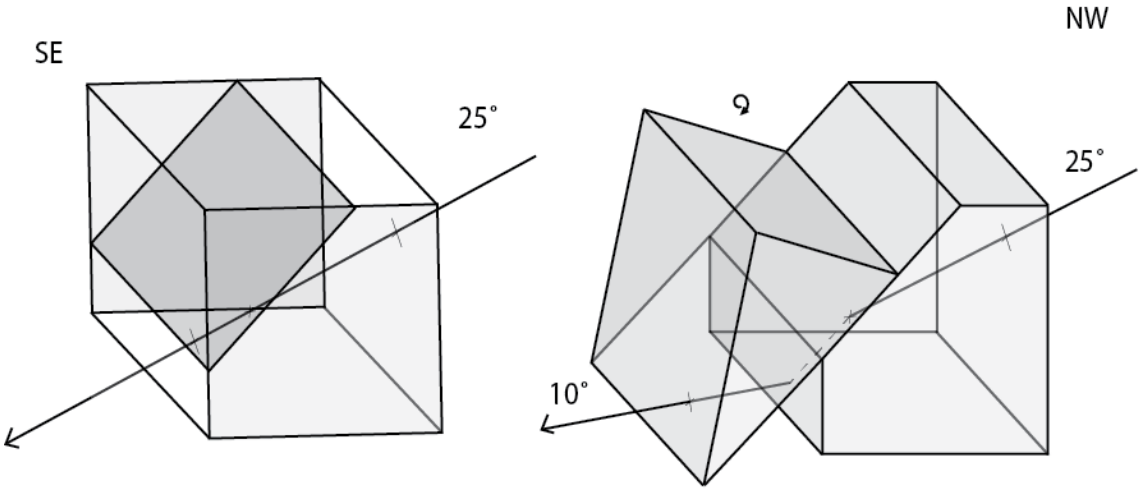

Figure 59: The block diagrams show how the orientation of a geologic line can change when involved in hangingwall rotation from a normal fault. At top, the case involves a 25˚ southeast plunging line cut by a northwest dipping fault. The line becomes steeper in the hangingwall. The lower case shows the same line offset by a southeast dipping fault, resulting in a shallower line in the hangingwall. I suggest the axial line of the Chaos Syncline was first steepened by the Sheephead Fault, and then brought to a shallower angle by the Amarogsa Fault. The current angle is still steeper than originally because the hangingwall of the Amargosa Fault did not experience as much rotation.

line by the Amargosa and Sheephead-Jubilee faults is consistent with the steeper plunge observed in the Chaos Syncline.

The Desert Hound Anticline has been correlated to the Mormon Point Turtleback (Noble, 1941; Curry, 1954; Mancktelow and Pavlis, 1994). Figure 60 shows a modified version of a diagram from Mancktelow and Pavlis (1994) showing the fold's relationship to the extension direction. The folds form as footwall corrugations or mullions during detachment faulting, though the modern geometry is probably more suggestive of the active range front normal fault (Miller and Pavlis, 2005). Detachment faulting requires the maximum principle stress to be vertical, while the minimum stress is in the direction of extension. Orthogonal to the maximum and minimum stress is a stress that is also slightly compressive, which is termed a "transcurrent stress" by Mancktelow and Pavlis (1994). The Black Mountain Turtlebacks and Desert Hound, Rhodes, and Graham Anticlines are expressions of the transcurrent stress (Mancktelow and Pavlis, 1994).

The Copper Canyon Turtleback has an associated Copper Canyon syncline that formed syn-depositionally with the Copper Canyon Formation ~6-3 ma (Holm *et al*., 1994). I suggest the Chaos Syncline formed similarly to the Copper Canyon Syncline, but the Chaos Syncline started deforming much earlier. While the Chaos Syncline was interrupted by strike-slip faulting, the Copper Canyon syncline continued to deform and become a basin that collected the sediments composing the Copper Canyon Formation.

D4: Amargosa Fault

This fault is characterized by its structural uniformity, especially when compared to the previously described structures. The Amargosa Fault clearly truncates the earlier

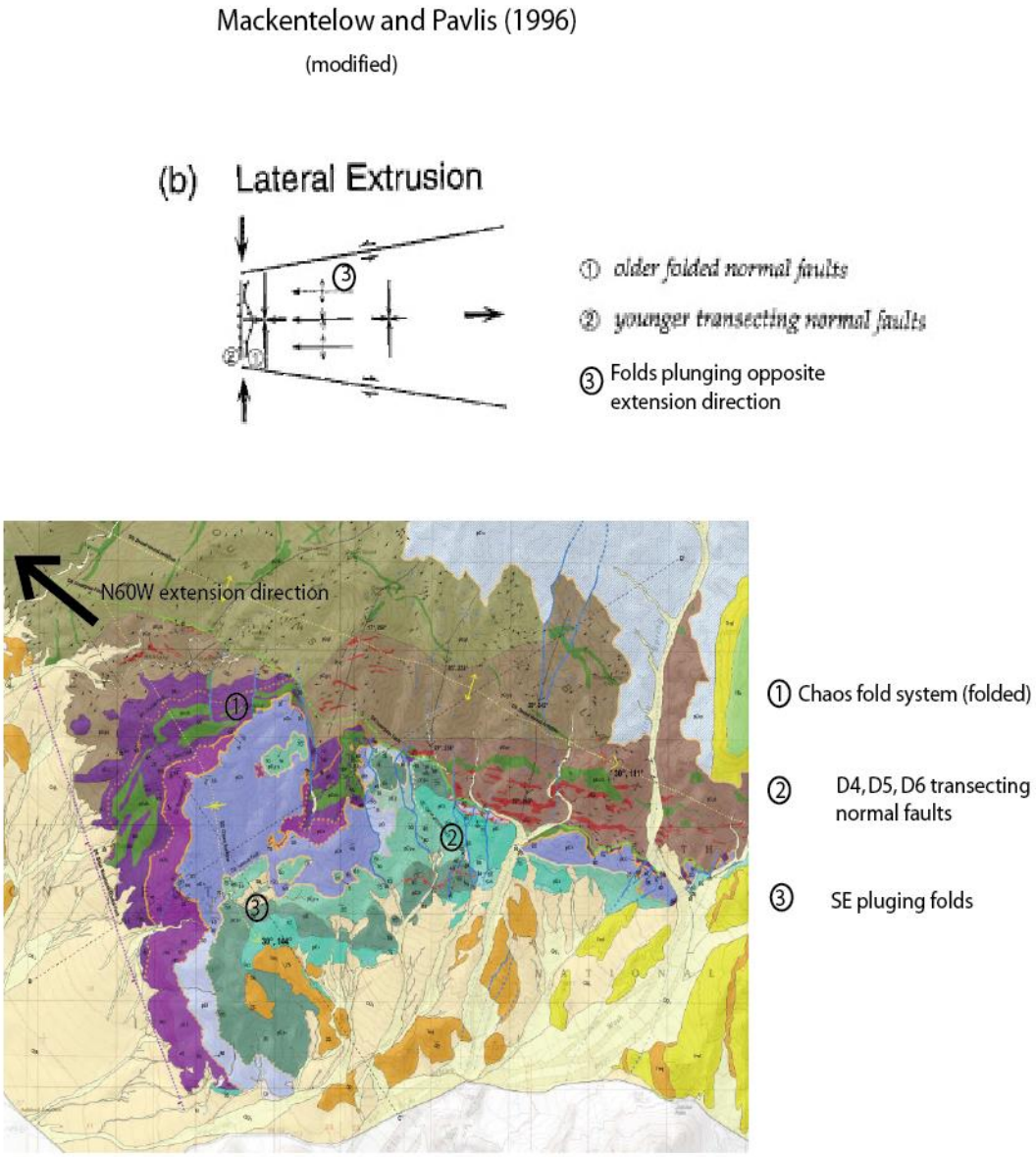

Figure 60: Mackentelow and Pavlis (1996) suggested three models for the relationships seen between detachment faults and folds. I propose their model (b) Lateral Extrusion best fits the local situation. In general, the extension is accommodated by a frontal normal fault and lateral strike-slip. Normal faults form perpendicular to maximum extension direction, while fold axes form parallel to elongation. When a N60˚W extension direction is imposed, the same relationships and geometries are seen in the study area.

structures. The fault has a moderately steep dip (60º-70º) and I've estimated a pure dip-slip motion on the fault between 8-14 km, which is similar to previously suggested slip of <15 km (Miller, 2002). This estimate decreases substantially with increasing strike-slip and may be as little as 3 km if pure strike-slip.

This fault is not deformed about D3 and is not a continuous structure with the basal surface of the northern Chaos in the stripped pattern on the opposite side of Desert Hound Anticline. This difference suggests the two previously lumped structural assemblages may have different geologic histories, which was also concluded by Rogers (2000). Beyond the field area the fault must continue along strike. To the southeast, it is covered by the undeformed Funeral Formation and projects toward Sheephead Pass and the Sheephead Fault. To the northwest, the fault may eventually die-out into a left stepping, en-echelon relationship with the Black Mountains Frontal Fault.

D5: Domino Faults

The domino faults were activated as brittle accommodation faults sub-parallel to the main extension structure of the time, which was either the early Black Mountains Frontal Fault or the Turtleback fault system. Though the individual fault slips along these structures may be minute, the collective system may have several kilometers of slip (Topping, 2003). These faults apply yet another level of complexity to the previously assembled Chaos, but are not responsible for the stratigraphic attenuation.

D6: Black Mountains Frontal Fault

The Black Mountain Frontal Fault is the active trace of the Death Valley System and is a manifestation of the higher-angle extensional system that cut the older lower-angle Turtleback System. Locally, this fault cuts all of the previously described

structures. The fault drops the valley side down and allowed for Quaternary sedimentary cover. Slip on this fault is not well documented, but is estimated at approximately 15 km or as little at 1 km (Topping, 2003; Keener *et al*., 1993). The relationships in cross-section B-B' suggest a pure dip-slip offset of ~3 kilometers, which is within the range of other suggestions.

CHAPTER VI

REGIONAL IMPLICATIONS AND CONCLUSIONS

This section of Virgin Spring Phase of the Amargosa Chaos records multiphase deformation throughout the Neogene and also documents earlier compression. I have shown evidence that the Amargosa Fault is a relatively minor structure; a conclusion that implies regional models suggesting ~80 kilometers of northwest transport need to be revised. I have identified a new local system of faults, the Chaos Fault System, which is essentially responsible for the appearance of the Virgin Spring Phase of Chaos. Many outstanding questions were raised during this study, the answers to which could modify the current hypotheses regarding extension in southern Death Valley (Figure 61). But more importantly, the two main questions that inspired the study can now be answered.

Order to the Chaos

The shingle-like structure described by (Noble, 1941) is indeed the primary structure of the Virgin Spring Phase of the Amargosa Chaos. The Chaos Fault System dictates the arrangement of rock types, but subsequent deformation distorted the arrangement into the chaotic appearance.

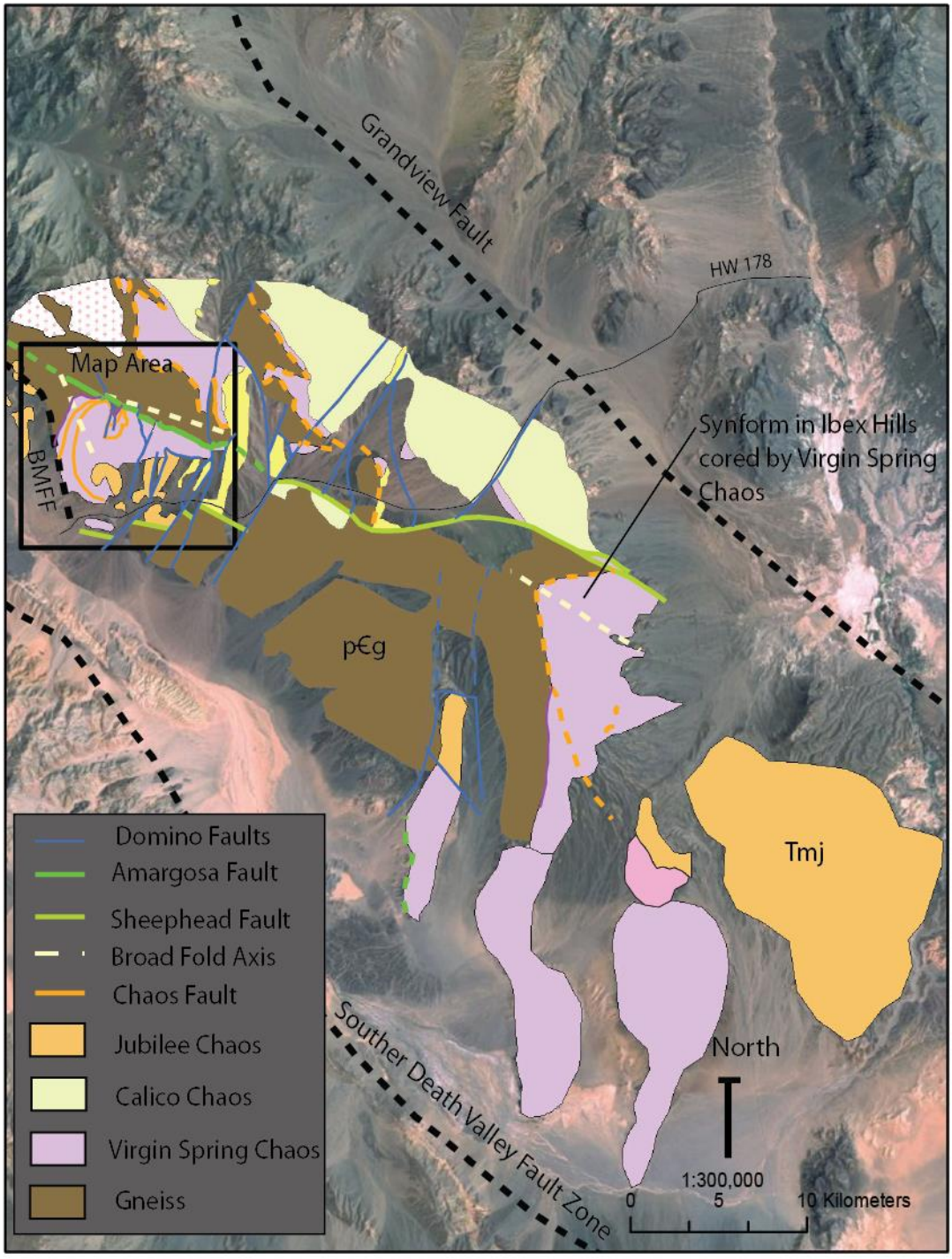

Figure 61: This map is modified after Topping (2003) and depicts the distribution of rock units and major structures throughout southern Death Valley.

Relationship between Amargosa Fault and Virgin Spring Chaos

This section of the Virgin Spring Phase of the Amargosa Chaos did not form in response to the Amargosa Fault. Instead, the pre-existing structure of Virgin Spring Chaos was truncated by the Amargosa Fault.

Many of the structures identified and described here–D4, D5, D6–correlate with the interpretations of Topping (2003) regarding the distribution of the GABS basin via distributed faults. Topping (2003) gave estimates for the timing and slip of the structures and constructed a sequence of tectonostratigraphic events during the mid-Miocene. In this hypothesized sequence, D4-D6 occurred between ~10.1 Ma to <4 Ma.

Other structures described and interpreted here are newly identified and are relatively poorly understood in the regional context. D1 structures represent ~25% shortening across the field area that probably formed when the western North American margin was undergoing compression. The Chaos Fault System, D2, needs more detailed study. Most urgently, the other areas of Virgin Spring Phase of Chaos should be mapped in similar detail to identify whether the Chaos Fault System is the defining feature of the Virgin Spring Phase or if the system is exclusive to this section. I've hypothesized here the Chaos Fault System could be Oligocene in age, but this hypothesis is not robust and needs further study to be conclusive. The broad anticline of D3 has been previously correlated to the Mormon Point Turtleback (Mancktelow and Pavlis, 1994). A correlation that suggests the structures had a similar mode and timing of formation by transcurrent stress or lateral extrusion ~14-8 Ma (Miller and Pavlis, 2005). The Chaos Syncline is

structurally reminiscent of the Copper Canyon Syncline, but the two cannot be confidently correlated.

In conclusion, the structures described in this manuscript fit into the existing paradigm of tectonic evolution of southern Death Valley. The multiphase deformation recorded by D2-D6 supports a tectonic model of distributed-faulting to form the arrangement of the modern geologic features of southern Death Valley.

APPENDIX A

SOURCES FOR FIGURE 4

Atwater, T., and Stock, J., 1988, Pacific-North American Plate Tectonics of the Neogene Southwestern United States-An update: International Geologic Review, v. 40, p. 375-402.

Bacon, C.R., Lanphere, M.A., and Champion, D.E., 1999, Late Quaternary slip rate and seismic hazards of the West Klamath Lake fault zone near Crater Lake, Oregon Cascades: Geology, v. 27., p. 43-46.

Bennet, R.A., Wernicke, B.P., Davis, J.L., Elósegui, P., Snow, J.K., Abolins, J., House, M.A., Stirewalt, G.L., and Ferrill, D.A., 1997, Global Positioning System constraints on fault slip rates in the DV region, California and Nevada: Geophysical Research Letters, v. 24., no. 23, p. 3073-3076.

Brady, R.J., Wernicke, B.P., and Niemi, N.A., 2000, Reconstruction of Basin and Range extension and westward motion of the Sierra Nevada Block, in Lageson, D.R., Peters, S.G., and Lahren, M.M., eds., Great Basin and Sierra Nevada: Boulder Colorado, Geologic Society of America Field Guide 2, p. 75-96.

Dokka, R.K., and Ross, T.M., 1995, Collapse of the Southwestern North America and the evolution of early Miocene detachment faults, metamorphic core complexes, the Sierra Nevada orocline, and the San Andreas fault system: Geology, v. 23., p. 1075-1078.

Faulds, James E., Christopher D. Henry, Hinz H. Nicholas, 2005, Kinematics of the northern Walker Lane: An incipient transform fault along the Pacific-North American plate boundary: Geology, v. 33, p. 505-508

Flesch, L., and Bendick, R., 2012, The relationship between surface kinematics and deformation of the whole lithosphere: Geology, v. 40, no. 8, p. 711-714.

Hammond, W.C., and Thatcher, W., 2007, Crustal deformation across the Sierra Nevada, northern Walker Lane Basin and Range transition, western Unites States measure with GPS, 2000-2004: Journal of Geophysical Research, v. 112, p. 26-52

Hammond, W.C., Blewitt, G., Li, Z., Plag, H., and Kreemer, C., 2012, Contemporary uplift of the Sierra Nevada, western United States, from GPS and InSAR measurements: Geology, v. 40, p. 667-670.

Levy, M., and Christie-Blick, N., 1989, Pre-Mesozoic Palinspastic Reconstruction of the Eastern Great Basin (Western United States): Science, v. 245, no. 4925, p. 1454-1462.

McCaffrey, R., Qamar, A.I., King, R.W., Wells, R., Khazaradze, G., Williams, C.A., Stevens, C.W., Vollick, J.J., and Zwick, P.C., 2007, Fault locking, block rotation and crustal deformation in the Pacific Northwest: Geophysics Journal International, v. 169, p. 1315-1340.

Parson, T., and Thatcher, W., 2011, Diffuse Pacific-North American plate boundary: 1000 km of dextral shear inferred from modeling geodetic data: Geology, v. 39, p. 943-946

Plattner, C., Malservisi, R., Furlong, K.P., Govers, R., 2010, Development of th Eastern California Shear zone- Walker Lane belt: The effects of microplate motion an pre-existing weakess in the Basin and Range: Tectonophysics, v. 485, p. 78-84.

Popov, A.A., Sobolev, S.V., and Zoback, M.D., 2012, Modeling evolution of the San Andreas Fault system in northern and central California: Geochemistry, Geophysics, Geosystems, v. 13, no. 8, p 21-42.

Schmandt, B., and Humphreys, E., 2011, Seismically imaged relict slab from the 55 Ma Siletzia accretion to the northwest United States: Geology, v. 39, no. 2, p. 175-178.

Schmidt, M.E., and Grunder, A.L., 2009, The evolution of North Sister: A volcano shaped by extension and ice int eh central Oregon Cascade Arc: Geological Society of America Bulletin, v. 121, no. 5-6, p. 643-662.

Wernicke, B.P., Davis, J.L., Niemi, N.A., Luffi, P., and Bisnath, S., 2008, Active Megadetachment beneath the western United States: Journal of Geophysical Research, v. 113, B11409, p. 26-52.

APPENDIX B

ROCK DESCRIPTIONS: FROM FIELD AND LITERATURE

Precambrian Crystalline Rocks

*p€g- 1.790 Ga World Beater Complex (*Wasserberg *et al.* 1959*)*

This metamorphic complex is the local basement rock throughout the northeastern Mojave Desert and Death Valley and is similar to basement complexes throughout the southwest desert (Karlstrom, 1986). Wasserberg *et* al. (1959) determined a K-Ar age for this complex of 1.790 Ga implying metamorphism ended in the Paleoproterozoic. This age is extrapolated to be the age of the metamorphic basement rocks of the Black Mountains, Nopah Range, and Kingston Range. I have observed many metamorphic lithologies throughout the region, including fine grained graphitic schist, coarsely crystalline marble, well-foliated quartz-biotite schist, and granitic gneiss. I interpret these rocks are representing Neoarchean sediments deposited on the passive margin of the Supercontinent Columbia (Zhao *et al*., 2004) and later metamorphosed during Paleoproterozoic orogenies, such as the Grenvillian, Yavapai, or Mazatzal (Zhao *et al*., 2002).

Within the map area, three major lithologies are present: fine-grained quartz-feldspar augen gneiss, fine-grained quartz-biotite-feldspar gniess, and a well-foliated quartz-biotite schist. Wright and Troxel (1984) note the distinctive field characteristic of the basement as "monotonous gray slopes". Though monotonous from a distance, the charismatic nature of this rock when observed in detail encourages the young geologist to "get naked and roll in it" (Miller, personal communication; Castonguay, personal experience).

A traverse from Virgin Spring Wash to the east flank of Desert Hound Peak crosses representative sections of the foliated quartz-biotite schist and poorly layered biotite-feldspar augen gneiss. The augen gneiss of Desert Hound Peak has poorly developed augens. Between the feldspar rich unit and the foliated unit resides a quartz-feldspar-biotitie gneiss. Foliation of the units is steeply dipping to the south-southeast. I assume the contacts between metamorphic rock types is parallel or sup-parallel to foliation, suggesting that north is structurally down into the World Beater Complex (locally).

pЄp- Precambrian Pegmatite

The pegmatite consists primarily of clear to light smokey quartz and plagioclase feldspar. The rock displays graphic intergrowth texture. It also contains scattered to abundant sheets of muscovite and often small semi-euhedral crystals of black tourmaline (schorl), usually near the intrusive contact.

The white quartz-feldspar pegmatite dikes are easily recognizable from a distance and only exist within the Precambrian basement. Abundance varies between units of the World Beater Complex. Locally, this variation can be seen on the west side of the map area, where the pegmatite dikes are less abundant.

No radiometric age constraint exists for the pegmatite dikes, though it is somewhat bracketed by dated events. The dikes do not display any sign of metamorphism, so emplacement must post-date the metamorphism of the World Beater Complex. The pegmatite does not intrude the sedimentary Crystal Springs formation that unconformably overlies the metamorphic basement so the emplacement of the pegmatite must have been after the 1.8 Ga thermal metamorphic date and before the ~1.4 Ga age of

the deposition of the Crystal Springs basal conglomerate.

*p€db- Precambrian 1.08 Ga Diabase (*Heaman and Grotzinger, 1992*)*

This basic intrusive igneous rock is uniformly dark green to greenish black both in outcrop and on fresh surfaces. The rock contains pockets of abundant plagioclase laths and coarse biotite sheets. Wright (1968) described the mineral components of the rock as containing 30-60% plagioclase, 30-60% mafic minerals (hypersthene and augite) and from 2-10% magnetite and ilmenite. Wright (1968) also determined that the chemical composition of this diabase has less silica than other world-wide diabase, but elevated ferric and ferrous iron. As suggested by Wright (1968), the diabase probably intruded poorly consolidated material of the lower Crystal Springs formation that was still saturated with marine water, which created the contact metamorphism. The alteration produced talc-tremolite schist that was exploited commercially in the region.

The diabase forms steep blocky slopes around Ashford Peak. The intrusion is not seen to intrude the upper Cyrstal Springs Member or Beck Springs Dolomite (Wright and Troxel, 1984).

The diabase sills of this region have been correlated temporally with sills in both the Unbar Group in the Grand Canyon and the Apache Group in Central Arizona (Heaman and Grotzinger 1992).

Pahrump (Super)group

These Neoproterozoic marine and non-marine sedimentary rocks primarily represent a syndepositional tectonic basin that formed and received sediments from ~1.4 to 0.6 Ga (Levy and Christie-Blick, 1989; Heaman and Grotzinger, 1992). This basin is

classically termed the Amargosa aulacogen and predated the Cordilleran miogeosyncline (Wright *et al.* 1976). The basin is now interpreted (Levy and Christie-Blick, 1989) to have been oriented north-south. Isotopic Nd data suggest the detritus composing this group, with the exception of the basal conglomerate, was derived from local Proterozoic basement rocks (Farmer and Ball, 1997). Mahon (2012) suggested elevating the Pahrump Group to Supergroup status based on the relative time of accumulation.

p€cs- Precambrian Crystal Springs formation

This unit contains several lithologies of mixed carbonate-siliciclastic marine and fluvial facies ranging from arkosic sandstone to algal dolomite. Mahon (2012) proposed to split the formation and named the upper Crystal Springs Member as the Horse Thief Springs Formation. The stratigraphic order of the Crystal Springs members is as follows: Blue arkosic sandstone member with basal conglomerate, white feldspathic sandstone member, purple shale member, orange lime (dolomite) member, black chert member, and upper siltstones and red carbonates (Horse Thief Springs Formation). Each of these units can be described in further detail for the study area, but are ultimately described and published elsewhere (Wright 1968; Roberts 1976; Mahon 2012).

The contact between the Crystal Springs Formation and the metamorphic basement is an unconformity. Observation of this surface shows a poorly-developed, 1.5 m thick paleosol (Figure 1.6b), where the micas and feldspars have been altered to white micas and clays.

Blue arkosic sandstone member with basal conglomerate

The basal conglomerate has abundant white, vitreous, zircon-bearing quartzite clasts with a unimodel age distribution of 1.68 Ga (Mahon 2012) (Figure 1.6b, upper

right). No source rocks of this age are known, but imbricate clasts suggest water flow from the north (Roberts, 1976). Three sections of this conglomerate were measured and described in the field area. The results show some variation in thickness, clast composition, and clast abundance. Roberts (1976) recorded thicknesses of this conglomerate of up to 8 meters though locally the average thickness is under 2 meters. This basal conglomerate of the arkosic member is interpreted (Wright 1968; Roberts 1976; Wright *et al*. 1976) as deposits of braided streams debouching into a newly formed basin.

The overlying arkosic sandstone is notably blue-gray to light blue in outcrop. Though the member contains occasional thin beds of shale and carbonate, it is mostly composed of fine- to coarse-grained sands with regular zones of pebble conglomerate. The average composition (Roberts 1976) is 35% quartz, 22% matrix, 20% lithic fragments, and 17% feldspars, with 6% accessory minerals (calcite, mica, opaque minerals). These deposits are interpreted to be from a complex near-shore system with high energy environments (Roberts 1976).

The best-exposed section of the blue arkosic sandstone member within the field area is on the steep slopes on the west and southwestern side of Ashford peak near 'Prospect Canyon'. An accessible sedimentary section from the basal conglomerate upward is exposed in the head of Ashford Canyon west of 'Gray Wizard Pass'. The following field descriptions of the remaining Crystal Spring Formation are all derived from that exposure.

White feldspathic sandstone member

Wright (1968) and Roberts (1976) describe the sandstone as being red, purple, blue, green, and gray; I have observed it to be white to light gray. The lower section of this member is composed of fine- to coarse-grained sands with abundant sedimentary features, from cross laminations to ripple marks. Roberts (1976) also noted mudcracks, though none were observed locally. Up section from the coarser sands are sequences of fining-upwards sediments, from medium sand to silt. As reported by Roberts (1976), this whole member represents a fining-upwards sequence to the overlying mudstone member.

Compositionally, the sandstone contains much less feldspar than the arkosic member and is 35-70% quartz (Roberts 1976). This decrease in feldspar abundance suggests more complete chemical weathering at the source, signifying a more subdued, low-relief source area landscape (Roberts 1976).

This fining-upwards deposit is interpreted to be that of a tidal sand body transitioning to a tidal flat of a prograding delta. The ripple marks show multi-model directions like that of tidally influenced depositional environments with a northerly flood tide and southerly ebb tide (Roberts 1976). The bedding structures, sequences, shallow water structures, composition, and context all suggest a tidal environment.

Purple Shale (mudstone) Member

The purple shale member is described as "massive to poorly bedded, purple to red, silty to sandy mudstone" by Roberts (1976), but Wright (1968) notes it is "chiefly shale" in many locations. In the field area, only one location exists where this member is primarily well-bedded shale, but does contain thick sections of massive sand-rich silty mudstone. Another local observation that differs from Roberts (1976) description is the

presence of thin carbonate beds, which are absent here. The rock's composition is a 75-80% illite-hematite mixture, giving rise to the purple color, 15-20% quartz, and <5% feldspars (Roberts 1976).

One striking feature is the abundance of pale green to pale blue, often spheroidal, blotches. Wright (1968) found, under thin section, these spots to be the centers where ferric oxide had been reduced to ferrous oxide. These blotches are thus termed reduction spots. I think that these reduction spots represent early iron-reducing organisms, as are typical in paleosols (Retallack 2001).

The purple shale member represents the last predominately clastic unit of the Crystal Springs and is interpreted to represent a low gradient stream estuary system or a tidal marsh (Roberts 1976).

Orange Carbonate (Dolomite and algal Member)

The orange carbonate member is dull to burnt orange in outcrop with 2-5 cm brown interbeds of chert. The lower portion of the member is dolomitic, while the upper portion of the member has abundant algal features. These differences compelled Roberts (1976) to split the carbonate into a dolomite member and algal member.

The dolomitic member is a thinly-bedded, gray, siliceous sandy dolomite with thin layers of chert that protrude as brown ribs (Roberts 1976). The algal portion looks similar from a distance, but the algal features become more prominent with closer observation. The interpreted depositional environment for the two portions differs somewhat, but mainly records a persistent carbonate shelf that was mildly affected by an uplifting source region with transgressions and regressions (Roberts, 1976).

Black Chert Member

Locally, this member is almost invariably black, but one section shows thin banding of red jasperoid bands. It is well bedded, with beds from 5-10 cm thick. Wright (1968) stated that this chert in other areas contains more variety of color, is more common, and is also massive in sections. The chert is often associated with diabase; In many places small bodies of this chert can be found in the diabase. Neither Wright (1968) not Roberts (1974) describe this member in detail; thus it remains an understudied member of the Crystal Springs Formation. Roberts (1974) hypothesized that this member represents the first deposit of northerly transport from an uplifting southerly source region.

Stratigraphically above the black chert member is a disconformity representing a ~300 Ma hiatus (Mahon 2012) followed by deposition of well-bedded siltstones and red limestones of the Horse Thief Formation. This section was not typically observed in the field.

<u>pЄbs</u>- Precambrian Beck Springs formation

The Beck Spring Dolomite is a blue-gray, well-laminated dolomite. It has abundant stromatolitic features in discontinuous, wavy, and non-parallel patterns, as well as other interesting sedimentary textures of shallow-marine carbonates, such as laminations and giant ooids. The dolomite is very fine grained with little variation throughout, though a set of one meter-thick red chert beds were observed in the middle of the section. The laminae are very light blue in color, which stand out in the darker blue-gray matrix. Overall, it is a very thick unit with no large scale lithologic characteristics that can be used as structural markers.

Shafer (1980) contains extensive descriptions and measured sections of the unit from throughout the region. One of the measured sections is from the central Black Mountains where the unit was split into three main members. These members remain informal and were not used during this study.

The depositional environment recorded by the Beck Spring Dolomite is a shallow-marine carbonate shelf. The individual members record tectonic uplifts of the southern upland of the Amargosa aulacogen (Shafer, 1980).

p€kp- Precambrian Kingston Peak Formation

The Kingston Peak Formation is an assemblage of lithologies that represent a variety of depositional environments, which are separated into a western and eastern facies (Petterson *et al.,* 2011). The most illustrious of these are the glacial diamictites. In combination with the overlying Noonday Dolomite, these rocks have been used as evidence to support the global and diachronous climate event during the Neoproterozoic Cryogenian period (Mrofka and Kennedy, 2011) that has been called the Snowball Earth hypothesis (Hoffman *et al.* 1998), first recognized by Kirschvink (1992). Mrofka and Kennedy (2011) explain that a combination of glaciation and tectonics are responsible for the complex mix of lithologies throughout the Kingston Peak formation, which is not seen in most Cryogenian glacial deposits. Extension and uplift provide accommodation space in shallow marine and terrestrial environments that preserves the glacial sediments (Mrofka and Kennedy 2011). Microfossils in the formation, from a variety of eukaryotes, confirm the survival of life throughout Earth's Snowball times (Corsetti *et al*., 2003; Corsetti *et al*., 2006).

The age of deposition of the Kingston Peak Formation is not well constrained, but if correlated with the Rapitan-Sturtian glaciation, the formation is ~700 Ma (Young, 1995). Conversely, the formation has also been correlated with the Marinoan glacial episode of ~650 Ma (Peterson *et al*., 2011). These correlations of the tectonostratigraphic deposits of the formation represent the initial fragmentation of the Neoproterozoic Supercontinent Rodina (Young, 1995; McMenamin and McMenamin 1990).

While the Kingston Peak appears to be missing throughout much of the field area it does outcrop in two mapped areas. The southernmost section, exposed near the mouth of 'Scallywag Canyon' and throughout the South Hills, contains a thick section of the formation. This section thickens southward, to expose the lower shale units of KP1, the black Virgin Spring Limestone, and a red diamictite (Surprise Member of Peterson *et al*., 2011). The northernmost outcropping near 'Gray Wizard Pass', contains a diamictite, probably of the KP4 member (Mrofka, personal communication; Wright, 1974).

The diamictite is by far the most recognizable unit of this formation. It is a matrix- supported sedimentary breccia that contains rare striated clasts of the lower formations of the Pahrump group, most commonly the Beck Spring Dolomite. The Kingston Peak Formation in the field is typically in fault contact with the overlying and underlying unit, but elsewhere the contacts are unconformities.

Noonday Dolomite Formation

pЄn-Noonday Dolomite

Within the study area, the Precambrian Noonday Dolomite presents as a thick mostly massive body of creamy tan dolomite. The formation is exposed throughout the

field area, and is probably the most extensive unit. Lack of textural variation and pervasive intraformational faulting and brecciation, reliable bedding orientations are rare.

One striking field observation is the pervasive brecciation in the Noonday Dolomite, which exists throughout the mapped area. It is ambiguous whether this brecciation is sedimentary or tectonic in nature because of the lack of sedimentary structures or a clear relation to discrete faults. Study of the stratigraphic section suggests the brecciation is sedimentary in nature (Peterson *et al.,* 2011). Rogers (2000) suggested the pervasive brecciation may have been caused by implosion during hydrothermal fluid injection.

The Snowball Earth hypothesis (Hoffman *et al.,* 1998) has raised many interesting questions and other hypotheses about the Noonday Dolomite. It is believed to be a cap-carbonate after the recession of the Cryogenian global ice sheets (Mrofka and Kennedy, 2011). Cap carbonates represent the global sequestration of atmospheric CO_2 following the Snowball events (Hoffman *et al.,* 1998; Kennedy, 1996). Rivaling this hypothesis is the idea that many of the so-called cap-carbonates are actually glacial loess deposits that have been calcified by soil processes (Retallack, 2011a).

pЄi-Ibex Formation

The Ibex formation is mappable in two distinct members, the lower of which has limited outcropping. The lower member consists of a purple shale and prominent orange to tan carbonate beds. The upper member is a characteristic lavender (on fresh surfaces) sandy dolomite that stands as resistant, rough, high, conical peaks and sharp ridges. Similar to the Noonday Dolomite, the Ibex Formation is brecciated throughout much of the field area.

It was once thought that the Ibex was the time-correlative basin facies of the Noonday Dolomite (Wright and Troxel, 1984). The formation was first described by Willams *et al.* (1974) as an arkosic dolomite deposited in the mature Amargosa aulocogen with a southwesterly transport direction. It has now been recognized that a ~100Ma hiatus occurred between the lower and upper Noonday Dolomite. Because the Ibex Formation resides above the unconformity, the lower Noonday Dolomite must have deposited and eroded before the Ibex Formation began to deposit (Corsetti and Kaufman, 2005). The upper Noonday and the Ibex Formation remain as time-correlative units.

In 'Scallywag Canyon', the Noonday and Ibex show a sedimentary interfingering relationship, but elsewhere this relationship is not clear. South of this area, in the outcroppings south from peak 387T, a superb section of the lower Ibex is exposed in fault contact with Kingston Peak diamictite below, and has been a focus in several studies (Peterson *et al.,* 2011; Corsetti and Kaufman, 2005; DeYoung 2005). A superb section it may be, but it is in fault contact with the upper member above that underlies peak 387T.

Johnnie Formation

pЄjl-lower Johnnie Formation

pЄjm-middle Johnnie Formation

pЄju- upper Johnnie Formation

This Ediacran formation (Verdel *et al.,* 2011*)* is unmistakable and striking in the field. The formation is named after the town of Johnnie 50 miles east of Death Valley and is informally split into three members: a lower white quartzite member, the middle shale member, and the upper carbonate-siliciclasic member (Hunt and Mabey, 1966). The upper member of this formation is widely distributed throughout the field area. Four

conical buttes of upper Johnnie Formation are referred to as the east and west 'Tall Johnnie Hills' and 'Short Johnnie Hills' (Figure 1.2b). The well-bedded stratigraphy of the middle and upper members provides great marker beds to detect small faults as well as control on structural orientation. The formation contains abundant sedimentary structures, including ripple marks, cross bedding and load casts, among others. The single best stratigraphic marker in this formation, or any other in these Precambrian sedimentary rocks, is the Johnnie Oolite. This ooid grainstone crops out as a prominent burnt orange ridge among the immediately surrounding fine-grained siliciclastics.

The bottom and top of the formation are marked by unconformities. Other unconformities exist within the formation. These unconformities are the result of eustatic fluctuations and/or tectonic uplifts (Summa, 1993).

The mixed sediments of the formation indicate deposition off a continental margin. The margin was dominated by low-gradient braided fluvial system (siliciclasic sediments) emptying northward into a broad low-energy inner-shelf basin (mixed sediments) and a carbonate shelf (Summa, 1993). These sediments represent the passive continental margin after the breakup of the Neoproterozoic supercontinent Rodinia (Summa, 1993). The upper member preserves high energy oscillatory sheet-flow conditions. Among these is the Johnnie Oolite, a relatively high-energy deposit, which is interpreted to be a landward-prograding transgressive sheet that tracked sea-level rise (Summa, 1993). This observation has been used with $\delta^{13}C$ from the ooid member to correlate the Shuram Excursion in this Ediacaran basin (Bergmann *et al.,* 2011). The Shuram Excursion is a robust carbon isotopic excursion from the Shuram Formation in Oman that suggest changes in the carbon isotopic composition of the global ocean. The

well-calibrated curve is used to correlate global basins. Further studies on this correlation have been conducted (Verdel, 2010; Verdel *et al.,* 2011), and yield similar results. Verdel *et al.* (2011) adds to this by reporting a young detrial zircon dated at 640 +/- 0.09 Ma in the upper Johnnie, confirming the formation as Ediacaran. Detrial zircon dates throughout the formation suggest a Meso- to Neoproterozoic source, which is correlated to formations in Sonora, Mexico (Schoenborn, 2010).

Sterling Quartzite and Wood Canyon Formation

pЄsq-Stirling Quartzite Formation

The Sterling Quartzite consist of three mappable members: Lower siliciclastic-carbonate, middle white and purple quartzite, and upper white quartzite. The stratigraphy and sedimentology of this formation is similar to the underlying Johnnie formation, though it has less carbonate material. The middle member of the unit is particularly characteristic because of the alternating bands of purple shale-rich quartzite and white quartzite. Fedo and Cooper (2001) interpret these member subdivisions as representing fluvial dominated upper and lower members separated by an intertidal marine middle member.

Schoenborn (2011; 2012) found that this formation has the same provenance as the Johnnie Formation. He reports detrial zircon peaks in the Meosproterozoic and Paleoproterozoic that correlate with the local Grenvillian, Yavapai and Mazatzal provinces underlying southwest North America and the Colorado Plateau.

Єwc-Wood Canyon Formation

The Wood Canyon Formation is divided into four distinct members: 1) lower carbonate-bearing member, 2) conglomeratic arkose member, 3) arkosic-feldspathic

quartzite member, and 4) upper carbonate-bearing member (Diehl, 1979). The sediments have been interpreted as deposited in a tidally-influenced delta system and deposited on the edge of an evolving cratonic margin (Diehl, 1979). A similar environment is recorded in the lower formations, though there are two distinct differences. The first is the appearance of macroscopic fossils of the Ediacaran fauna, marking the beginning of the "Cambrian Explosion" (McMenamin and McMenamin, 1995). These fossils include: *Swarptuntia, Treptichnus pedum, Ernietta, Helminthoidichnites, Onuphionella, Planolites,* Mineralized Tubes, and Arthropod Traces (Diehl, 1979). The upper member includes Archaeocyathids, Trilobites, *Skolithos*, and *Tirasiana* (Hagadorn *et al.*, 2000). The second distinction is the eastern extant of the provenance of the upper two members, which on-lap the craton. The lower conglomeratic member includes a granitic provenance in the east (Farmer and Ball, 1997) while Fedo and Cooper (2001) interpret ~1.1 Ga detrial zircons in the upper member as indicating the return of a more distal Grenvillian source area. Either way, the conglomerate-rich member marks the basal deposits of the Cordilleran passive margin (Fedo and Cooper, 2001).

Relatively little Wood Canyon Formation is present within the mapping area. It is most distinct in the head of the Charles Pride Mine wash, where the Pleistocene fan materials have eroded down to expose paleotopography. A similar occurrence east of Jubilee Wash exposes a small section of the formation. At both locations the basal carbonate-bearing member is missing. The exposures of the formation are clearly portions of the conglomeratic arkose member, ranging from granule to pebble size clast-supported conglomerate.

Overlying Cambrian Formations

Above the Wood Canyon Formation exists a rich sedimentological record that extends well into the Paleozoic. For complete exposure to the stratigraphy of the area, I will list the remaining Paleozoic formations: the lower Cambrian Zabriskie Quartzite, Carrera Formation, and Bonanza King Formation; the upper Cambrian Nopah Formation; Ordivician Pognip Group, Eureka Quartzite, Ely Springs Dolomite; the Devonian Hidden Valley Dolomite and Lost Burro Formation; and the Mississippian Tin Mountain Limestone and Perdido Formation. None of these formations will be described here, as they are not exposed within the mapping area.

Neogene Formations

Tmj-Middle-Late Miocene Landslide Deposits

-Jubilee Phase of Amargosa Chaos (Noble, 1941)

-OR-

-GABS Basin sediments (Topping, 1993)

This formation was first described and named by Noble (1941), as the Jubilee Phase of the Amargosa Chaos. It is more thoroughly described and interpreted by Topping (1993), who refers to the formation as the Greater Amargosa-Buckwheat-Sperry wash (GABS) basin sediments. Basically, the complex 'mosaic' of irregular blocks is composed of poorly consolidated and broken-up material (Noble 1941). The lithologies of this formation are highly variable, including clastics and rhyolitic tuffs. It is dominated by red matrix-rich, well-bedded conglomerate with clasts of granite, porphyritic andesite, quartz latite porphyry, and Pahrump group (Noble 1941).

Topping (1993) recorded detailed observations of these individual rock types within the formation and concluded the sediments represent a high-energy basin fill sequence or alluvial fans dominated by debris-sheet flows. Topping (1993) defined this assemblage as the GABS basin after the distributed localities. The formation is in depositional contact with the Precambrian gneiss, the Neoproterozoic-Cambrian sedimentary rocks (Virgin Spring Phase of Amargosa Chaos), and various volcanic rocks (Noble 1941; Wright and Troxel 1984; Topping 1994), suggesting a lithologically diverse bottom to the GABS basin. The intermediate and silicic volcanic rocks below the basal basin unconformity are dated and span the time between 14-10 Ma (Topping 1994), indicating deposition in the basin did not occur until ~10.5 Ma.

The formation can be split into three main conglomerate members that differ in sediment transport direction and composition (Topping 1994): a west-derived conglomerate and two east-derived conglomerates. Within these three members are various tuff deposits have used to constrain the age of the deposits (Topping, 1993). The upper east-derived conglomerate is interpreted as rock-avalanche deposits from the Kingston Range. When Noble (1934) first attempted to describe these rock-avalanche deposits, it was noted that many of the rock fragments are so coarse with so little matrix that “at first they resemble granite in place.” An estimate of the rock-avalanche volumes indicates that the mass could have traveled no more than 10 km from the source and also indicates the basin width was about 20 km (Holm *et al.*, 1994).

The prominent 'Chaos Ridge', including peak 331T, is made up of this formation. Cavernous weathering, which can be seen from afar, characterizes this formation (Noble, 1941), occurring where cobbles and boulders weather out. The basal unconformity of this

formation is very well exposed near the mouth of Ashford Canyon where the west-derived conglomerate overlies the 13.01+/- 0.42 Ma Ashford latite flow (***Til***) (Topping, 1993; Holm et al., 1994).

Tff-Pliocene Funeral Formation (fanglomerate)

As described and named in Noble (1941), derived from unpublished data of Thayer, the type section of this formation is from the Funeral Range approximately 30 km to the north, indicating is it wide-spread. This formation has been referred to as the Black Mountains unroofing sequence (Topping, 1994).

In this location, this formation unconformably overlies the Jubilee Chaos and is interpreted to represent the fragmentation of the GABS basin by stike-slip faulting and the simultaneous unroofing of the Black Mountains by low-angle normal faulting (Topping, 2003). The formation is mainly rock-avalanche deposits and can be split into three informal sections based on clast composition. The basal section is composed of Crystal Spring Formation and Beck Spring Dolomite clasts, while the middle section consists of metamorphic basement clasts only. The upper section includes metamorphic basement clasts, but also contains Shoshone Volcanics, basalt clasts, and the Sheephead Andesite. The uppermost section of the formation, atop the rock-avalanche deposits, is the capping Funeral Basalt (**T*fb***) dated at 4.9 +/- 0.1 Ma (Holm and Lux, 1991) and 4.14 +/- 0.12 Ma (McAllister 1973).

This formation only occurs in the extreme eastern boundary of the map area. The middle section, composed of metamorphic basement clasts, makes up the hills surrounding Jubilee Pass (471T), while the Funeral Basalt can be seen capping a high ridge to the north of Jubilee Pass (1027T).

Qg_1-Pleistocene fan deposits-cemented

Ashford Canyon contains several isolated outcrops of a quartz-cemented alluvial fan deposit. The clasts range from sub-angular to sub-rounded of various lithologies, which were not studied in detail. The unit is peculiar because of its geographic position within Ashford Canyon as well as its striking difference to any other fan deposits in the area. No literature exists on the subject. A Pleistocene age is assumed for the unit based on local sediment aggradation in the basin required to deposit such sediments and the degree of induration.

Qg_1-Pleistocene fan deposits-unconsolidated

The topographically lower portions of the field are dominated by these deposits, which where presumably deposited *in situ* on top of Virgin Spring and Jubilee phases of the Amargosa Chaos. These fan deposits where once much broader and thicker, but have undergone significant erosion by the modern wash tributaries that carry sediment down slope during storms and flash floods.

Qa-Holocene Sand Deposits

Small amounts of windblown dune sand have collected in the southern portion of the mapping area, where they are a prominent feature of the landscape.

Qg_2-Holocene Wash Deposits

These deposits define the modern (at time of mapping and satellite imagery) washes throughout the area. This unit was mapped primarily using the base layer satellite imagery available on ArcMap, with minor field mapping.

The deposits are made of unconsolidated materials of the fan deposits on which they form and minor input from rock outcrops. Therefore, these deposits are composed of

the same material as described above. However, the channels migrate through time, particularly after flash flooding events. For example, minor changes in channel margins could be detected between the 2011 and 2012 field excursions due to a late summer 2012 rainstorm.

APPENDIX C:

INSTRUMENTAL NEUTRON ACTIVATION ANALYSIS RESULTS

Sample ID	Al2O3		CaO		K2O		Na2O		Fe2O3	
	%	± 1 σ	%	± 1 σ	%	± 1 σ	%	± 1 σ	%	± 1 σ
DUH304-1	0.75	0.04	18.00	0.50	-0.51	0.02	0.02	0.00	41.91	0.50
DUH304-2	0.76	0.04	18.48	0.51	-0.52	0.02	0.02	0.00	42.19	0.51
DUH324-1	0.92	0.03	8.03	0.27	-0.36	0.01	0.01	0.00	66.92	0.80
DUH324-2	0.98	0.03	7.59	0.27	-0.37	0.01	0.01	0.00	65.48	0.78
DUH306-1	3.32	0.04	1.50	0.11	-0.29	0.01	0.02	0.00	66.50	0.80
DUH306-2	3.35	0.04	1.60	0.11	-0.29	0.01	0.02	0.00	64.86	0.78
DUH327-1	3.84	0.05	4.72	0.20	-0.39	0.01	0.37	0.01	64.23	0.77
DUH327-2	3.68	0.05	5.23	0.21	-0.39	0.01	0.34	0.01	64.26	0.77

Sample ID	Ti		Sc		V		Cr		Mn	
	ppm	± 1 σ	ppm	± 1 σ	ppm	± 1 σ	ppm	± 1 σ	ppm	± 1 σ
DUH304-1	374.81	241.24	1.13	0.03	21.44	3.27	6.18	1.28	2666.56	69.92
DUH304-2	655.16	243.29	1.17	0.03	24.84	3.82	8.30	1.40	2685.24	70.41
DUH324-1	780.63	235.24	1.68	0.04	25.43	3.27	-4.59	0.08	1450.18	38.09
DUH324-2	999.86	237.35	1.71	0.04	21.26	2.83	7.02	1.70	1451.34	38.12
DUH306-1	1663.16	282.27	2.38	0.05	44.97	4.90	7.41	1.88	936.12	24.64
DUH306-2	1311.09	284.20	2.30	0.05	43.91	4.89	8.75	1.94	966.72	25.44
DUH327-1	1627.99	257.64	5.68	0.10	46.30	5.11	50.33	2.52	1571.33	41.26
DUH327-2	1421.77	255.94	5.59	0.10	44.28	5.11	49.53	2.56	1480.00	38.87

Sample ID	Co		Zn		Rb		Cs		Ba	
	ppm	± 1 σ	ppm	± 1 σ	ppm	± 1 σ	ppm	± 1 σ	ppm	± 1 σ
DUH304-1	42.49	0.62	150.72	6.88	-21.55	0.97	-0.48	0.01	-80.82	3.24
DUH304-2	43.51	0.63	164.93	7.17	-21.61	0.98	-0.49	0.01	-80.24	3.22
DUH324-1	48.04	0.70	56.81	5.01	-26.61	1.20	-0.60	0.01	102.46	34.12
DUH324-2	47.53	0.69	56.02	5.17	-26.88	1.21	-0.60	0.01	85.36	31.84
DUH306-1	56.69	0.82	78.97	7.00	-27.31	1.23	-0.61	0.01	1106.79	73.47
DUH306-2	54.50	0.78	86.78	6.53	-26.81	1.21	-0.59	0.01	1019.92	71.02
DUH327-1	50.17	0.73	232.41	9.49	-27.00	1.22	-0.61	0.01	226.48	49.25
DUH327-2	49.76	0.72	242.39	9.93	-27.57	1.25	-0.62	0.01	150.05	47.25

Sample ID	Sr		La		Ce		Nd		Sm	
	ppm	± 1 σ	ppm	± 1 σ	ppm	± 1 σ	ppm	± 1 σ	ppm	± 1 σ
DUH304-1	-240.30	25.37	3.64	0.05	6.08	0.69	-12.74	0.86	0.96	0.01
DUH304-2	-244.83	25.85	3.66	0.05	6.80	0.75	-13.07	0.88	1.00	0.01
DUH324-1	-291.21	30.75	6.56	0.07	12.39	0.95	-16.29	1.10	2.31	0.02
DUH324-2	-290.13	30.63	6.60	0.07	12.57	0.94	-16.19	1.09	2.26	0.02
DUH306-1	-297.79	31.44	2.07	0.04	-2.44	0.02	-16.32	1.10	0.87	0.01
DUH306-2	-292.39	30.87	1.91	0.04	-2.38	0.02	-16.10	1.09	0.83	0.01
DUH327-1	-305.92	32.30	1.54	0.05	-2.46	0.02	-16.94	1.14	0.91	0.01
DUH327-2	-310.76	32.81	1.66	0.05	-2.51	0.02	-17.38	1.17	0.92	0.01

Sample ID	Eu		Tb		Dy		Yb		Lu	
	ppm	± 1 σ	ppm	± 1 σ	ppm	± 1 σ	ppm	± 1 σ	ppm	± 1 σ
DUH304-1	0.19	0.02	-0.37	0.02	-1.62	0.08	1.23	0.08	0.22	0.02
DUH304-2	0.19	0.02	-0.39	0.02	-1.65	0.08	1.05	0.07	0.24	0.02
DUH324-1	0.34	0.02	-0.46	0.03	2.02	0.51	1.13	0.09	0.21	0.01
DUH324-2	0.32	0.02	-0.45	0.03	-1.18	0.06	1.19	0.09	0.18	0.01
DUH306-1	0.17	0.02	-0.47	0.03	-1.21	0.06	0.77	0.09	0.10	0.02
DUH306-2	0.15	0.02	-0.46	0.03	-1.25	0.06	0.53	0.08	0.10	0.02
DUH327-1	0.24	0.02	-0.46	0.03	-1.27	0.06	0.66	0.08	0.10	0.01
DUH327-2	0.25	0.02	-0.45	0.03	-1.25	0.06	0.63	0.09	0.11	0.01

Sample ID	Sb		As		Hf		Ta		Th	
	ppm	± 1 σ	ppm	± 1 σ	ppm	± 1 σ	ppm	± 1 σ	ppm	± 1 σ
DUH304-1	3.19	0.14	14.91	0.29	-0.30	0.01	-0.30	0.02	0.14	0.10
DUH304-2	3.37	0.15	14.74	0.29	-0.31	0.01	-0.31	0.02	0.28	0.10
DUH324-1	-0.22	0.01	1.29	0.19	-0.38	0.01	-0.38	0.02	10.49	0.23
DUH324-2	-0.21	0.01	1.02	0.19	-0.38	0.01	-0.37	0.02	10.53	0.23
DUH306-1	0.90	0.12	6.47	0.33	-0.39	0.01	-0.38	0.02	-0.38	0.00
DUH306-2	1.11	0.12	6.48	0.31	-0.38	0.01	-0.38	0.02	-0.37	0.00
DUH327-1	1.17	0.11	13.39	0.45	0.58	0.17	-0.38	0.02	0.83	0.14
DUH327-2	1.54	0.12	13.89	0.42	0.73	0.18	-0.38	0.02	1.01	0.15

	U	
	ppm	± 1 σ
DUH304-1	1.39	0.26
DUH304-2	1.08	0.23
DUH324-1	5.54	0.42
DUH324-2	5.75	0.45

	U	
	ppm	± 1 σ
DUH306-1	1.23	0.41
DUH306-2	0.82	0.31
DUH327-1	0.79	0.33
DUH327-2	0.78	0.30

REFERENCES CITED

Allmendinger, R.W., and Jordan, T.E., 1981, Mesozoic evolution, hinterland of the Sevier orogenic belt: Geology, v. 9, p. 308-313.

Allmendinger, R. W., Cardozo, N., and Fisher, D., in press, Structural geology algorithms: Vectors and tensors in structural geology: Cambridge University Press , 302p.

Anders, M.H., Christie-Blick, N., Walker, C.D., 2005, Distinguishing between Rooted and Rootless detachments: A Case Study from the Mormon Mountains of Southeastern Nevada: Geology, v. 114, p. 645-664.

Anderson, R.E., 1971, Thin Skin Distension in Tertiary Rocks of Southeastern Nevada: Geologic Society of America Bulletin, v. 82, p. 43-58.

Axen, G.J., and Bartley, J.M., 1997, Field tests of rolling hinges: Existence, mechanical types, and implications for extensional tectonics: Journal of Geophysical Research, v. 102, no. B9, p. 20,515-20,537.

Barton, M.D., and Johnson, D.A., 1996, Evaportic-source model for igneous-related Fe oxide--(REE-Cu-Au-U) mineralization: Geology, v. 24, p. 1559-262.

Barton, M.D., Girardi, J.D., Kreiner, D.C., Seedorff, E., Zurcher, L., Dilles, J.H., Haxel, G.B., and Johnson, D.A., 2011, Jurassic igneous-related metallogeny of southwestern North America, p. 373-396.

Bergmann, K.D., Zentmyer, R.A., and Fischer, W.W., 2011, The stratigraphic expression of a large negative carbon isotope excursion from the Ediacaran Johnnie Formation, Death Valley: Precambrian Research, v. 188, p. 45-56.

Burchfiel, B.C., and Stewart, J.H., 1966, "Pull-Apart" origin of the central segment of Death Valley, California: Geological Society of America Bulletin, v. 77, p. 439-442.

Butler, P.R., Troxel, B.W., Verosub, K.L, 1988, Late Cenozoic history and styles of deformation along the southern Death Valley fault zone, California: Geological Society of America Bulletin, v. 100, p. 402-410.

Calzia, J.P. and Ramo, O.T., 2000, Late Cenozoic crustal extension and magmatism, southern Death Valley region, California, *in* Lageson, D.R., Peters, S.G, and Lahren, M.M., eds., Great Basin and Sierra Nevada: Boulder, Colorado, Geologic Society of America Field Guide 2, p. 135-164.

Corsetti, F.A., Awramik, S.M., Pierce, D., 2003, A complex microbiota from snowball Earth times: Microfossils from the Neoproterozoic Kingston Peak Formation, Death Valley, USA: Proceedings of the National Academy of Sciences, v. 100, no. 8, p. 4399-4404.

Corsetti, F. A., Kaufman, A.J., 2005, The relationship between Neoproterozoic Noonday Dolomite and the Ibex Formation: New Observations and their bearing on 'snowball Earth': Earth-Science Reviews, v. 73, p. 63-78.

Corestti, F.A., Olcott, A.N., Bakermans, C., 2006, The biotic response to Neoproterozoic snowball Earth: Paleogeography, Paleoclimatology, Palaeoecology, v. 232, p. 114-130.

Cloud, P., Wright, L.A., Willams, E.G., Diehl, P., and Walter, M.R., 1974, Giant Stramatolites and Associated Vertical Tubes from the Upper Proterozoic Noonday Dolomite, Death Valley Region, Eastern California: Geological Society of America Bulletin, v. 85, no. 12, p. 1869-1882.

Curry, D.H., 1938, "Turtleback" fault surfaces in Death Valley, California (abstract): Geological Society of America Bulletin, v. 49, p. 1875.

Curry, D.H., 1954, Turtlebacks in the Central Black Mountains, Death Valley, California *in* Geology of Southern California: California Division of Mines and Geology, Bulletin 170, v. 2, p. 53-59.

DeYoung, D.P., 2005, The Neoproterozoic Ibex Formation, Eastern California: Stratigraphic and Sedimentological constraints on ice age and carbonate precipitation events of southern Death Valley, [M.Sc. Thesis]: University of California, Riverside, 344 p.

Diehl, P.E., 1979, The Stratigraphy, Depositional Environments, and Quantitiative Petrography of the Precambrian-Cambrian Wood Canyon Formation, Death Valley. [Ph.D Dissertation]: Pennsylvania State University, 363 p.

Drewes, H., 1959, Turlteback Faults of Death Valley, California: A Reinterpretation: Geologic Society of America Bulletin, v. 70, no. 12, p. 1497-1508.

Farmer, G.L., and Ball, T.T., 1997, Sources of Middle Proterozoic to Early Cambrian siliciclastic sedimentary rocks in the Great Basin: a Nd isotope study: Geologic Society of America Bulletin, v. 109, no. 9, p. 1193-1205.

Federal Geographic Data Committee [prepared for the Federal Geographic Data Committee by the U.S. Geological Survey], 2006, FGDC Digital Cartographic Standard for Geologic Map Symbolization: Reston, Va., Federal Geographic Data Committee Document Number FGDC-STD-013-2006, 290 p., 2 plates.

Fedo, C.M. and Cooper, J.D., 1990, Braided Fluvial to Marine Transition: The Basal lower Cambrian Wood Canyon Formation, Southern Marble Mountains, Mojave Desert, California: Journal of Sedimentary Petrology, v. 60, no. 2, p. 220-234.

Fowler, T.K., Jr., and Calzia, J.P., 1999, The Kingston Range detachment fault, southeastern Death Calley region, California: Relation to Tertiary deposits and reconstruction of initial dip, *in* Wright, L.A., and Troxel, B.W., eds., Cenozoic Basins of the Death Valley Region: Boulder, Colorado, Geologic Society of America Special Paper 333.

Fedo, C.M. and Cooper, J.D., 2001, Sedimentology and sequence stratigraphy of Neoproterozoic and Cambrian units across a craton-margin hinge zone, southeastern California, and implications for the early evolution of the Cordilleran margin: Sedimentary Geology, v. 141, p. 501-522.

Fedo, C.M., 2001, Constraints on the Evolution of the Cordilleran Margin from Detrial Zircon analyses in the middle member wood canyon formation, marble mountains, southeastern California. Geologic Society of America Annual Meeting, November 5-8, 2001, Session No. 94: Geochemistry of Siliciclasic Materials: Provenance, Paleoclimates, and Plate Tectonic Settings, Paper No. 94-0.

Fleck, R.J., 1970, Age and Tectonic Significance of Volcanic Rocks, Death Valley Area, California: Geologic Society of America Bulletin, v. 81, no. 9, p. 2807-2816.

Flesch, L., and Bendick, R., 2012, The relationship between surface kinematics and deformation of the whole lithosphere: Geology, v. 40, no. 8, p. 711-714.

Fraiser, M.L., and Corsetti, F.A., 2003, Neoproterozoic Carbonate shrubs: Interplay of Microbial Activity and Unusual environmental conditions in Post-Snowball Earth: PALAIOS, v. 18, no. 4, p. 378-387.

Friedmann, S.J., and Burbank, D.W., 1995, Rift Basins and supradetachment basins: intracontinental extensional end-members: Basin Research, v. 7, no. 2, p. 109-127.

Guest, B., Pavlis, T.L., Golding, H., and Serpa, L., 2003, Chasing the Garlock: A study of tectonic response to vertical axis rotation: Geology, v. 31, no. 6, p. 553-556.

Hagadorn, J.W., Fedo, C.M., and Waggoner, B.M., 2000, Early Cambrian Ediacran-Type Fossils from California: Journal of Paleontology, v. 74, no. 4, p. 731-740.

Hammond, J.G, 1986, Geochemistry and petrogenesis of Proterozoic diabase in the southern Death Valley region of California: Contributions to mineralogy and petrology, v. 93, no. 3, p. 312-321.

Hammond, W.C., Blewitt, G., Li, Z., Plag, H., and Kreemer, C., 2012, Contemporary uplift of the Sierra Nevada, western United States, from GPS and InSAR measurements: Geology, v. 40, p. 667-670.

Hayman, N.W., Knott, J.R., Cowan, D.S., Nemser, E., and Sarna-Wojcicki, A.M., 2003, Quaternary low-angle slip on detachment faults in Death Valley, California: Geology, v. 31, p. 343-346.

Hayman, N.W., 2006, Shallow crustal fault rocks from the Black Mountain detachments, Death Valley, CA: Journal of Structural Geology, v. 28, p. 1767-1784.

Heaman, L.M., and Grotzinger, J.P., 1992, 1.08 Ga diabase sills in the Pahrump Group, California: Implications for development of the Cordilleran miogeocline: Geology, v. 20, p. 637-640.

Heizer, R.F., 1954, Indian Occupation in Southern California *in* Geology of Southern California: California Division of Mines and Geology, Bulletin 170, v. 2, p. 45-53

Hoffman, P.F., Kaufman, A.J., Halverson, G.P., and Schrag, D.P., 1998, A Neoproterozoic Snowball Earth: Science, v. 281, p. 1342-1346.

Holm, D.K., and Dokka, R.K., 1993, Interpretation and tectonic implications of cooling histories: An example from the Black Mountains, Death Valley extended terrane, California: Earth and Planetary Science Letters, v. 116, p. 63-80.

Holm, D.K., Geissman, J.W., and Wernicke, B.K., 1993, Tilt and rotation of the footwall of a major normal fault system: Paleomagnetism of the Black Mountains, Death Valley extended terrane, California: Geologic Society of America Bulletin, v. 105, p. 1373-1387.

Holm, D.K., and Lux, D.R., 1991, The Copper Canyon Formation: A record of unroofing and Tertiary folding of the Death Valley turtleback surfaces: Geologic Society of America Abstracts with Programs, v. 23, no. 2, p. 35.

Holm, D.K., Snow, J.K., and Lux, D.R., 1992, Thermal and Barometric constraints on the intrusive and unroofing history of the Black Mountains: Implications for timing, initial dip, and kinematics of detachment faulting in the Death Valley Region, California: Tectonics, v. 11, no. 3, p. 507-522.

Holm, D.K., and Wernicke, B.P., 1990, Black Mountains crustal section, Death Valley extended terrain, California: Geology, v. 18, p. 520-523.

Holm, D.K, Pavlis, T.P., Topping, D.J., 1994, Black Mountains Crustal Section, Death Valley Region, California, *in* McGill, S.F., and Ross, T.M., eds., Geological investigations of an active margin: Geologic Society of America Cordilleran Section Guidebook: Redlands, California, San Bernardio County Museum Association, p. 31-54.

Holm, D.K., Fleck, R.J., and Lux, D.R., 1994, The Death Valley Turtlebacks Reinterpreted as Miocene-Pliocene Folds of a Major Detachment Surface: Geology, v. 102, p. 718-727.

Hill, M.L., and Troxel, B.W., 1966, Tectonics of Death Valley Region, California: Geological Society of America Bulletin, v. 77, p. 435-438.

Hunt, C.B., and Mabey, D.R., 1966, Stratigraphy and Structure Death Valley, California: U.S. Geologic Survay Professional Paper 494-A, 162 p.

Karlstrom, K.E., and Conway, C.M., 1986, Early Proterozoic geology of Arizona: Geology 1986, v. 14., p. 625-626.

Kupfer, D.H., 1960, Thrust Faulting and Chaos structure, Silurian Hills, San Bernardio County, California: Geologic Society of America Bulletin, v. 71, no. 2, p. 161-214.

Keener, C., Serpa, L., and Pavlis, T.L., 1993, Faulting at Morman Point, Death Valley, California: A low-angle normal fault cut by high-angle faults: Geology, v. 21., p. 327-330.

Kirschivink, J.L., 1992, Late Proterozoic Low-Latitude Global Glaciation: the Snowball Earth *in* Schopf, J.W., and Klein, C. (eds.): The Proterozoic Biosphere: A Multidisciplinary Study. Cambridge University Press, p. 51-52.

Kirsch, S.A., 1971, Chaos Structure and Turtleback Dome, Mineral Ridge, Esmeralda County, Nevada: Geologic Society of America Bulletin, v. 82, no. 11, p. 3169-3176.

Levy, M., and Christie-Blick, N., 1989, Pre-Mesozoic Palinspastic Reconstruction of the Eastern Great Basin (Western United States): Science, v. 245, no. 4925, p. 1454-1462.

Lingenfelter, Richard E., 1988, Death Valley and the Amargosa: A Land of Illusion, University of California Press, 622 p.

Losh, S., Purvance, D., Sherlock, R., Jowett, E.C., 2005, Geologic and geochemical study of the Picacho gold mine, California: gold in a low-angle normal fault environment: Mineralium Deposita, v. 40, p. 137-155.

Low, J.W., 1957, Geologic Field Methods, First Edition, Harper and Brothers Publishing, New York, 489 p.

Lowenstein, T.K., Li, J., Brown, C., Roberts, S.M., Ku, T., Luo, S., and Yang, W., 1999, 200 k.y. Paleoclimate record from Death Valley salt core: Geology, v. 27, p. 3-6.

Mancktelow, N.S., and Pavlis, T.L, 1994, Fold-fault relationships in low-angle detachment systems: Tectonics, v. 13, no. 2, p. 668-685.

Mahon, R.C., 2012, Detrial Zircon Provenance, Geochrology and revised stratigraphy of the Mesoproterozoic and Neoproterozoic Pahrump (super)group, Death Valley Region, California, [M.S. Thesis] Idaho State University, 182 p.

McAllister, J.F., 1973, Geologic map and section of the Amargosa Valley borate area—southeast continuation of the Furnace Creek area—Inyo County, California: U.S. Geological Survey Miscellaneous Geological Investigations Map 1-782.

McMenamin, M. A. S., and McMenamin, D. L. S., 1990, The Emergence of Animals: The Cambrian Breakthrough, Columbia University Press, 217 pp.

Miller, M.G., 1999, Implications of ductile strain on the Badwater Turtleback for pre-14-Ma extension in the Death Valley region, California, *in* Wright, L.A., and Troxel, B.W., eds., Cenozoic Basins of the Death Valley Region: Boulder, Colorado: Geologic Society of America Special Paper 333.

Miller, M.G., and Friedman, R.M., 1999, Early Tertiary magmatism and probable Mesozoic fabrics in the Black Mountains, Death Valley, California: Geology, v. 27, p. 19-22.

Miller, M.G., 2002, Constraints on the Slip and Magnitude of the Amargosa Fault: Implications for Extension in Death Valley, California, USA: Geologic Society of America Annual Meeting, Paper No. 79-3.

Miller, M.G., and Prave, A.R., 2002, Rolling hinge or fixed basin?: A test of continental extension models in Death Valley, California, United States: Geology, v. 30, p. 847-850.

Miller, M.G., 2003, Basement-involved thrust faulting in a thin-skinned fold-and-thrust belt, Death Valley, California, USA: Geology, v. 31, p. 31-34.

Miller, M.B., and Pavlis, T.L., 2005, The Black Mountains turtlebacks: Rosetta stones of the Death Valley tectonics: Earth-Science Reviews, v. 73, p. 115-138.

Miller, J.M.G, 1987, Paleotectonic and Stratigraphic Implications for the Kingston Peak-Noonday Contact in the Panamint Range, Eastern California: Geology, v. 95, no. 1, p. 75-85.

Mrofka, D., and Kennedy, M., 2011, The Kingston Peak Formation in the eastern Death Valley region, *in* Arnaud, E., Halverson, G.P., and Shields-Zhou, G., (eds.) The Geologic Record of Neoproterozoic Glaciations, Geologic Society, London: Memoirs, v. 36, p. 449-458.

Noble, L.F., 1934, Rock formations of Death Valley, California: Science, v. 80, no. 2069, p. 173-178.

Noble, L.F., 1941, Structural Features of the Virgin Spring Area, Death Valley, California: Bulletin of the Geologic Society of America, v. 52, p. 941-1000.

Noble, L.F. and Wright, L.A., 1954, Geology of the Central and Southern Death Valley Region, California *in* Geology of Southern California: California Division of Mines and Geology, Bulletin 170, v. 2, p. 143-160.

Norton, I., 2011, Two-stage formation of Death Valley: Geosphere, v. 7, p. 171-182.

Pavlis, T.L., Serpa, L.F., and Keener, C., 1993, Role of seismogenic processes in fault-rock development: An example from Death Valley, California: Geology, v. 21, p. 267-270.

Peterson, R., Prave, A.R., Wernicke, B.P., and Fallick, A.E., 2011, The Neoproterozoic Noonday Formation, Death Valley Region, California: Geological Society of America Bulletin, v. 123, no. 7-8, p. 1317-1336.

Plattner, C., Malservisi, R., Furlong, K.P., Govers, R., 2010, Development of th Eastern California Shear zone- Walker Lane belt: The effects of microplate motion an pre-existing weakess in the Basin and Range: Tectonophysics, v. 485, p. 78-84.

Powell, C.M., and Young, G.M., 1995, Are Neoproterozoic Glacial Deposits preserved on the margins of Laurentia related to the fragmentations of two supercontinents? Comment and Reply: Geology, v. 23, p. 1053-1055.

Prave, A.R., 1999, Two diamictites, two cap carbonates, two $\delta^{13}C$ excursions, two rifts: The Neoproterozoic Kingston Peak Formation, Death Valley, California: Geology, v. 27, p. 339-342.

Pruss, S.B., Corsetti, F.A., Fischer, W.W., 2008, Seafloor-precipitated carbonate fans in the Neoproterozoic Rainstorm Member, Johnnie Formation, Death Valley Region, USA: Sedimentary Geology, v. 207, p. 34-40.

Proffett, J.M., JR., 1977, Cenozoic geology of the Yerington district, Nevada, and implications for the nature and origin of Basin and Range faulting: Geological Society of America Bulletin, v. 88, p. 247-266.

Roberts, M.T., 1976, Stratigraphy and Depositional Environments of the Crystal Spring Formation, Southern Death Valley Region, California, *in* Geologic Features of Death Valley, California: California Division of Mines and Geology Special Report 106, p. 35-43.

Roberts, M.T., 1974, Stratigraphy and Depositional Environments of the lower part of the Crystal Spring Formation, Southern Death Valley Region, California, [Ph.D. Dissertation] Pennsylvania State University, 199 p.

Renik, B., Chrisite-Blick, N., Troxel, B.W., Wright, L.A., Niemi, N.A., 2008, Re-evaluation of the Middle Miocene Eagle Mountain Formation and its significance as a piercing point for the interpretation of extreme extension across the Death Valley Region, California, U.S.A: Journal of Sedimentary Research, v. 78, p. 199-219.

Retallack, G.J., 2011a, Neoproterozoic glacial loess and limits to snowball Earth: Geological Society of London Journal 168, 1-19.

Retallack, G.J. 2001. Soils of the Past: an Introduction to Paleopedology. Second Edition, Blackwell, Oxford, 600 p.

Rogers, C.E., 2000, The geometry and kinematics of the Amargosa Fault, Southern Black Mountains, Death Valley, California. [M.S. Thesis]: University of Oregon, 79 p.

Schmandt, B., and Humphreys, E., 2011, Seismically imaged relict slab from the 55 Ma Siletzia accretion to the northwest United States: Geology, v. 39, no. 2, p. 175-178.

Schoenborn, W.A., and Fedo, C.M., 2011, Provenance and paleoweathering reconstruction of the Neoproterozoic Johnnie Formation, southeastern California: Chemical Geology, v. 285, p. 231-255.

Schoenborn, W.A., Fedo, C.M., Farmer, G.L., 2012, Provenance of the Neoproterozoic Johnnie Formation and Stirling Quartzite, southeastern California, determined by detrial zircon geochronology and Nd isotope geochemistry: Precambrian Research, v. 206-207, p. 182-199.

Sears, D.H., 1953, Origin of the Amargosa Chaos, Virgin Spring Area, Death Valley, California: The Journal of Geology, v. 61, no. 2, p. 182-186.

Serpa, L., DE Voodoo, B., Wright, L.A., Willem in, J., Oliver, J., Hauser, E., and Troxel, B., 1988, Structure of the central Death Valley pull-apart basin and vicinity from COCORP profiles in the southern Great Basin: Geological Society of America Bulletin, v. 100, p. 1437-1450.

Serpa, L. and Pavlis, T.L., 1996, Three-dimensional model of the late Cenozoic history of the Death Valley region, southeastern California: Tectonics, v. 15, no. 6, p. 1113-1128.

Shafer, D.C., 1983, Petrology and depositional environments of the Beck Spring Dolomite, Southern Death Valley Region, California, [M.S. Thesis], University of California Davis, 90 p.

Snow, J.K., and Wernicke, B.P., 1989, Uniqueness of geologic correlations: an example from the Death Valley extended terrain: Geologic Society of America Bulletin, v. 101, no. 11, p. 1351-1362.

Snow, J.K., and Wernicke, B.P., 2000, Cenozoic Tectonics in the central basin and range magnitude, rate, and distribution of upper crustal strain: American Journal of Science, v. 300, p. 659-719.

Stewart, J.H., 1983, Extensional tectonics in the Death Valley area, California: Transport of the Panamint Range structural block 80 km northwestward: Geology, v. 11, p. 153-157.

Summa, C.L., 1993, Entomological, stratigraphic, and tectonic controls of a mixed carbonate-siliciclastic succession: Neoproterozoic Johnnie Formation, southeast California, [Ph.D. Dissertation, Massachusetts Institute of Technology, 616 p.

Topping, D.J., 1993, Geographical reconstruction of the Death Valley extended region: Evidence from Miocene large rock-avalanche deposits in the Amargosa Chaos Basin, California: Geological Society of America Bulletin, v. 105, p. 1190-1213.

Topping, D.J., 2003, Stratigraphic Constraints on the Style and Magnitude of Extension in the Southern Black Mountains, Death Valley, California, 10.5 Ma to present: Geological Society of America Abstracts with Programs, v. 35, no. 6, p. 347.

Verdel, C., Wernicke, B.P, and Bo wring, S.A., 2011, The Shuram and Subsequent Ediacaran carbon isotope excursions from southwest Laurentia, and implications for environmental stability during the Smetana radiation: Geological Society of America Bulletin, v. 123, p. 1539-1559.

Wernicke, B.P., Axen, G.J., and Snow, K.J., 1988, Basin and Range extensional tectonics at the latitude of Las Vegas, Nevada: Geological Society of America Bulletin, v. 100, p. 1738-1757.

Wernicke, B.P., and Snow, K.J., 1998, Cenozoic Tectonism in the Central Basin and Range: Motion of the Sierran-Great Valley Block: International Geology Review, v. 40, p. 403-410.

Wernicke, B.P., Davis, J.L., Niemi, N.A., Luffi, P., and Bisnath, S., 2008, Active Megadetachment beneath the western United States: Journal of Geophysical Research, v. 113, P. 26-52.

Williams, E.G., Wright, L.A., and Troxel, B.W., 1976, The Noonday Dolomite and equivalent stratigraphic units, southern Death Valley Region, California *in* Wright, L.A., and Troxel, B.W. (Eds.),1976, Geologic Features, Death Valley California: California Division of Mines and Geology, Special Report 106, 72p.

Wright, L.A., and Troxel, B.W., 1954, Western Mojave Desert and Death Valley Region Geologic Field Guide no. 1, *in* Geology of Southern California: Department of Natural Resources, Division of Mines and Geology, Bulletin 170, 50 p.

Wright, L.A., 1968, Talc Deposits of the Southern Death Valley Region, California: Division of Mines and Geology, Special Report 95, 78 p.

Wright, L.A., and Troxel, B.W., 1969, Chaos Structure and Basin and Range Normal Faults: Evidence for a Genetic Relationship: Geologic Society of America Abstract with Programs Part 7, p. 242.

Wright, L.A., and Troxel, B.W. (Eds.),1976, Geologic Features, Death Valley California: California Division of Mines and Geology, Special Report 106, 72 p.

Wright, L.A., Williams, E.G., Cloud, P., 1978, Algal and cyptalgal structures and platform environments of the late pre-Phanerozoic Noonday Dolomite, eastern California: Geologic Society of America Bulletin, v. 89, p. 321-333.

Wright, L.A., and Troxel, B.W., 1984, Geology of the northern half of the Confidence Hills quadrangle, Death Valley region, California; the area of the Amargosa chaos: California Division of Mines and Geology Map Sheet 34, scale 1:24,000, 31 p.

Wright, LA., Thompson, R.A., Troxel, B.W., Pavlis, T.L., DeWitt, E.H., Otton., J.K., Ellis, M.A., Miller, M.G., and Serpa, L.F., 1991, Cenozoic magmatic and tectonic evolution of the east-central Death Valley region, California, *in* Walawender, M.J., and Hanan, B.B., eds., Geologic excursions in southern California and Mexico: San Diego, California: Geological Society of America 1991 Annual Meeting Guidebook, p. 93-127.

Wright, L.A., Greene, R.C., Çemen, I., Johnson, F.C., and Prave, A.R., 1999, Tectonostratigraphic development of the Miocene-Pliocene Furnace Creek Basin and related features, Death Valley region, California, *in* Wright, L.A., and Troxel, B.W., eds., Cenozoic Basins of the Death Valley Region: Boulder, Colorado, Geologic Society of America Special Paper 333, p. 87-114.

Wright, L.A., and Troxel, B.W., 1999, Levi Noble's Death Valley, a 58 year Perspective *in* Moores, E.M., Sloan, D., and Stout, D.L., eds., Classic Cordilleran Concepts: A View from California: Boulder, Colorado: Geologic Society of America, Special Paper 338, p. 399-411

Wright, L.A., and Troxel, B.W., 2002, Levi Noble: Geologist, His Life and Contributions to understanding the Geology of Death Valley, the Grand Canyon, and the San Andreas Fault: U.S. Geologic Survey Open-File Report 02-422, 38 p.

Wasserburg, G.J., Wetherill, G.W., and Wright, L.A., 1959, Ages in Precambrian Terrane of Death Valley, California: Journal of Geology, v. 67, no. 6, p. 702-708.

Yin, A., and Dunn, J.F., 1992, Structural and stratigraphic development of the Whipple-Chemehuevi detachment fault system, southeastern California: Implications for the geometrical evolution of domal and basinal low-angle normal faults: Geological Society of America Bulletin, v. 104, p. 659-674.

Young, G.M., 1995, Are Neoproterozoic Glacial Deposits preserved on the margins of Laurentia related to the fragmentations of two supercontinents?: Geology, v. 23, p. 153-156.